2017

The Role of Protease-Activated Receptor-2 During Wound Healing in Intestinal Epithelial Cells

Fernando, Elizabeth

UNIVERSITY OF CALGARY

The Role of Protease-Activated Receptor-2 During Wound Healing in Intestinal Epithelial Cells

by

Elizabeth Hannah Fernando

A THESIS

SUBMITTED TO THE FACULTY OF GRADUATE STUDIES

IN PARTIAL FULFILMENT OF THE REQUIREMENTS FOR THE

DEGREE OF DOCTOR OF PHILOSOPHY

GRADUATE PROGRAM IN MEDICAL SCIENCE

CALGARY, ALBERTA

JANUARY, 2017

Abstract

The intestinal epithelial barrier is a single layer of epithelial cells that functions to regulate absorption and secretion, in addition to protecting our bodies from the contents of the intestinal lumen. When the barrier becomes damaged, uncontrolled passage of bacterial and antigenic factors generates an immune response that can result in intestinal inflammation. One principal step in the resolution of inflammation is epithelial barrier healing, which stops the entry of inflammatory triggers. The mechanisms of intestinal epithelial wound healing are not completely understood, especially in the context of proteases and their receptors. The intestinal epithelial barrier is exposed to numerous proteases originating from luminal bacteria, host immune cells, and proteases expressed by the epithelial cells themselves. It was recently shown that activation of protease-activated receptor-2 (PAR2) on epithelial cells induced the expression of cyclooxygenase-2 (COX-2), which has protective functions in the gastrointestinal tract.

It was hypothesized that PAR2-induced COX-2 could enhance wound healing in intestinal epithelial cells.

In the first part of this study, PAR2-induced COX-2 was characterized using western blotting and ELISA techniques to perform time-course and dose-response experiments. Actinomycin D was used to determine that PAR2-induced COX-2 was transcriptionally regulated. Potential components of the PAR2-COX-2 signaling pathway, including Rac1 and CUX1, were studied using pharmacological inhibitors and siRNA. However, both Rac1 and CUX1 were not involved in the PAR2-COX-2 signaling pathway.

In the second part of this study, the Caco2 cell model was used for epithelial wound healing. Contrary to our hypothesis, PAR2 activation inhibited wound healing, independently of COX-2 activity. The inhibition of wound healing was due to reduced migration associated with a PAR2-mediated reduction in lamellipodia formation at the wound edge, and an increase in E-cadherin expression surrounding the wound. Conversely, when wound healing was investigated in T84 intestinal epithelial cells, PAR2 activation was found to enhance wound healing through increased cell migration, with opposite effects on actin dynamics and E-cadherin expression compared to the data obtained from Caco2 cells.

These findings represent a novel effect of PAR2 activation on the mechanisms of epithelial cell wound healing that could influence the resolution of intestinal inflammation.

Acknowledgements

First and foremost, I need to thank my supervisor, Dr. Wallace MacNaughton. Wally, the patience and support you've shown me since I started in your lab has completely transformed me (in a good way, don't worry). You've helped me survive so many highs and lows, I don't know how I would have made it through without you. I'll forever be grateful for your mentorship and your friendship. **high five**

The guidance from my committee members has been invaluable in shaping this project, as well as my personal development. Dr. Morley Hollenberg has taught me to ask the three most important questions to guide my research: what is your working hypothesis, what is your data telling you, and… oh shoot. I forgot the third one. Dr. Donna-Marie McCafferty provided much needed direction in times where I lost my focus (which was often). Dr. Paul Beck, although late to the ball game, was really the reason this project began and lent me his ear and support when I needed it most. Last, but certainly not least, Dr. Chris Waterhouse: I'm having trouble finding words that express just how much I value and appreciate your investment in both my academic and personal growth. To each of you, I can't thank you enough.

All of the previous and current members of the MacNaughton lab, as well as IRN, created the perfect environment to "do science". This project, and my incredibly positive experience as a graduate trainee, would not have been possible without Mike, Marilyn, Tie, Christina, Sonia, Cris, Vadim, Michael, Natalie, Judie, and Andrew. I'm certain there are others I haven't mentioned – please know I am thankful to everyone for their friendship.

The Snyder Live Cell Imaging Facility is one of the main reasons this project became what it is, not only because of the amazing tools offered, but also the unwavering support of Pina and Rima, and their passion to help everyone around them succeed.

Kathy Baer and Dr. Mark Ropeleski were my guides into research during my undergraduate degree, and without them I never would have caught the research bug, nor would I have realized I was even remotely capable of fitting in to an academic environment.

My family is the reason I chose to do a PhD, so I guess I should thank them too (thanks a lot, Steph /s). But seriously, my parents, brother, sister-in-law, and friends have kept me sane. I especially owe a huge thank-you to my husband, John. I'm the luckiest girl in the world with your unconditional love and support.

Finally, this work would not have been possible without support from Crohn's and Colitis Canada, and graduate scholarships from the Alberta Cancer Foundation, Alberta IBD Consortium, Queen Elizabeth II, and the Pepsi Bottling Group.

Table of Contents

List of Tables

List of Figures and Illustrations

List of Symbols, Abbreviations and Nomenclature

15-PGDH	15-prostaglandin dehydrogenase
2fLI	2-fluroyl-LIGRLO
2fO	2-fluroyl-OLRGIL
AA	arachidonic acid
AChE	acetylcholinesterase
ACHRI	Alberta Children's Hospital Research Institute
ADP	actin depolymerizing factor
AJ	adherens junction
ANOVA	analysis of variance
ARP	actin-related protein
ATCC	America Type Culture Collection
BSA	bovine serum albumin
cAMP	cyclic adenosine monophosphate
CD	cluster of differentiation
CD	Crohn's disease
CIM	cell invasion and migration
CO_2	carbon dioxide
COX	cyclooxygenase
CREB	cAMP response element binding protein
CRISPR	clustered regulatory interspaced short palindromic repeats
CUX1	Cut homeobox
DAMP	danger-associated molecular pattern
DAPI	4',6-diamino-2-phenylindole
DC	detergent compatible
DHA	docosahexaenoic acid
Dll4	delta-like ligand 4
DME/F12	Dulbecco's modified Eagles medium and Ham's F-12 nutrient mixture
DMSO	dimethyl sulfoxide
DP	D prostanoid receptor
dsLNA	double stranded locked nucleic acid
DSS	dextran sodium sulfate
EC_{50}	effective concentration
ECM	extracellular matrix
EDTA	ethylenediaminetetraacetic acid
EdU	5-ethynyl-2'-deoxyuridine
EGF	epidermal growth factor
EGFR	epidermal growth factor receptor
ELISA	enzyme-linked immunosorbent assay
EMT	epithelial mesenchymal transition
EP	E prostanoid receptor

EPA	eicosapentaenoic acid
ERK	extracellular signal-related kinase
FA	fatty acid
F-actin	actin filaments
FBS	fetal bovine serum
G-actin	globular actin
GALT	gut-associated lymphoid tissue
GEF	guanine exchange factor
GFP	green fluorescent protein
GI	gastrointestinal
GPCR	G-protein coupled receptor
GTP	guanosine triphosphate
IBD	inflammatory bowel disease
IFN	interferon
Ig	immunoglobulin
IL	interleukin
IU	international units
JAK	Janus kinase
Lgr5	leucine-rich repeat containing G-protein coupled receptor 5
LOX	lipoxygenase
LPS	lipopolysaccharide
LT	leukotriene
LX	lipoxin
MAPK	mitogen-activated protein kinase
MCP-1	monocyte chemoattractant protein-1
MHC	major histocompatibility complex
MLC	myosin light chain
MLN	mesenteric lymph nodes
MMC	mitomycin C
MMP	matrix metalloproteinase
MPO	myeloperoxidase
mRNA	messenger ribonucleic acid
MUC2	mucin 2
NADPH	nicotinamide adenine dinucleotide phosphate
NET	neutrophil extracellular trap
NK	natural killer
ns	not significant
NSAID	non-steroidal anti-inflammatory drug
NSB	non-specific binding
NW-C	non-wounded control
NW-PAR2	non-wounded PAR2 activated
PAMP	pathogen-associated molecular pattern
PAR	protease activated receptor
PBS	phosphate-buffered saline

PG	prostaglandin
PGEM	prostaglandin E metabolite
PGES	prostaglandin E synthase
PGHS	prostaglandin H synthase
PI3K	phosphatidylinositol-4,5-bisphosphate 3-kinase
PLA_2	phospholipase A_2
PRR	pattern recognition receptors
PUFA	polyunsaturated fatty acid
r.t.	room temperature
RELM	resistin-like molecule
ROCK	Rho-associated protein kinase
ROS	reactive oxygen species
RTCA	real-time cell analyzer
SDS	sodium dodecyl sulfate
siRNA	small interfering ribonucleic acid
STAT	signal transducer and activator of transcription
TA	total activity
TBST	tris buffered saline with tween
Tcf	T-cell factor
TGF	Transforming growth factor
TJ	tight junction
TNBS	2,4,6-trinitrobenzenesulfonic acid
TNF	tumour necrosis factor
TTF	trefoil factor peptides
TX	thromboxane
UC	ulcerative colitis
V	volt
Vh	volt hours
W-C	wounded control
W-PAR2	wounded PAR2 activated
ZO	zonula occludens
α	alpha
β	beta
γ	gamma
ω	omega

Epigraph

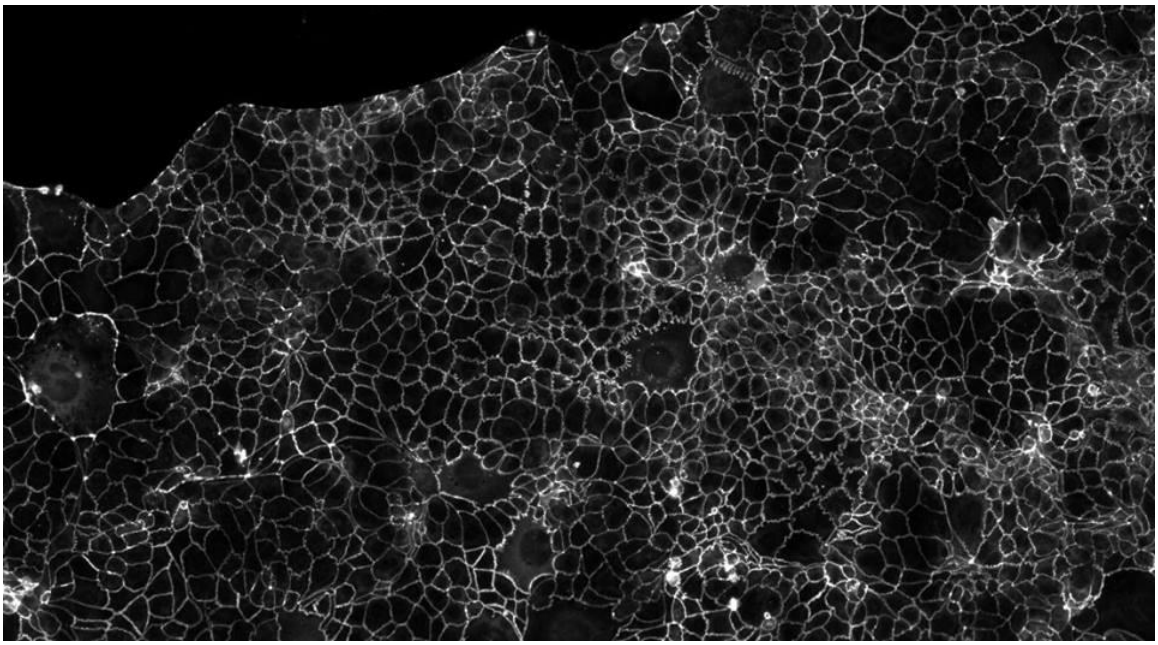

I am among those who think that science has great beauty. A scientist in his laboratory is not only a technician: he is also a child placed before natural phenomena which impress him like a fairy tale.

– Marie Curie

In Eve Curie Lahouisse, Eve Curie and Vincent Sheean, *Madame Curie* (1937), 341

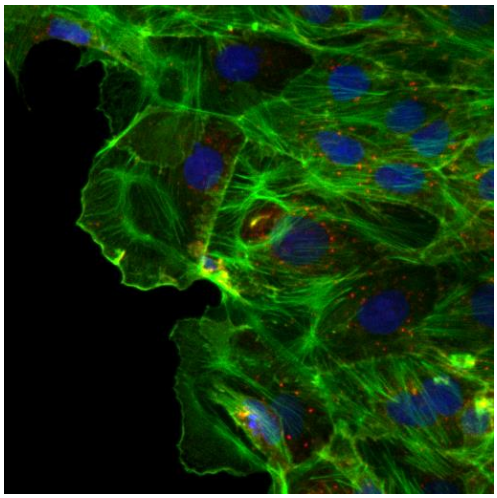

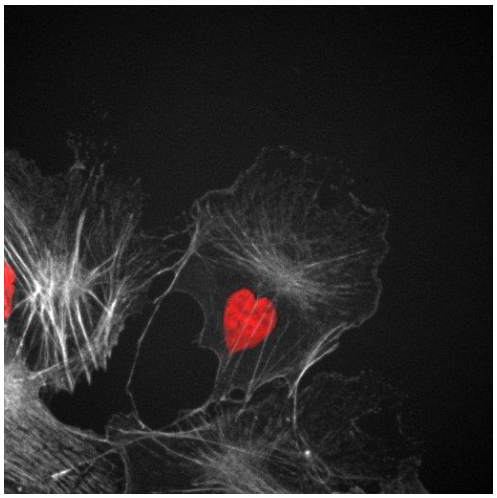

CHAPTER 1

Background

1.1 Relevance

The intestinal mucosal barrier of the gastrointestinal (GI) tract is often taken for granted, yet it is critically important for health considering it has a surface area of ~32 m^2 that exposes our bodies to the external environment (Helander and Fändriks 2014). An important component of the GI mucosal barrier is a single layer of epithelial cells, which can become damaged due to a variety of common factors including GI disease, bacterial infection, food allergies, alcohol consumption, or even over-the-counter non-steroidal anti-inflammatory drugs (NSAID). Although each of these factors initiates damage or ulceration of the intestinal epithelium through unique mechanisms, the underlying result is shared: intestinal inflammation. With the presence of an inflammatory stimulus, there will likely be further damage to the epithelial barrier that must be repaired in order to prevent uncontrolled passage of luminal contents into our bodies. The mechanisms of wound healing, which require a balance of cellular proliferation and epithelial sheet migration, are not completely understood. Additionally, the GI tract contains the highest level of endogenous and exogenous proteases within the body (Antalis et al. 2007), but very little is known regarding the role of proteases in modulating intestinal epithelial wound healing. Importantly, protease-dependent signaling has been shown to increase the expression of cyclooxygenase (COX)-2 (Hirota et al. 2012), an enzyme that produces protective lipid mediators in the GI tract, which could contribute to wound healing.

The purpose of this study was to investigate the mechanisms of intestinal epithelial wound healing, specifically in the context of proteases and their receptors, and how these mechanisms may relate to COX-2-derived lipid mediators.

1.2 The intestinal mucosal barrier

The intestinal mucosal barrier of the GI tract encounters many challenges including physical abrasion by luminal contents, exposure to numerous ingested antigens, and 10^{13}-10^{14} bacteria (Sekirov et al. 2010; Sender, Fuchs, and Milo 2016) that comprise the intestinal microbiota. A healthy mucosal barrier is able to withstand these stresses while facilitating the absorption of nutrients and secretion of regulatory factors. The mucosal barrier can be divided into extrinsic and intrinsic components.

1.2.1 The extrinsic mucosal barrier

Principal components of the extrinsic barrier include layers of mucus, antimicrobial peptides, as well as secreted antibodies. The main structural component of the secreted mucus is the glycoprotein mucin 2 (MUC2), which acts to lubricate as well as provide a physical barrier, separating intestinal epithelial cells from intestinal bacteria and other luminal components (Johansson, Sjövall, and Hansson 2013). Although there is only a single layer of loosely adherent mucus in the small intestine, colonic mucus forms two distinct layers: a tightly adherent inner layer next to the intestinal epithelium that is absent of bacteria, and a loosely adherent outer layer that supports much of the commensal

microbiota (Johansson et al. 2011). Embedded in both layers of mucus are antimicrobial peptides, including α-defensins, β-defensins, cathelicidins, and S100 proteins (reviewed in (Robinson et al. 2015), as well as secreted immunoglobulin (Ig)A antibodies (reviewed in (Pabst, Cerovic, and Hornef 2016). The protective properties of the extrinsic barrier also depend on water secretion mediated by the epithelial cells of the intrinsic barrier (Barrett and Keely 2000). In addition to hydration of the mucus layer, colonic epithelial secretion is required during health to limit bacterial colonization (Asfaha et al. 2001).

1.2.2 The intrinsic mucosal barrier

The intrinsic barrier is comprised of intestinal epithelial cells and the tight junctions (TJ) that hold the cells together. Four main types of epithelial cells differentiate from $Lgr5^{+}$ stem cells found at the base of the crypts (Barker et al. 2007), and each cell type carries out specific functions. *Enterocytes*, the most common, are columnar epithelial cells that facilitate absorption of nutrients, electrolytes and water, and secretion of electrolytes and water. *Goblet cells* secrete components of the extrinsic mucosal barrier including the main structural glycoprotein of the mucus layer, MUC2, as well as trefoil factor peptides (TTF), resistin-like molecule β (RELMβ), and Fc-γ binding protein (Kim and Ho 2010). *Enteroendocrine cells* are the hormone-producing cells of the GI tract (Gunawardene, Corfe, and Staton 2011), and *Paneth cells* of the small intestinal secrete antimicrobial factors into the lumen (Clevers and Bevins 2013). Except for Paneth cells that migrate toward the base of the crypt, enterocytes, enteroendocrine cells, and goblet cells

differentiate as they migrate up from the dale of the crypt. With a life span of only 3-5 days, epithelial cells undergo apoptosis and are shed into the lumen once they reach the tip of the villus in the small intestine, or the surface epithelium in the colon (Pinto and Clevers 2005; Marshman, Booth, and Potten 2002).

The TJ is the most apical point of cell-cell contact between epithelial cells, and is comprised of intercellular proteins (claudins, occludin, tricellulin, and junctional-adhesion molecules), and scaffolding proteins (zonula occludens (ZO) 1-3) which anchor the TJ to an actomycin ring of the cell cytoskeleton. In addition to serving a fence-like function for the epithelial cell itself, by restricting the localization of proteins to either the apical or basolateral side of the cell, paracellular permeability is determined by the protein composition of the TJ and the contractile state of the actomycin ring (Groschwitz and Hogan 2009; Turner 2009).

1.2.3 Additional factors relating to the intestinal mucosal barrier

There are many additional factors contributing to barrier function that can play roles in the maintenance, damage, or healing of the epithelial barrier. Of particular interest in the context of wound healing are other cell-cell junctions, and the GI-specific immune system.

Although the TJ is the principal epithelial junction associated with barrier function, two additional epithelial junctions are required for intestinal health and homeostasis, specifically the adherens junction (AJ), and the desmosome. The AJ contains the

intercellular membrane-spanning protein E-cadherin, which interacts with members of the catenin family (α, β, p120) that act as scaffolding proteins to anchor the AJ to the cell cytoskeleton (Harris and Tepass 2010). The main purpose of the AJ, as the name suggests, is to adhere cells together. However, many other functions and signaling pathways are associated with AJ components and will be discussed in subsequent sections. The desmosome shares a structural similarity to the AJ, with desmosomal cadherins (desmoglein and desmocollin) interacting within the intercelluar space, and desmoplakin anchoring the junction to intermediate filaments of the cell cytoskeleton (Kowalczyk and Green 2013). The desmosome mechanically couples cells, which functions to help tissues resist mechanical stress.

In addition to the epithelial and mucus barriers, resident innate immune cells contribute to host defense in the GI tract. The GI tract contains specialized lymphoid organs collectively called the gut-associated lymphoid tissue (GALT) that functions to survey the luminal contents and homeostatic state of the GI tract. Consisting of mesenteric lymph nodes (MLN), Peyer's patches, isolated lymphoid follicles, cryptopatches, as well as scattered lymphocytes and dendritic cells in the lamina propria and epithelium, the GALT makes up the largest collection of lymphoid tissues in the body. As such, the majority of lymphocytes and macrophages in the human body are concentrated in the intestinal wall (Schenk and Mueller 2008).

1.3 Initiation and resolution of intestinal inflammation

There are many challenges that the intestinal mucosal barrier must protect against, including bacterial infection (Papaconstantinou and Thomas 2007), excessive alcohol consumption (Patel et al. 2015), as well as chronic NSAID use (Graham et al. 2005). When these external factors overcome the extrinsic mucosal barrier, they can gain access to and damage the intrinsic mucosal barrier, resulting in ulceration of the intestinal epithelium. In a subset of the population, epithelial damage can also result from food allergies (Weinberger et al. 2016) and GI-related diseases (Xavier and Podolsky 2007). Importantly, once the epithelial barrier has become damaged, there is unregulated passage of luminal contents into our bodies, which evokes an inflammatory immune response that can further damage the epithelium (Pastorelli et al. 2013).

1.3.1 Initiation of intestinal inflammation

In healthy individuals, the GALT is tailored to promote tolerance when sensing luminal components, which is important given the surface area and number of antigens in the GI tract. However, a strong immune response is triggered if antigens or endogenous danger signals are present in the lamina propria. In general, intestinal inflammation is initiated when innate immune cells within the lamina propria are triggered through the activation of pattern recognition receptors (PRR) by pathogen-associated molecular patterns (PAMP) or danger-associated molecular patterns (DAMP). When a PRR is bound by its cognate ligand, a signaling cascade leads to the activation of inflammatory genes,

that ultimately function to either eradicate invading microbes (eg. through the increased production of antimicrobial peptides), or attract additional immune cells to the area (reviewed in Takeuchi and Akira 2010; Chen and Nunez 2010)

Inflammatory cells are recruited to the area by activation of the endothelium and with a chemotactic gradient. With an activated endothelium, vascular leukocytes are able roll, adhere, and transmigrate through the endothelium to the tissue, and the chemotactic gradient will draw the leukocytes to the area they are needed (Ley et al. 2007). The first cell type to arrive is the neutrophil driven by an interleukin (IL)-8 chemotactic gradient (Yang et al. 1997). Neutrophils have a strong killing capacity through phagocytosis, oxidative bursts, and neutrophil extracellular trap (NET) formation, however these killing mechanisms also cause considerable collateral damage to surrounding tissue. The next main cell type recruited, by monocyte chemoattractant protein (MCP)-1, are monocytes/macrophages which function to engulf bacteria, apoptotic neutrophils, and to help clear any necrotic or damaged tissue (Reinecker et al. 1995). The neutrophils and macrophages are recruited as long as there is a stimulus resulting in a proinflammatory milieu.

1.3.2 Resolution of intestinal inflammation

In order for inflammation to resolve, the trigger must be eliminated, the normal resident cells in the tissue need to return to their original phenotype, and the infiltrating

inflammatory cells must be cleared from the tissue. Resolution is not a passive process, but rather is an active, defined phase of the inflammatory response (Serhan et al. 2007).

Eliminating the cause of inflammation: If neutrophils and macrophages are unable to clear the inflammatory stimulus (such as invading bacteria) on their own, adaptive T and B cells are recruited to the area. Helper T cells (T_h $CD4^+$) and cytotoxic T cells (T_c $CD8^+$) recognize proteins displayed on major histocompatibility complex (MHC)II or MHCI respectively. With T_h cells, the inflammatory milieu can shape their phenotype inducing T_h1, T_h2, T_h17 or T-regulatory (T_{reg}) cells, each with specific effector functions and unique cytokine profiles, whereas cytotoxic T cells function to kill infected cells (Zygmunt and Veldhoen 2011). B cells produce antibodies that will either neutralize the harmful agent or mark the cell to be targeted by other immune cells (Spencer and Sollid 2016).

Tissue restoration: One of the main events that must occur in order to achieve resolution is closure of the damaged epithelial barrier. This is accomplished by the migration, proliferation and differentiation of epithelial cells, driven by pro-resolution factors produced by the subepithelial myofibroblasts and other cell types (Serhan et al. 2007). Mechanisms of this process are described in detail in section 1.4. Once the barrier has been restored and no further noxious stimuli can enter, the underlying tissue can eliminate the remaining foreign/danger components and clear any damaged cells and tissue.

Clearing inflammatory infiltrate: Clearing recruited immune cells is the final necessary step for the resolution of inflammation, where tissue is returned to the normal

phenotype and architecture, and only the original cell types are present. Macrophages are the main cell type responsible at this stage, since they are able to phagocytose apoptotic immune cells before being cleared themselves through the lymphatics (Serhan and Savill 2005).

Importantly, all three of these processes are occurring simultaneously. The body will continuously be attempting to repair the breached area while recruiting cells to eliminate any dangerous components, and to clear cells that have served their purpose. However, it is important to emphasize that healing of the epithelial barrier is necessary to prevent the continual passage of luminal contents into our bodies. If a compromised epithelial barrier cannot be healed, chronic intestinal inflammation will develop due to the constant inflammatory stimuli freely crossing the damaged mucosal barrier. Unfortunately, this is the case for GI diseases such as inflammatory bowel disease (IBD).

1.3.3 Inflammatory Bowel Disease

Two main forms of IBD, Crohn's disease (CD) and ulcerative colitis (UC), are relapsing/remitting inflammatory conditions affecting over 1 in 150 Canadians, and costing $2.8 billion per year in direct and indirect costs (CCC 2012). IBD has no known cause, although it is suggested the disease is due to a loss of immunological tolerance to the colonic commensal microbiota in genetically susceptible individuals (Kaser, Zeissig, and Blumberg 2010). IBD is difficult to manage medically, has no cure, and incidence rates are increasing each year (Molodecky et al. 2012). Patients are most commonly diagnosed in

late adolescence or early adulthood and must, therefore, deal with their disease for their entire lives. Understanding IBD is a necessary step to help minimize the time these patients spend suffering.

IBD involves chronic relapsing bouts of intestinal inflammation with symptoms including weight loss, abdominal pain and diarrhea. CD and UC differ in the key inflammatory cytokines involved, and their distribution of inflammation. CD is classified as a T_h1/T_h17-mediated disease, due to the high levels of the classic T_h1/T_h17 cytokines: IL-12(p40), interferon (IFN)-γ, tumour necrosis factor (TNF)-α and IL-6. The resulting inflammation can become transmural, and may occur in a patchy distribution in any region of the GI tract (Brand 2009). In contrast, UC is considered to take on a T_h2-like phenotype due to the high expression of IL-13 that appears to drive strictly mucosal inflammation by disrupting the epithelial cells (Heller et al. 2005). UC inflammation generally begins in the distal colon and advances toward the proximal colon.

Although the etiology of IBD is unknown, it is believed to develop as an inappropriate immune response to resident microbes in genetically susceptible individuals. Genetic studies in IBD emphasize the complexity of the disease, with recent reports highlighting 231 independent single nucleotide polymorphisms within 200 loci associated with increased IBD risk (Jostins et al. 2012; Liu et al. 2015). Many IBD-associated loci are involved with regulating cytokine production, in particular IFN-γ, IL-12, TNF-α, and IL-10 signaling, along with lymphocyte activation and JAK/STAT signaling pathways. Additionally, many IBD-associated genes display cell-type expression specificity with dendritic cells

having the strongest enrichment, along with $CD4^+$ T cells, natural killer (NK) cells, NKT cells, and bone marrow-derived macrophages. Even though many genetic associations have been identified, the genetic components only explain a fraction of IBD cases: 13.1% in CD and 8.2% in UC (Jostins et al. 2012; Liu et al. 2015), which again emphasizes the complexity of the disease while implicating major roles for microbial and environmental factors in disease pathogenesis.

The clinical outcome of IBD could be remission, with or without the help of medication, or the disease could result in a variety of complications. The long-term pathology of CD is well characterized, with increased adipose tissue and fat wrapping near the inflamed areas, muscularization, neuronal and vascular changes, as well as fibrosis (Shelley-Fraser et al. 2012). Although both CD and UC can eventually resolve after a number of years for unknown reasons, the long-term sequelae of CD can be very dangerous, resulting in altered GI function and obstruction of the lumen due to fibrosis. The curative treatment for UC is partial or complete colectomy, however long-term issues involved with colectomy include possible osteomy complications or pouchitis.

Importantly, the primary goal of IBD treatment is now mucosal healing, and not merely symptom relief, since mucosal healing is a strong predictor of sustained clinical remission and reduced rates of hospitalization and surgery (Pineton de Chambrun, Blanc, and Peyrin-Biroulet 2016).

1.4 Damage and restitution of the intestinal epithelial barrier

The epithelial barrier is an important component of the host defence provided by the intestinal mucosal barrier. Once the epithelial barrier is damaged, there is no longer a regulated exchange of factors between the intestinal lumen and our bodies, and the intestinal microbiota gains access to the lamina propria where it no longer serves a commensal role but instead evokes an immune response. It is important to understand how the barrier becomes damaged, and how the epithelial cells heal the wounded area and restore barrier function.

1.4.1 Common factors that damage the intestinal epithelial barrier

The epithelial barrier can be damaged by both external and host-derived factors. External factors include chemical substances including alcohol (Beck and Dinda 1981; Kelly et al. 1995) and NSAIDs (Allison et al. 1992; Graham et al. 2005), as well as bacterial factors such as *C. difficile* toxins (Riegler et al. 1995; Fordtran 2006). Most often, the damage to the epithelium caused by host-derived factors is due to the harsh local tissue environment created by an immune response, specifically associated with neutrophils and the production proteolytic enzymes, reactive oxygen species (ROS), and NET formation. The structure of NETs is formed by extruded DNA and histones, and there are many antimicrobial enzymes (elastase, cathepsin G, myeloperoxidase (MPO) and nicotinamide adenine dinucleotide phosphate **(**NADPH) oxidase) embedded within the NET that cause

considerable collateral damage to the epithelial barrier (Grisham and Granger 1988; Gao et al. 2015; Kaplan and Radic 2012).

1.4.2 Mechanisms of intestinal epithelial barrier restitution

Epithelial cells at the edge of a damaged area do not experience contact inhibition and will lose their columnar polarity to flatten and cover more surface area while migrating into the denuded area (Ito et al. 1984; Lacy 1988). This migration, or restitution, is in a large part mediated by the Rho family guanosine triphosphate (GTP)ases that organize and remodel the actin cytoskeleton through the formation of stress fibers, lamellipodia, and filopodia. There is also a requirement for epithelial cells to modulate the cell-cell junctions in order to allow for migration. Additionally, epithelial cells will proliferate to increase the number of cells available to cover the wound, and then differentiate into mature columnar epithelial cells restoring the original phenotype of the epithelium.

Single cell migration vs epithelial sheet migration: An important distinction to make when studying cell migration is the presence or absence of cell-cell junctions that could influence cell movement. Single cell migration is more simple, with one cell that needs to respond to an extracellular signal, whereas sheet migration requires intercellular integration of signals in order to achieve any movement. An important paradigm in collective cell movement is the formation of leader cells and follower cells. Leader cells are formed through multiple signaling pathways including MAPK/ERK, PI3K/Akt, Notch, and Rho GTPase signaling (Chapnick and Liu 2014; Yamaguchi et al. 2015; Riahi et al. 2015;

Zegers and Friedl 2014). Importantly, Delta-Notch interaction is necessary for negative feedback signaling that will lead to the establishment of a single leader cell in contact with multiple follower cells (Riahi et al. 2015). These signaling pathways also help to develop the front-rear polarity characteristics of leader cells. Using the localization of Rho-GTPases as an example, Rac1 activation in the anterior of the cell is associated with lamellipodia and filipodia protrusions, and RhoA/Rho-associated kinase (ROCK) activity in the posterior of the cell inhibits actomyosin contractility (Zegers and Friedl 2014). In addition to leader and follower cell behaviour signaling, sheet migration also involves chemical guidance (chemotaxis), and electrical guidance (electrotaxis). Chemotaxis in collective cell movement can involve a self-generated chemokine gradient (Dona et al. 2013), or a chemical gradient created by altered pH or ROS production (Majumdar, Sixt, and Parent 2014). In the case of electrotaxis, when epithelial sheets are disrupted, an endogenous weak electrical gradient is induced that enhances migration into the open space (Zhao et al. 2006).

Actin regulation: During cell migration, there is a dynamic regulation of monomeric globular actin (G-actin) and actin filaments (F-actin), which are polymers of G-actin. This regulation includes components of actin nucleation, actin treadmilling, and actin severing. Nucleation is the first step in filament formation, where actin monomers are first stabilized into a polymer by actin-nucleating proteins, including the actin-related protein (ARP) 2/3 complex, formins, or tandem-monomer-binding nucleators (Firat-Karalar and Welch 2011). Treadmilling involves the growth of the actin filament from one end, and the

recycling of G-actin from the opposite end, which is dependent on the concentration of available monomers (Schaus, Taylor, and Borisy 2007). Severing helps to reorganize actin filaments, and is regulated by actin depolymerizing factors (ADF) and cofilin (McGrath et al. 2000). Actin regulation during epithelial wound healing depends on the size of the wound. Small epithelial wounds (with fewer than 10 cells at circumference of the wound) do not require protrusions from wound edge cells, but instead heal through purse-string wound closure. This purse string closure is simply a contraction of a cable of actin at the wound edge that is transmitted through adherens junctions (Russo et al. 2005). Conversely, larger wounds require filipodia and lamellipodia formation in leader cells at the wound edge. Importantly, leader cells can only form protrusions when the actin cable at the wound edge is no longer present (Reffay et al. 2014). The formation of lamellipodia and filipodia is mainly controlled by Rho-GTPases, including RhoA, Rac1, and Cdc42 that regulate actin contractility through myosin light chain (MLC), actin polymerization through the Arp2/3 complex, and actin turnover through cofilin (Sadok and Marshall 2014; Ladwein and Rottner 2008).

Cell-cell junction regulation during epithelial sheet migration: Importantly, leader cells do not resemble epithelial cells, but instead take on fibroblast-like appearance and behaviour (Poujade et al. 2007), which is the observation behind wound healing-associated epithelial-mesenchymal transition (EMT). One of the first changes associated with EMT is a decrease in E-cadherin. This decrease can be mediated transcriptionally, with the EMT-associated transcription factors SNAIL and TWIST repressing E-cadherin expression,

or it can be mediated through increased internalization using both clathrin and non-clathrin-associated mechanisms (de Beco, Amblard, and Coscoy 2012). However, although E-cadherin is entirely lost during complete EMT, it is important to note that E-cadherin expression and interactions are still required during epithelial sheet migration (Hwang et al. 2012; Li et al. 2012). Interestingly, during one study of epithelial sheet migration stimulated by the chemokine CXCL12, increased E-cadherin membrane localization is required (Hwang et al. 2012). Conversely, it has also been shown that endocytosis of E-cadherin is necessary for proper actomyosin regulation during wound closure (Hunter et al. 2015), highlighting the complex nature of E-cadherin and cell-cell junction regulation during sheet migration.

Principal mediators of intestinal epithelial restitution: There are numerous factors that mediate intestinal epithelial wound healing through either increased migration or proliferation. These mediators include growth factors, cytokines, and peptides, such as transforming growth factor (TGF)-α, TGF-β, epidermal growth factor (EGF), fibroblast growth factor (FGF), insulin-like growth factor (IGF)-I and IGF-II, IL-1β, IL-2, IL-6 as well as trefoil factors (TFF) (Iizuka and Konno 2011; Kuhn et al. 2014). Of these, TGF-β is considered a central factor of wound healing (Dignass and Podolsky 1993), and the mechanisms of other regulatory signaling molecules can therefore be described as either TGF-β-dependent (TGF-α, EGF, FGF, IL-1β, IL-2) or TGF-β-independent (TFF) (Iizuka and Konno 2011; Dignass et al. 1994). Within the intestine, TGF-β has been shown to enhance colonic crypt regeneration (Miyoshi et al. 2012), and mediate wound healing through direct effects

on the epithelium (Beck et al. 2003). Importantly, and of relevance to the present work, it was recently demonstrated in pancreatic cells that TGF-β-induced migration requires the presence of protease-activated receptor (PAR) 2 (Zeeh et al. 2016).

1.5 Intestinal proteases and protease-activated receptors

Proteases, also called proteinases or peptidases, can be divided into five main categories: cysteine, aspartic, serine, threonine and metalloproteinases, which are based on the amino acid (or metal ion) in the active site of the enzyme, necessary for the catalytic reaction. Several proteases, particularly in the serine, cysteine and metalloproteinase families, can exert biological activity through activation of PARs. PARs are G protein-coupled receptors (GPCR) that are activated when the extracellular N-terminus is cleaved at specific consensus amino acid sequences, revealing a new N-terminal sequence that acts as a "tethered ligand" to bind to and activate the receptor.

1.5.1 Endogenous and exogenous intestinal proteases

The intestine is constantly exposed to numerous proteases, and although intestinal proteases were historically associated solely with digestive functions, they have since been shown to play numerous roles in homeostasis as well as disease development (Antalis et al. 2007). Endogenous proteases found in the GI tract include luminal (trypsin, chymotrypsin, elastase), brush border, epithelial (zonulin, matriptase, prostasin, matrix metalloproteinases (MMP)), immune cell (tryptase, MMPs, granzymes, elastase),

circulating (plasminogen, coagulation factors), and bacterial proteases generated by the commensal microbiome. These endogenous proteases are in addition to exogenous proteases produced by enteric pathogens (Sears 2001). Considering the numerous proteases in the intestinal environment, they are an important component to study in the context of intestinal epithelial wound healing and resolution of inflammation.

1.5.2 Protease-activated receptors

There are four members in the PAR family of receptors, which belong to the GPCR superfamily. GPCRs are plasma membrane proteins with seven membrane-spanning domains, functioning to transduce extracellular signals to intracellular signaling cascades, through G-protein dependent or independent pathways. The receptor activation of PARs is unique compared to other GPCRs since the receptor does not bind soluble ligands *in vivo*. Instead, a protease cleaves the N-terminus of the protein, revealing a new N-terminal sequence that acts as a tethered ligand to bind intra-molecularly and activate the receptor. This proteolytic mechanism of receptor activation was first described with the identification of the receptor for the serine protease α-thrombin, later named PAR1 (Rasmussen et al. 1991; Vu et al. 1991). Three years later, PAR2 was described as the second example of a proteolytically activated GPCR (Nystedt et al. 1994), with PAR3 and PAR4 described shortly after (Ishihara et al. 1997; Kahn et al. 1998; Xu et al. 1998).

Protease-activated receptor 2: Thrombin canonically cleaves PAR1, PAR3, and PAR4. However, thrombin was also recently shown to cleave PAR2 (Mihara et al. 2016).

Canonical PAR2 signaling occurs when proteases cleave the N-terminal R^{34}-S^{35} bond, freeing the new N-terminal sequence SLIGKV in human (SLIGRL in rat) that can bind the receptor (Nystedt et al. 1994). This type of signaling is most common with cleavage by trypsin-like serine proteases, including trypsin (Nystedt et al. 1994), mast cell tryptase (Molino et al. 1997), and coagulation factors VIIa and Xa (Camerer, Huang, and Coughlin 2000; Riewald and Ruf 2001). Downstream, pathways associated with canonical PAR2 activation include calcium signaling through $G\alpha_{q/11}$, inhibition of cyclic adenosine monophosphate (cAMP) through $G\alpha_{i}$, activation of Rho-GTPases through $G\alpha_{12/13}$, and MAPK/ERK signaling mediated by β-arrestin recruitment and receptor internalization (Soh et al. 2010; McCoy, Traynelis, and Hepler 2010; DeFea et al. 2000). However, certain proteases can cleave different N-terminal sites, resulting in either distinct signaling (biased agonism), or disarming the receptor by removing the tethered ligand sequence. Examples of antagonism through receptor disarming include cleavage by neutrophil elastase, cathepsin-G, and proteinase-3 (Ramachandran et al. 2011). Interestingly, neutrophil elastase has also been shown to act as a biased agonist by inducing ERK activation independently from β-arrestin recruitment and receptor endocytosis (Ramachandran et al. 2011). These data emphasize the importance of considering mechanisms of receptor activation when studying PAR-dependent signaling.

1.5.3 Proteases, protease-activated receptors, and inflammatory bowel disease

There is some evidence that implicates PAR2 in IBD since mast cell involvement during active inflammation was shown to significantly increase the levels of mast cell tryptase in CD and UC (Raithel et al. 2001). However, it was only in UC that the increase was also seen in non-inflamed areas, suggesting tryptase plays an important role in UC pathogenesis. Additionally, in canine IBD, the expression of PAR2 was increased in intestinal epithelial cells (Maeda et al. 2014). Interestingly, when PAR2 agonists were administered intrarectally to mice, the mice developed acute colonic inflammation and tissue damage (Cenac et al. 2002). These results suggested that the increased levels of luminal proteases in IBD patients might be involved in sustaining inflammation as part of the IBD pathogenesis. Importantly, using three different models of colitis, PAR2 was found to be pro-inflammatory since PAR2-deficient mice displayed significantly reduced MPO activity, lower macroscopic damage scores, decreased bowel thickness, and less leukocyte rolling and adhesion that Wt mice (Hyun et al. 2008). Similarly, mice treated with antagonists of PAR2 are also protected during experimental colitis (Lohman et al. 2012).

1.5.4 Proteases, protease-activated receptors, and epithelial wound healing

The main proteases studied in relation to wound healing are MMPs, due to their regulation of extracellular matrix (ECM) components (McCarty et al. 2012). However, in the context of intestinal epithelial wound healing, the roles of both PAR1 and PAR2 have been investigated using the endogenous activating proteases as well as activating peptides

that mimic the receptor tethered ligand (Swaminathan 2004). In this study, PAR1 and PAR2 activation with thrombin and trypsin respectively, or with receptor-specific activating-peptides, were able to enhance wound healing through epidermal growth factor receptor (EGFR), PI3K, and Rho kinase signaling. There is additional evidence in the literature of PAR2-mediated increased migration and proliferation in many tissues, including colon (Darmoul et al. 2004; Zhou et al. 2011; Wu et al. 2014), pancreas (Shimamoto et al. 2004; Shi et al. 2013), prostate (Mize, Wang, and Takayama 2008), and breast (Ge et al. 2004; Morris et al. 2006), which could also contribute to PAR2-mediated enhanced wound healing.

1.6 Lipid mediators of intestinal inflammation and wound healing

An interesting body of literature connects diet and inflammation, with a special emphasis on polyunsaturated fatty acid (PUFA) intake. Importantly, PUFAs can be converted into lipid mediators called eicosanoids, which are involved with numerous physiological and pathophysiological processes. PUFAs include both omega-3 (ω-3) and ω-6 fatty acids (FA) that are essential to health.

The production of eicosanoids is a complex and tightly regulated process. In general, ω-3s such as EPA and DHA are converted to resolvins, protectins, maresins, and 3-series prostaglandins that are anti-inflammatory and pro-resolution, whereas ω-6 FAs give rise to both inflammatory and anti-inflammatory mediators (Stables and Gilroy 2011). Arachidonic acid (AA), an ω-6 FA, is released from cell membrane phospholipids by

phospholipase A_2 (PLA_2). Once free, AA can be converted into prostaglandin (PG)H_2 through a cyclooxygenase reaction and a peroxide reaction by prostaglandin H synthase (PGHS)-1 or -2 (Smith, Urade, and Jakobsson 2011). The more common names for the PGHS enzymes are derived from the first reaction: cyclooxygenase (COX)-1 and -2. PGH_2 can then be acted on by a variety of PG synthases to form many eicosanoids, including the classical prostanoids PGD_2, PGE_2, $PGF_{2\alpha}$, and prostacyclin (PGI_2) as well as thromboxane A_2 (TXA_2) (Smith, Urade, and Jakobsson 2011). AA can also be acted on by lipoxygenases (LOX) to form leukotrienes (LTs), which are pro-inflammatory mediators, and lipoxins (LXs), which are the first anti-inflammatory and pro-resolution mediators produced during inflammation (Stables and Gilroy 2011). Of particular interest for this project are COX-2, PGE_2 and PGD_2.

1.6.1 COX-2

In contrast to constitutively expressed COX-1, COX-2 expression is readily up regulated in response to inflammation and tissue damage. Some consider COX-2 a pro-inflammatory enzyme since it is expressed very early during inflammation. When studying COX-2 in pleurisy, an initial peak of COX-2 was identified at 2 h, but a second peak (350% greater than the first) appeared at 48 hr, during the resolution phase (Gilroy et al. 1999), suggesting dual function of the enzyme with an emphasis on resolution. However, there have been reports of COX-2-dependent negative effects following resolution of intestinal

inflammation, including modulation of secretory and barrier dysfunction that remained up to 6 wk after TNBS colitis (Zamuner et al. 2003).

COX-2 and IBD: It has been known since the 1970s that PGs play a role in IBD, where it was shown in both CD and UC that inhibition of PGs was able to ameliorate disease (Gould, Brash, and Conolly 1977; Shafran, Maurer, and Thomas 1977). However, the precise role of PGs remains controversial. COX enzymes, which form PGs from FA precursors, were later implicated as factors in IBD when COX-2 messenger RNA (mRNA) (Hendel and Nielsen 1997) and protein (Singer et al. 1998) were shown to be increased in areas of active chronic IBD. Although inhibiting COX enzymes can reduce inflammation and pain at sites of tissue injury, there are considerable GI side effects due to endogenous PG control of physiological function within the GI tract. Importantly, inhibiting COX-2 in animal models of colitis can exacerbate disease (Reuter et al. 1996), and small-intestinal injury is common in humans who take COX inhibitors (Graham et al. 2005). With respect to wound healing, mice deficient for COX-2 are unable to heal biopsy-induced intestinal wounds (Manieri et al. 2012). In summary, COX-2 can be regarded as an anti-inflammatory mediator in experimental colitis with an important role in mucosal protection, resolution of inflammation, and wound healing (Ajuebor, Singh, and Wallace 2000; Wallace and Devchand 2005). Additional studies focusing on the role of COX-2 during inflammation and resolution will help to further elucidate its complex role.

COX-2 and PAR2: PAR2-induced up regulation of COX-2 was first demonstrated in endothelial cells (Houliston et al. 2002). The mechanism was later investigated in airway

epithelial cells, and found to involve EGFR transactivation independent of MMP activity (Kawao et al. 2005). Further mechanistic details of PAR2 signaling in airway epithelium found a dependence on ERK1/2 signaling to allow accumulation of β-catenin, which interacted with the transcription factors T-cell factor (Tcf)4 and cAMP response element binding (CREB) protein to up regulate COX-2 (Wang et al. 2008). Recently, our lab demonstrated PAR2-induced COX-2 expression in intestinal epithelium, although the initial signaling pathways identified are different than in airway epithelium. EGFR transactivation was still necessary, but it was dependent on MMP activity and independent of ERK1/2 signaling (Hirota et al. 2012). PAR2-induced expression of COX-2 plays a functional role in intestinal epithelial chloride secretion (van der Merwe, Hollenberg, and MacNaughton 2008) that also requires PAR2-induced increases of $cPLA_2$ and PGE_2 (van der Merwe et al. 2009). However, the effects of PAR2-induced COX-2 expression on wound healing are unknown.

1.6.2 PGE_2

PGE_2 plays important roles throughout the body, including nociception, regulation of blood pressure, regulation of mucosal integrity, and smooth muscle function. Every cell in the body is able to produce PGE_2, with epithelial cells, fibroblasts, and inflammatory cells being the major sources during an immune response. The amount of PGE_2 present depends on 1) the availability of the precursor PGH_2, 2) the levels of PGE-synthases (PGES) and 3) the levels of 15-PG dehydrogenase (15-PGDH) which degrades PGE_2. The effect of

PGE_2 is dictated by which of the four E prostanoid receptors it binds, termed EP1 through 4. As a major lipid mediator during inflammation, PGE_2 might be a key mediator of IBD, however the effects of PGE_2 vary greatly depending on its target receptor and cell type. For example, PGE_2 supports the proinflammatory Th17 phenotype by acting through EP2/EP4 receptors, thereby exacerbating inflammation (Sheibanie et al. 2007). However, also acting through EP4 it can lessen symptoms of DSS-induced colitis by protecting epithelial cells (Jiang et al. 2007). When studying wound healing specifically, PGE_2 has been shown to enhance wound closure in both airway epithelial cells (Savla et al. 2001) and intestinal epithelial cells (Miyoshi et al. 2016), which may be due to increased migration (Li et al. 2015). Interestingly, this same study that showed PGE_2-mediated enhanced migration in airway epithelial cells, also showed an inhibition of migration when these cells underwent EMT and developed a fibroblast phenotype (Li et al. 2015). These data could have important implications in the specific mechanisms of PGE_2-mediated wound healing when considering wound healing-associated EMT.

1.6.3 PGD_2

Similar to PGE_2, PGD_2 has a wide variety of effects including regulation of body temperature and the sleep-wake cycle in mammals, hormone release, olfactory function, and pain response. It is important to note that the effects of PGD_2 can be complicated to decipher due to 15d-PGJ_2, the dehydration product of PGD_2 which can also signal through the DP receptors (Scher and Pillinger 2005). Nonetheless, during inflammation PGD_2 can

serve as an inflammatory or anti-inflammatory mediator depending on the inflammatory milieu present and the tissue-specific receptor expression of DP1 and DP2. The DP1 receptor is known to have anti-inflammatory effects whereas the DP2 receptor mediates allergic responses by PGD_2. In the context of intestinal inflammation, PGD_2 acts as an early anti-inflammatory signal attenuating granulocyte infiltration (Ajuebor, Singh, and Wallace 2000) and has been found expressed at high levels in UC patients who have reached long-term remission (Vong et al. 2010). Interestingly, in dermal wounds made *in vivo*, there is a shift from PGE_2 to PGD_2 production during wound healing (Kapoor et al. 2007), similar to the shift seen during general resolution of inflammation. Although a review of the literature reveals that PGD_2 has apparently not been studied specifically in the context of epithelial wound healing, it has been shown to inhibit fibroblast migration (Kohyama et al. 2002), similar to PGE_2.

Hypothesis: PAR2 activation in intestinal epithelial cells will drive a pro-wound healing response through the effects of COX-2-derived lipid mediators.

Objectives:

1) To further characterize PAR2-induced COX-2 expression using the Caco2 intestinal epithelial cell line
2) To determine the role of PAR2-induced COX-2 in wound healing using different models of wounding in several intestinal epithelial cell lines
3) To explore additional mechanisms of PAR2-dependent effects on wound healing

CHAPTER 2

Materials and Methods

2.1 General Materials and Reagents

Ultrapure water was supplied by a Barnstead NANOpure Water Purification System (Thermo Scientific, Waltham, MA) at a purity of 18.2 MΩ.cm. Non-sterile phosphate-buffered saline (PBS) was made in ultrapure water from tablets (p4417, Sigma, St. Louis, MO). The following were purchased from Fisher Scientific (Hampton, NH): sodium chloride (S271), Tris-HCl (BP153), sodium dodecyl sulfate (SDS, BP166), as well as 12 mm (12-545-80), and 18 mm (12-545-100) #1 glass cover slips. Sterile dimethyl sulfoxide (DMSO, D2438), Triton-X (X100), sodium orthovanadate (S6508), protease inhibitor cocktail (p2714), and ponceau S (P3504) were purchased from Sigma. Sodium fluoride (ASC 798), β-mercaptoethanol (44143), and acetic acid (B27013) were from BDH Inc (Darmstadt, Germany), and ETDA was from EMD Millipore (4010-OP, Darmstadt, Germany). Bovine serum albumin (BSA) was purchased from VWR (0332, West Chester, PA).

2.2 Cell culture

2.2.1 General Culture Conditions. All cells were cultured in an incubator at 37°C in 5% carbon dioxide (CO_2), fed every 2 days with pre-warmed media, and subcultured every 4-5 days. Polystyrene flasks and plates were purchased from Greiner (658175 – T75, 657160 – 6 well, 665180 – 12 well, 662160 – 24 well, 655180 – 96 well, Monroe, NC).

2.2.2 Subculturing. Cells maintained in T75 flasks were passaged once they reached 80-90% confluence by rinsing the flask with sterile PBS (without Ca^{2+} or Mg^{2+}) (HyClone GE

SH30028.02, Chicago, IL) before adding 1.5 mL trypsin-EDTA (Sigma T4174). Flasks were returned to the incubator until all the cells were lifted (~3 min for Caco2, ~10 min for T84), at which time complete media with 10% fetal bovine serum (FBS) was added to inactivate the trypsin. Cells were transferred to a 15 mL conical centrifuge tube and spun down at 243 x *g* for 3 min. Media containing trypsin was aspirated, and the cell pellet was resuspended in fresh complete media. A small aliquot of the cell suspension was diluted in PBS, and cells were manually counted using a hemocytometer prior to plating an experiment.

2.2.3 Freezing and raising cells. Freezing: cells were lifted and washed after reaching 80-90% confluence, similar to the subculturing protocol. The cell pellet resulting from a single flask was resuspended in 2 mL of freezing media (10% DMSO in FBS). The cells were transferred to cryovials (1 mL of cell suspension/vial), and frozen slowly in a Nalgene Cryo 1°C Freezing Container at -80°C. Once frozen, the vials were moved to liquid N_2. Raising: the vials were quickly thawed in a warm water bath, mixed with complete media in a conical tube, spun down (243 x *g* for 3 min) to remove the freezing media, and resuspended in fresh complete media that was transferred to a T75 flask. Cells were subcultured at least twice after being brought up from frozen before being used for an experiment.

2.2.4 Caco2 cells were kindly provided by Dr. Simon Hirota (University of Calgary, Calgary, AB) at passage 38, originally from ATCC (Manassas, VA). Cells were cultured in DME/F12 media (HyClone SH30023.01) supplemented with 10% FBS (Gibco 12483-020,

Burbury, ON), 100 IU/mL penicillin and 100 µg/mL streptomycin (HyClone SV30010), as well as a low maintenance dose of plasmocin (5 µg/mL) (InvivoGen ant-mpt, San Diego, CA). Due to the high variability in Caco2 cell phenotypes and their ability to differentiate post-confluence, an initial low density cell stock was prepared according to published Caco2 cell culture practices (Natoli et al. 2012). Cells were subcultured before reaching 50% confluence for 10 passages (from p43-53), and a large number of cryovials were frozen at p54. All experiments with Caco2 cells were performed from p56-80.

2.2.5 T84 cells were kindly provided by Dr. Derek McKay (University of Calgary), originally from ATCC. Cells were cultured in DME/F12 media supplemented with 10% FBS, 1mM sodium pyruvate (HyClone SH30239.01), 100 IU/mL penicillin, 100 µg/mL streptomycin, and 5 µg/mL of plasmocin. T84 cells were brought up from frozen at p81 and used for experiments between p83-92.

2.3 PAR2 receptor activation

PAR2 was activated using 2-furoyl-LIGRLO-NH_2 (2fLI), a small peptide with sequence similarity to the endogenous post-cleavage tethered ligand, SLIGKV. The inactive reverse sequence peptide 2-furoyl-OLRGIL (2fO) was used as a control (Hollenberg et al. 2008). Peptides were kindly provided by Dr. Hollenberg (University of Calgary).

2.4 Western blot

Cells were washed once with cold PBS and cold SDS lysis buffer was added directly to the well (NaCl (100 mM), Tris-HCl (20 mM pH 8.0), SDS (0.1%), EDTA (0.9 mM), protease

inhibitor cocktail (1:50), triton-X (0.5%), activated sodium orthovanadate (2 mM), and sodium fluoride (50 mM)). Cells were collected with a cell scraper, transferred to a microcentrifuge tube, and frozen at -80°C to further lyse the cells.

Whole-cell lysates were thawed on ice, centrifuged (max speed 20817 x *g*, 10 min, 4°C), and the supernatant was transferred to a clean microcentrifuge tube. The pellet was discarded. A protein estimation was performed in a 96-well plate with diluted samples using the detergent compatible (DC) Protein Assay kit (BioRad 500-0112, Hercules, CA) according to the manufacturer's instructions, with the provided BSA used to prepare a standard curve with each plate. After determining the protein concentration, samples were made up to a final concentration of 1 µg/mL of protein in PBS, with 5X SDS loading buffer and fresh β-mercaptoethanol. The samples were boiled for 5 min, and frozen at -20°C.

Gels were run with either 12-well or 26-well Criterion™ XT precast 4-12% Bis-Tris gels (BioRad 345-0123, 345-0125) that were placed in a Criterion™ Vertical Electrophoresis Cell (BioRad) with XT MOPS running buffer (BioRad 161-0788). After adding the samples and the ladder (Precision Plus Protein Kaleidoscope, BioRad 161-0375), the gel was run at 120 – 140 volts (V) for 1.5 – 2 h. The gel was then transferred to a nitrocellulose membrane (0.2 µm, BioRad 162-0112) with a Criterion™ Blotter in Tris-Glycine transfer buffer with 20% methanol for 100 Vh. To ensure an even transfer, the membrane was stained with Ponceau Red (0.1% Ponceau S, 5% acetic acid in ultrapure water) for 5 minutes and rinsed with distilled water, to visualize the proteins on the blot.

The Ponceau stain was removed with Tris-buffered saline with Tween (TBST) and the membrane was blocked for 1 h at room temperature (r.t.) in blocking solution before being rinsed with TBST and incubated in 1° antibody (Table 2.1) overnight at 4°C on a rocking platform. The following day, the membrane was washed 3 x 5 min in TBST and incubated with secondary antibody (Table 2.2) for 2 h at r.t. on a rocking platform. The membrane was washed 2 x 5 min in TBST, and lastly washed 1 x 5 min in TBS, before being incubated with enhanced chemiluminescence substrate (Clarity Western ECL Substrate, BioRad) for 1 – 5 min. The membrane was placed in a plastic sheet protector and imaged on a ChemiDoc XRS+ imager (BioRad) with Quantity One basic software (4.6.5 BioRad).

Table 2.1 Details of primary antibodies used in western blotting.

Protein Detected	Size (kDa)	Catalog # and Company	Block (5%)	[1° Ab] made in 5% BSA	[2° Ab] made in 5% milk
COX-2	72	sc-1745: Santa Cruz	BSA	1:500	α-goat 1:5000
β-actin	42	AC5441: Sigma	milk	1:10000	α-mouse 1:10000
pERK1/2	44/42	9106S: Cell Signaling	BSA	1:2000	α-mouse 1:5000
tERK1/2	44/42	9102: Cell Signaling	milk	1:2000	α-rabbit 1:5000
Rac1	21	05-389: Millipore	milk	1:1000	α-mouse 1:5000
CUX1	180	sc-13024: Santa Cruz	BSA	1:500	α-rabbit 1:5000

Table 2.2 Details of secondary HRP-conjugated antibodies used in western blotting.

	Catalog # and Company
Goat α-rabbit	111-035-144: Jackson
Goat α-mouse	115-035-146: Jackson
Donkey α-goat	705-035-147: Jackson

2.4.1 Pharmacological inhibitors used when assessing PAR2-induced COX-2 by western blot. To inhibit transcription, actinomycin D (5 μg/mL, Sigma A1410) was added to Caco2 cells for 1 h during serum-starvation, before the addition of 2fO or 2fLI (0.5 μM) for 4 h. DMSO (1:200) was used as the vehicle control. To inhibit Rac1 activation, confluent Caco2 cells were serum starved and treated with varying concentrations of NSC23766 (0 – 200 μM) (2161 Tocris, Minneapolis, MN) or EHop-016 (0.5 - 3 μM) (Sigma SML0526) for 1 hr, prior to the addition of 2fO or 2fLI (0.5 μM) for either 5 min or 3 h to assess ERK1/2 phosphorylation and COX-2 expression respectively. In experiments using T84 cells, some wells were treated with a cocktail of TNFα (10 ng/mL, R&D Systems 210-TA, Minneapolis, MN), IFNγ (10 ng/mL, R&D Systems 285-IF) and lipopolysaccharide (LPS) (1 μg/mL, Sigma L4391), as a positive control for induction of COX-2 expression.

2.4.2 Analysis of western blotting. Densitometry was performed using the same Quantity One basic software used to acquire the images, and the protein of interest was expressed relative to total protein (pERK/tERK) or β-actin.

2.5 PGE-metabolite enzyme-linked immunosorbent assay

Caco2 cells were serum-starved for 1 h prior to the addition of 2fO or 2fLI (0.5 μM). At various time points from 0 h – 12 h, supernatants were collected and centrifuged (max speed 20817 x *g*, 5 min, 4°C) for analysis of PGE metabolite levels using the PGEM ELISA kit (Cayman 514531, Ann Arbor, MI) according to the manufacturer's instructions. The PGEM kit was chosen since PGE_2 is unstable, and the outputs of the first experiment with the

PGE_2 ELISA kit (Cayman 514010) were below the standard curve (data not shown). Briefly, the standard and samples were allowed to fully derive the PGE metabolite overnight at 37°C in carbonate buffer. The samples from cells treated with 2fLI for 3-12 h were diluted 1:2 in media prior to derivation, while all other samples were used undiluted. The following day, phosphate buffer and ELISA buffer were added. The standard was prepared by serially-diluting the derived standard in PGEM assay buffer (0.39 – 50 pg/mL). Standards and samples were run in duplicate (50 µL/well). After preparing the non-specific binding (NSB) and B_0 wells, 50 µL of acetylcholinesterase (AChE) tracer was added to each well (not total activity (TA) or Blnk wells). Finally, 50 µL of PGEM ELISA anti-serum was added to each well (not TA, NSB, or Blnk wells). The plate was covered and incubated for 18 h at r.t. The following day, the wells were rinsed (x5) with wash buffer. Ellman's reagent was reconstituted immediately prior to use, and 200 µL was added to each well. AChE tracer (5 µL) was added to the TA well, and the plate was covered and placed on the orbital shaker for 90 min to develop. The plate was read on a Spectramax Plus 384 microplate reader (Molecular Devices, Sunnyvale, CA) at 405nm, with SoftMax Pro 5 software. Data was analysed with the provided spreadsheet from Cayman Chemical (www.caymanchem.com/analysis/elisa) to calculate the B/B_0 value for each sample and compare it to the standard curve in order to determine the PGEM concentration.

2.6 Knock-down of Rac1 and CUX1

The small interfering (si)RNA protocol was optimized by treating the cells with either 100 nM or 300 nM of siRNA on day 2, 3 or 4 after plating, and then detecting the

level of protein knock-down on day 5, keeping with the time-point used for PAR2-induced COX-2 expression. Caco2 cells (8 x 10^4 cells/well) were plated in a 12-well plate. Two days after plating, the cells were washed and antibiotic-free media was added. A transfection solution (100 µL/well) containing 100 nM of either Rac1 or CUX1 siRNA (Life Technologies AM51331 and 110461, Grand Island, NY) with 5 µL Lipofectamine RNAiMAX (Invitrogen 56532, Carlsbad, CA) in Opti-MEM (Gibco 31985-070) was prepared at r.t. and allowed to sit for 20 min before being added dropwise to the cells. The transfection solution was on the cells for 6-8 h, and the cells were then washed and antibiotic-containing media was added. Cells were then used on day 5 to assess PAR2-induced COX-2 expression by western blotting.

2.7 Circular wound healing

Caco2 and T84 cells were plated and analyzed in a variety of conditions for wound healing experiments, including what will be referred to as standard, post-confluent, polarized, live-cell, and staining. Similarities in all 5 conditions involved starving the cells overnight in serum-free media, and wounding the cells the following morning. After wounding, cells were washed with PBS to remove cell debris and fresh media containing 10% serum was added. Cells were treated with peptides every 12 h to ensure continual activation of the receptor.

For standard wound healing experiments, Caco2 cells (8 x 10^4 cells/well) were plated in a 12 well dish and grown for 3 days to confluence. For post-confluent wound

healing, Caco2 cells (8 x 10^4 cells/well) were plated in a 12 well plate and grown for 21 days to induce differentiation. When using transwells to ensure polarization of the Caco2 cells, 1 x 10^5 cells/insert were plated on transwell supports (Corning 3460, Corning, NY) and grown for 5 days. In each of these experiments, individual wounds were all identified by drawing a grid on the bottom of each well to visually divide the monolayer into sections. In each section, one circular wound was made with a pipette tip attached to the end of an aspirator. Pictures of each wound were captured every 12 h (beginning at 0 h) with a Zeiss AxioCam MRc camera on a Zeiss AxioVert25 microscope (Oberkochen, Germany), using AxioVision Rel 4.6 software. Wounds were manually traced using ImageJ software, and percent initial wound area was calculated for each time point up to 48 h. In live-cell experiments, Caco2 cells (8 x 10^4/well) or T84 cells (5 x 10^5 cells/well) were plated in a 12 well plate and grown for 3 days, then starved overnight. Since there was no need to manually identify the same wound, multiple circular wounds were made randomly within the monolayer on day 4. Fresh media was added and cells were treated with peptides at 0 h before being transported to a pre-warmed live cell chamber. Within this chamber, cells were maintained at 37°C with 5% CO_2 (flow rate 40 mL/min) on an Olypus IX71 inverted microscope equipped with a Proscan™III motorized stage and a Hamamatsu OrcaR2 cooled CCD 12-bit camera. Using Volocity acquisition software and point visiting, which saved the x, y, and z coordinates that were manually set for each wound, the wounds were imaged every 15 min for 24 h and compiled for live-cell wound healing videos. With the MTrackJ plugin in FIJI, individual cells around the perimeter of the wound were tracked and the total

distance traveled by each cell was recorded. For Caco2 analysis, 10 cells around each wound were tracked, with 3 wounds/condition for each experiment. The results shown are from 4 separate experiments. For T84 analysis, 10 cells surrounding 1 wound/condition were tracked in 6 individual experiments. For staining experiments with Caco2 cells, sterilized 18 mm glass coverslips were placed within a 12 well plate, with 9 x 10^4 cells/well (or 12 mm coverslips were placed in a 24 well plate with 4.5 x 10^4 cells/well) and cells were grown for 3 days. With T84 cells, 5 x 10^5 cells/well were plated in a 12 well plate with sterilized 18 mm coverslips and grown for 3 days. Cells were starved overnight, wounded on day 4, and used at 2 time-points: cells were either treated with peptides at 0 h and fixed at 12 h, or treated with peptides at 0 h and 12 h and fixed at 24 h. These cells were used for both EdU and immunofluorescent staining.

2.7.1 Growth factors and pharmacological inhibitors used during wound healing.

The following additional components were used in specific experiments during the standard wound healing protocol above. Epidermal growth factor (EGF) (GF-010-8 Cedarlane, Burlington, ON) was added at 0 h and 24 h (5 and 20 ng/mL). The COX-2-selective inhibitor NS-398 (70590 Cayman) was added to cells at 0 h and 24 h (10 µg/mL), and as the vehicle control an equivalent volume of DMSO (1:2000) was added at the same time points. Actinomycin D (A1410 Sigma), used to inhibit transcription, was added to the cells at 0 h (5 µg/mL), and an equivalent volume of DMSO (1:200) was used as the vehicle control. To inhibit proliferation, cells were pre-treated with 5 µg/mL of the irreversible inhibitor mitomycin C (MMC) (sc3517 Santa Cruz, Dallas, TX) for 2 h, washed with PBS, and

then wounded. As a vehicle control, an equivalent volume of DMSO (1:750) was used to pre-treat the cells.

2.8 Scratch wound healing

Caco-2 cells (8 x 10^3 cells/well) were grown in a 96-well plate for 3 days. Cells were serum starved overnight, and the following day, the cells were wounded using the WoundMaker™ tool (Essen Biosciences, Ann Arbor, MI) according to the manufacturers instructions. After wounding, media was removed and fresh media containing 10% serum was added. Cells were then immediately treated with either 2fO or 2fLI (10 μM) and placed within the Incucyte microscope (Essen Biosciences). Incucyte ZOOM software was set for the microscope to capture one 4X image per well per hour for 24 h. Following the acquisition, the ZOOM software was set to detect the percentage of confluent cells relative to the total area for each well at each time point. Data were expressed as percent wound confluence.

2.9 Single-cell migration

Using the xCelligence Real-Time Cell Analyzer (RTCA) with the cell invasion and migration plate (CIM-Plate 16), the effect of PAR2 activation on the migration of single Caco2 epithelial cells through a microporous membrane was measured. The lower chamber of the CIM-Plate was filled with 170 μL of pre-warmed media (37°C, containing 1% serum), and the upper chamber was snapped onto the filled lower chamber and checked to ensure no air bubbles were trapped. Media (50 μL, 1% serum) was added to

the centre of the top well, and the CIM-Plate was allowed to equilibrate at 37°C for 1 h before taking a blank reading using the RTCA software. During this equilibration period, Caco2 cells were lifted with 2 mM EDTA, washed, and resuspended in fresh media (1% serum). Cells were counted, and two tubes were prepared with 1 mL media containing 10^5 cells. Immediately prior to adding the cells to the CIM-Plate, 2fLI (0.5 µM) was added to one of the tubes. The cell suspension (100 µL/10^4 cells) was added to the top wells, and the plate was equilibrated at room temperature for 30 min before being placed within the xCelligence instrument. The RTCA software was set to take measurements every 15 min for 24 h. Data were expressed as cell index, which was a measure of impedance detected by the electrodes on the underside of the upper chamber.

2.10 XTT proliferation

Caco2 cells (6 x 10^3 cells/well) were plated in a 96 well plate in either 0.5% FBS or 10% FBS phenol red-free media (HyClone SH30272.01). Beginning at 0 h, cells were treated with 2fO or 2fLI (10 µM) every 12 h. At 72 h, an XTT assay was performed according to the manufacturer's instructions (Cayman 10010200). Briefly, 10 µL of XTT reagent was added to each well and the plate was placed on an orbital shaker for 1 min before being returned to the incubator for 2 h. The plate was shaken again for 1 min before having the absorbance read on a microplate reader at 450 nm.

2.11 EdU proliferation

In order to assess proliferation in confluent, subconfluent, and wound-edge cells, the Click-iT EdU AlexaFluor488 Imaging Kit (Life Technologies C10337) was used according to the manufacturer's protocol. Briefly, Caco2 and T84 cells grown on glass coverslips were wounded using the circular wound healing model described. At the two time-points analyzed (12 h and 24 h), 50% of the media was replaced with fresh media containing 20 µM EdU (final concentration 10 µM EdU) and cells were returned to the incubator for 2 h. Cells were fixed with 4% paraformaldehyde (PFA, Alfa Aesar 43368, Ward Hill, MA) for 15 min, permeabilized with 0.5% Triton-X for 20 min, incubated with Click-iT reaction cocktail for 30 min (protected from light), and lastly incubated with DAPI (1:50000) for 30 min (protected from light), with washing between each step in PBS containing 3% BSA. Coverslips were then washed with PBS and mounted with FluorSave (34789 Calbiochem, Darmstadt, Germany). Widefield (10X) images were captured with an Olympus IX71 inverted microscope equipped with a Hamamatsu OrcaR2 12-bit camera. Using ImageJ software, cells were counted in DAPI images to determine total cell number, and in EdU images to determine number of proliferating cells. The detailed ImageJ process is described in Appendix A. Data was expressed as percent EdU-positive cells of total cell number.

2.12 Immunofluorescence staining

Caco2 and T84 cells grown on glass coverslips were wounded as per the circular wound healing model described. Either 12 h or 24 h after wounding, cells were fixed in 4%

PFA for 15 min. After washing 3 times with PBS, cells were blocked and permeabilized in 10% w/v BSA/PBS containing 0.1% Triton-X for 1 h at r.t. on a rocking platform. Cells were washed once with PBS/0.1% Triton-X, then primary antibody was added to the well and the coverslips were incubated at 4°C overnight on a rocking platform (Table 2.3). The following day, coverslips were washed twice with PBS/0.1% Triton-X, and the following steps were all performed with single wash steps in between, at r.t. and protected from light on a rocking platform: incubation with secondary antibody for 2 h (Table 2.4), incubation with phalloidin-488 (1:1000) for 30 min (only certain experiments), and finally incubation with DAPI (1:50000) for 30 min. Coverslips were then washed with PBS and mounted with FluorSave. Widefield images (20X) were captured with a Leica DMi6000 B inverted microscope equipped with a fully motorized XY stage and piezo Z stage insert. Metamorph software with a slide-scan function was used during acquisition to stitch the 20X images together in order to visualize the entire wound.

Table 2.3 Details of primary antibodies and isotype controls used in immunofluorescent staining.

Protein Detected	Catalog # and Company	[1° Ab] made in 2% BSA	[2° Ab] made in 2% BSA
E-cadherin	610182: BD	1:200	α-mouse 1:200
ZO-1	339100: Invitrogen	1:200	α-mouse 1:200
ppERK1/2	9106S: Cell Signaling	1:200	α-rabbit 1:200
Vimentin	sc5565: Santa Cruz	1:200	α-rabbit 1:200
N-cadherin	610921: BD	1:250	α-mouse 1:200
SNAIL	3879: Cell Signaling	1:200	α-rabbit 1:200
Mouse IgG	015-000-003: Jackson		
Rabbit IgG	011-000-003: Jackson		
Goat IgG	sc2028: Santa Cruz		

Table 2.4 Details of secondary antibodies and other markers used in immunofluorescent staining.

	Fluorophore	Catalog # and Company
goat-α-mouse secondary	488	A11029: Invitrogen
goat-α-rabbit secondary	488	A11034: Invitrogen
goat-α-mouse secondary	568	A11031: Invitrogen
donkey-α-rabbit secondary	568	A10042: Invitrogen
donkey-α-goat secondary	647	A21447: Invitrogen
Phalloidin	488	A12379: Invitrogen
DAPI	405	D1306: Invitrogen

2.13 LifeAct plasmid transfection and imaging

Transfection was optimized using an eGFP (green fluorescent protein) plasmid (CloneTech 6085-1, Mountain View, CA). Caco-2 cells (2.1 x 10^4 cells/well) were plated on an 8-well glass-bottom chamber slide (Ibidi 80827, Madison, WI), and transfected the following day with LifeAct-GFP (Ibidi p^{CMV}-LifeAct®-TagGFP2) using JetPrime reagents (PolyPlus 114-07, Illkirch, France): 0.5 µg plasmid, 1 µL JetPRIME, and 25 µL buffer (per well). Immediately after wounding, cells were imaged every 15 min for 24 h at 40X on a Leica DMi6000 B inverted spinning-disk confocal microscope (50 µm pinhole) equipped with live-cell instrumentation.

2.14 RNA sequencing

Caco-2 cells (plated at 2 x 10^5 cells/well) were grown to confluence in 6-well plates, serum-starved overnight, then used to create 4 conditions: non-wounded control (NW-C), wounded control (W-C), non-wounded with PAR2 activation (NW-PAR2) and wounded with PAR2 activation (W-PAR2) (10 µM of 2fLI). Wounding was performed using a pipette tip attached to the end of an aspirator to create a grid pattern in order to maximize the number of wounded/migrating cells (Figure 2.1). Three hours after wounding, RNA was isolated using the RNeasy kit (Qiagen 74106, Valencia, CA) according to the manufacturers instructions. The isolated RNA from biological triplicates of each condition were submitted for processing to the Alberta Children's Hospital Research Institute (ACHRI) Genomics and Informatics facility.

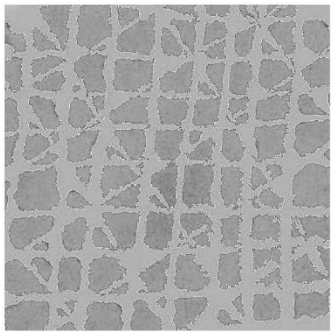

Figure 2.1 Example of grid wound pattern created in Caco2 cells used for RNA sequencing.

In order to maximize the number of wounded cells, grid wounds were made in confluent Caco2 monolayers using a pipette tip attached to the end of an aspirator. In order to standardize the number of wounded cells, the same grid pattern was made in each well: 10 vertical, 10 horizontal, and 5 across each diagonal.

The ACHRI facility performed the following: The quality of each sample was verified via Nanodrop, Qubit, and TapeStation. Total RNA samples were then prepared into libraries using an Illumina TruSeq Stranded mRNA sample preparation kit. The indexed libraries were then quantified with KAPA qPCR, normalized, and pooled for sequencing. Sequencing was performed on an Illumina NextSeq500 with a high output v2 sequencing kit (75 cycles). After sequencing, run metrics were verified and the data was uploaded to the Galaxy server.

Dr. Paul Gordon then performed the following: Raw NextSeq BCL files were converted to FASTQ format using bcl2fastq v2.15.0.4. In order to analyze the data with the web-interface of Galaxy, FASTQ files were mapped to the hg19(GRCh37) reference genome using TopHat v2.1.0 with the UCSC knownGenes track as a splice site guide, and underlying Bowtie v2.2.6 used in 'fast' mode. Multiple BAM files across lanes and runs were merged using samtools v0.1.9 to produce one final BAM file for each input biological sample.

BAM files were run with CuffDiff and differential gene expression testing results were exported for further analysis. Lists of genes that were significant and at least 2-fold increased or decreased were compiled and compared using an online tool to create Venn diagrams from gene lists (genevenn.sourceforge.net), and EnrichR (Chen et al. 2013).

2.15 Statistics

Data expressed as mean ± standard error were graphed and analyzed using GraphPad Prism 7.00 (GraphPad Software, La Jolla, CA). Student's T-test was used to compare 2 groups. One-way and two-way analysis of variance (ANOVA) were used when appropriate followed by a Bonferroni's multiple comparisons test. A p value < 0.05 was considered significant.

CHAPTER 3

Results

3.1 PAR2-induced COX-2 expression in Caco2 cells

3.1.1 PAR2 activation induced COX-2 expression on day 5

It was previously shown that PAR2 activation could induce COX-2 expression in Caco2 cells (Hirota et al. 2012), but the underlying mechanisms were not investigated completely. We sought to further characterize PAR2-induced COX-2 expression in the context of our hypothesis that PAR2 promotes wound healing in a COX-2-dependent manner. PAR2 signaling and COX-2 expression were investigated on day 5 and day 8 after plating. Caco2 cells were treated with 2fO or 2fLI (0.5 μM) for 3 h, or left untreated as the control. Although PAR2 signaling was confirmed on both day 5 and 8 with 2fLI-induced ERK phosphorylation, COX-2 up regulation was only detected on day 5 (Figure 3.1).

Concentration-response and time-course experiments were conducted to characterize the day 5 PAR2-induced COX-2 up regulation. For the concentration-response, cells were treated with 2fLI (5 nM – 10 μM) for 4 hr, and control cells were either left untreated, or treated with 2fO (10 μM, 4hr). Representative western blots for COX-2 and β-actin are shown (Figure 3.2 A), and the PAR2-COX-2 dose-response curve based on the densitometry was quantified from 4 separate experiments (Figure 3.2 B). PAR2-induced COX-2 using 2fLI in Caco2 cells was found to have an EC_{50} of 48 nM.

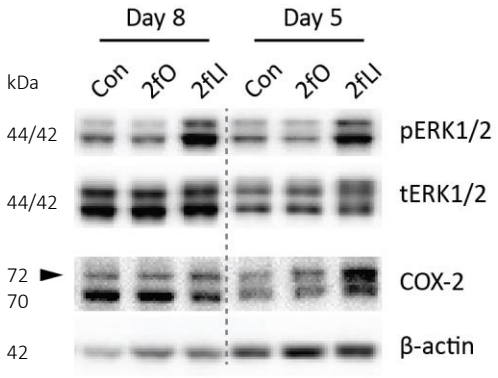

Figure 3.1 PAR2 activation induced expression of COX-2 in Caco2 cells.

Caco2 cells (2 x 10^5 cells/well, 6 well plate) grown for 5 or 8 days were serum-starved for 1 h, then treated with 2fO or 2fLI (0.5 µM) for 5 min or 3 h. Control cells were left untreated. Whole-cell lysates were analyzed by western blot for pERK1/2 and tERK1/2 (5 min) as well as COX-2 and β-actin (3 h). *(Small arrow indicates the COX-2 band at the correct size, 72 kDa.)*

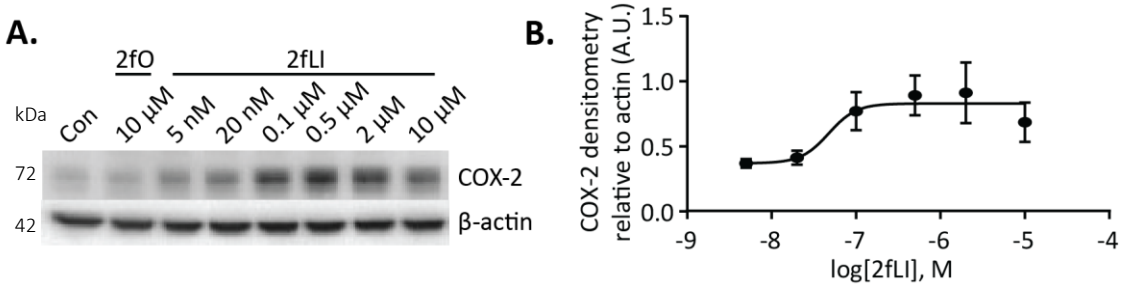

Figure 3.2 PAR2-induced COX-2 dose-response.

Caco2 cells (8 x 10^4 cells/well, 12 well plate) grown for 5 days were serum-starved for 1 h, then treated with varying concentrations of 2fLI (5 nM – 10 µM), or a high concentration of 2fO (10 µM) for 4 h. Control cells were left untreated. A: Whole-cell lysates were analyzed by western blot for COX-2 and β-actin (representative blot of n=6). B: A concentration-response curve was prepared according to the COX-2 densitometry relative to β-actin.

For the day 5 time-course, Caco2 cells were treated with 2fLI or 2fO (0.5 μM, 30 min – 12 h). In addition to western blots on whole-cell lysates to assess COX-2 expression, the supernatant was collected for a PGEM ELISA to determine COX-2 activity. COX-2 protein expression peaked 4 h after PAR2 activation, but was significantly increased compared to 2fO between 2 h – 9 h (Figure 3.3 A, B). COX-2 activity peaked at 6 h with 2fLI treatment, and was significant from 2fO at 30 min, and between 2 h – 12 h (Figure 3.3 C).

To test if PAR2-induced COX-2 was dependent on transcription[1], Caco2 cells were treated with actinomycin D (5 μg/mL, 1 h) prior to addition of either 2fO or 2fLI (0.5 μM, 4 h). Compared to untreated control cells, or cells treated with the vehicle control (DMSO), actinomycin D was able to prevent PAR2-induced COX-2 expression (Figure 3.4). Therefore, COX-2 up-regulation following PAR2 activation was dependent on transcription.

[1] These experiments were performed with Tina Sarkar, a high school student within the HYRS program.

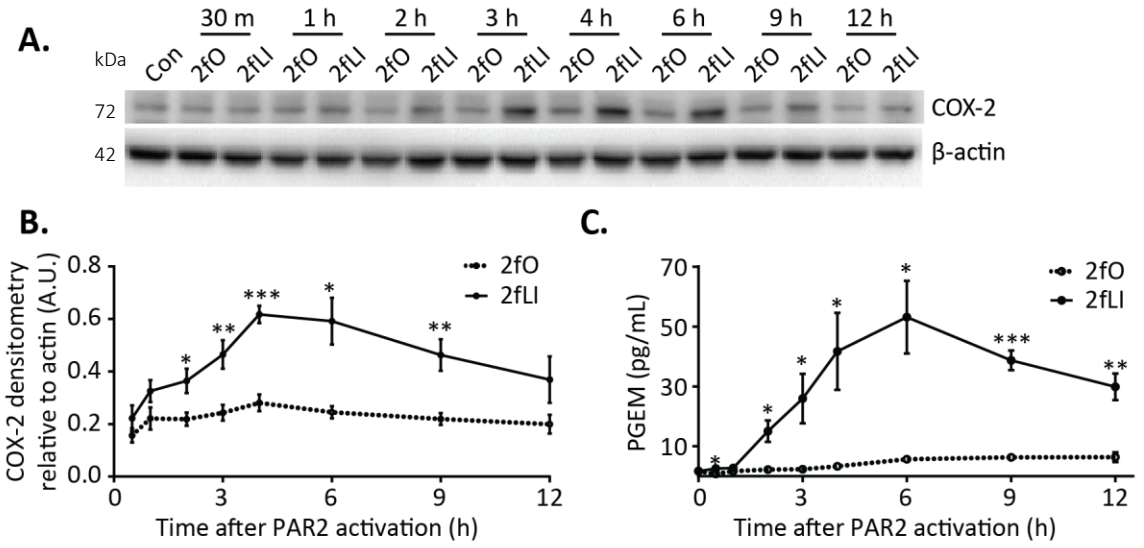

Figure 3.3 PAR2-induced COX-2 time-course.

Caco2 cells (2 x 10^5 cells/well, 6 well plate) grown for 5 days were serum-starved for 1 h, then treated with 2fO or 2fLI (0.5 µM) for times ranging from 30 min to 12 h. Control cells were left untreated. A: Whole-cell lysates were analyzed by western blot for COX-2 and β-actin (representative blot of n=8). B: Densitometry analysis of COX-2 expression relative to β-actin. C: Supernatants from the same experiments were collected and run on a PGEM EIA (n=6-9). *Statistics: data in B and C were analyzed using an unpaired two-tailed t-test with Welch's correction at each time point. (* p<0.05; ** p<0.01; *** p<0.001)*

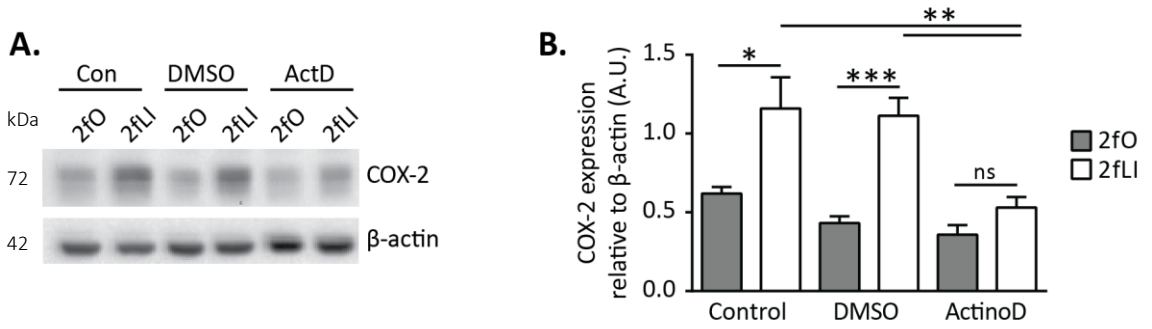

Figure 3.4 PAR2-induced COX-2 was dependent on transcription.

Caco2 cells (8 x 10^4 cells/well, 12 well plate) grown for 5 days were serum-starved and pre-treated with actinomycin D (5 µg/mL) or an equivalent volume of vehicle control (1:200 DMSO). After 1 h, cells were treated with 2fO or 2fLI (0.5 µM) for 4 h. A: Whole-cell lysates were analyzed by western blot for COX-2 and β-actin (representative blots of n=6). B: Densitometry analysis of COX-2 expression relative to β-actin. *Statistics: data in B were analyzed using a one-way ANOVA with Tukey's post-hoc test. (* p<0.05; ** p<0.01; *** p<0.001)*

3.1.2 Rac1 and CUX1 were not involved in the PAR2-COX-2 signaling pathway

Rac1 rationale: Previous studies have shown that both Ras and Rho families contribute to COX-2 up regulation, and the co-expression of constitutively active RhoA with Ras or Rac1 was required for maximum COX-2 expression (Chang et al. 2005). It was hypothesized that Rac1 would be involved in PAR2-induced COX-2 expression.

Rac1 was inhibited using NSC23766[2], which targets the Rac1-specific guanine exchange factors (GEF) TrioN and Tiam1, and using EHop-016, which targets the Rac-specific GEF Vav2. Inhibition of Rac1 with high doses of NSC23766 (100 and 200 µM) appeared to attenuate the increase in COX-2 seen following PAR2 stimulation (Figure 3.5 A, representative western blot of n=3), but there was no significant difference with densitometry (not shown). EHOP-016 did not have an effect on COX-2 expression (Figure 3.5 B). Since these data failed to conclusively show if Rac1 was involved in the PAR2-COX-2 signalling pathway, we chose to knock-down Rac1 with siRNA.

During siRNA optimization, Rac1 protein expression was most prominently reduced on day 5 by transfecting the cells with Rac1 siRNA (100 nM) 2 days after plating (Figure 3.6 A). When Rac1 was knocked-down using these conditions (to 27% of control) prior to the activation of PAR2 on day 5 (2fLI, 0.5 µM, 4 h), the increase in COX-2 protein was not changed from control (Figure 3.6 B-D), indicating that Rac1 did not play a role in the PAR2-COX-2 signaling pathway.

[2] These experiments were performed with Sharon Feng, a 3rd year undergraduate student in the U of C Health Sciences program.

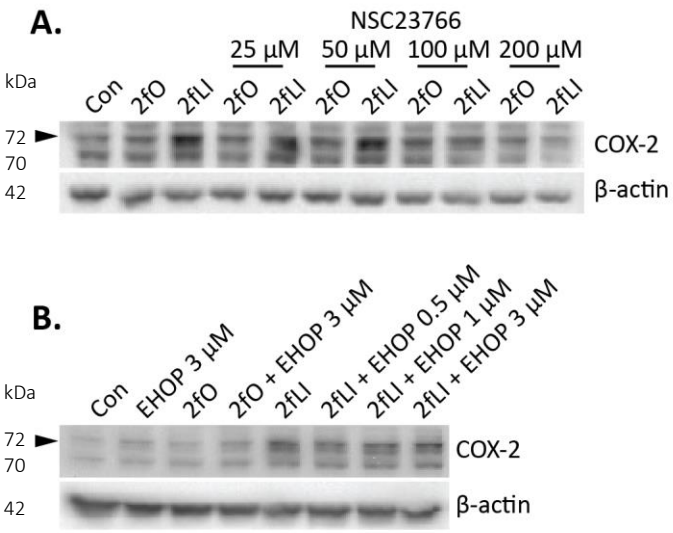

Figure 3.5 Pharmacological inhibition of Rac1 did not effect PAR2-induced COX-2 expression.

Caco2 cells (8 x 10^4 cells/well, 12 well plate) grown for 5 days were serum-starved and exposed to varying concentrations of pharmacological inhibitors known to affect the activation of Rac1. After 1 h, cells were treated with 2fO or 2fLI (0.5 µM) for 3 h. Control cells were left untreated. Whole-cell lysates were analyzed by western blot for COX-2 and β-actin. A: NSC23766 (25 µM - 200 µM, representative blot of n=3). B: EHOP-016 (0.5 - 3 µM, representative blot of n=2). (*Small arrow indicates the COX-2 band at the correct size, 72 kDa.)*

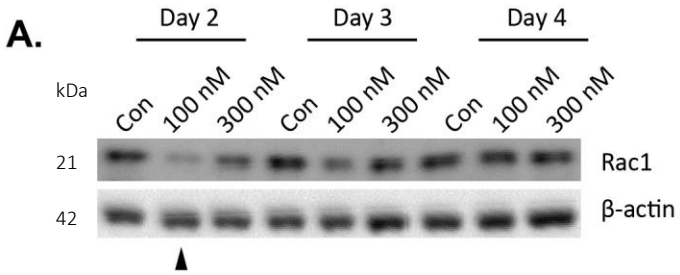
A.
Day 2
Day 3
Day 4
kDa
Con
100 nM
300 nM
Con
100 nM
300 nM
Con
100 nM
300 nM
21
Rac1
42
β-actin

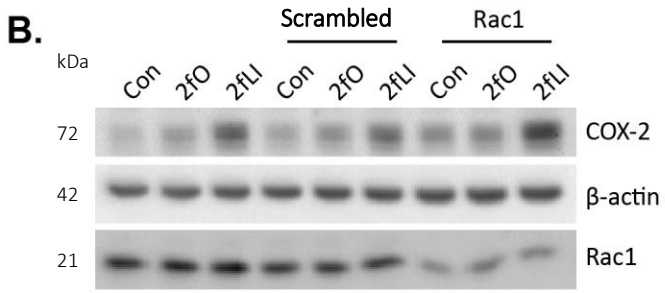
B.
Scrambled
Rac1
kDa
Con
2fO
2fLI
Con
2fO
2fLI
Con
2fO
2fLI
72
COX-2
42
β-actin
21
Rac1

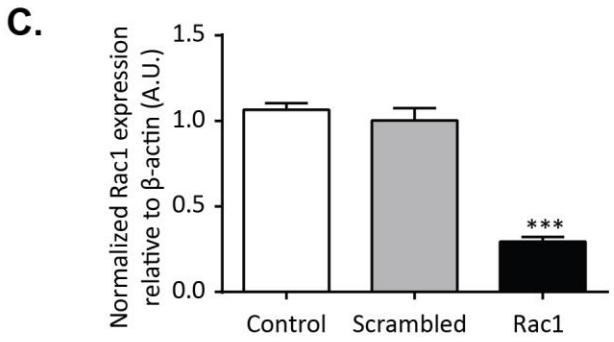
C.
Normalized Rac1 expression relative to β-actin (A.U.)
1.5
1.0
0.5
0.0
***
Control
Scrambled
Rac1

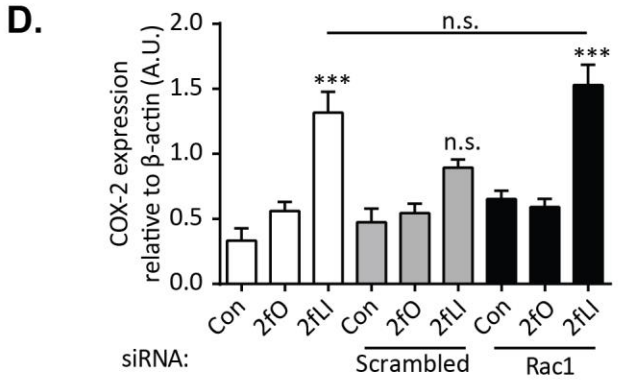
D.
COX-2 expression relative to β-actin (A.U.)
2.0
1.5
1.0
0.5
0.0
n.s.
***
n.s.
***
Con
2fO
2fLI
Con
2fO
2fLI
Con
2fO
2fLI
siRNA:
Scrambled
Rac1

Figure 3.6 Knock-down of Rac1 with siRNA had no effect on PAR2-induced COX-2 expression.

A: Transfection was optimized using 100 nM and 300 nM of Rac1 siRNA on day 2, 3 and 4 after plating, and analyzing the protein level on day 5. Most efficient knock-down was detected with a day 2 transfection using 100 nM siRNA (representative blot of n=2). B-D: Caco2 cells (8 x 10^4 cells/well, 12 well plate) were transfected with 100 nM Rac1 siRNA or a scrambled control siRNA 2 days after plating. On day 5, cells were serum-starved for 1 h, then treated with 2fO or 2fLI (0.5 μM) for 4 h. B: Whole-cell lysates were analyzed by western blot for COX-2, β-actin, and Rac1 expression (representative blots of n=4). C: Densitometry analysis of Rac1 expression relative to β-actin. D: Densitometry analysis of COX-2 expression relative to β-actin. *Statistics: data in C and D were analyzed using a one-way ANOVA with Tukey's post-hoc test. (*** p<0.001)*

CUX1 rationale: Of particular interest in PAR2-induced up regulation of COX-2 is CUX1 (*Cu*t homeobo*x*) (Wilson et al. 2009). CUX1 is a transcription factor involved in both the repression and activation of many genes, and generally affects cell cycle progression, cell motility, and cell invasion (Sansregret and Nepveu 2008). In order to test if CUX1 was involved in PAR2-induced COX-2 expression in Caco2 cells, CUX-1 was knocked-down using siRNA (100 µM, 2 days after plating) (Figure 3.7 A). Compared to the untreated control and scrambled siRNA, CUX-1 knock-down (35% of control) had no significant effect on the PAR2-mediated increase in COX-2 expression (Figure 3.7 B-D). Although CUX-1 could still be important following PAR2 activation, it is not likely involved in the PAR2-COX-2 signaling pathway.

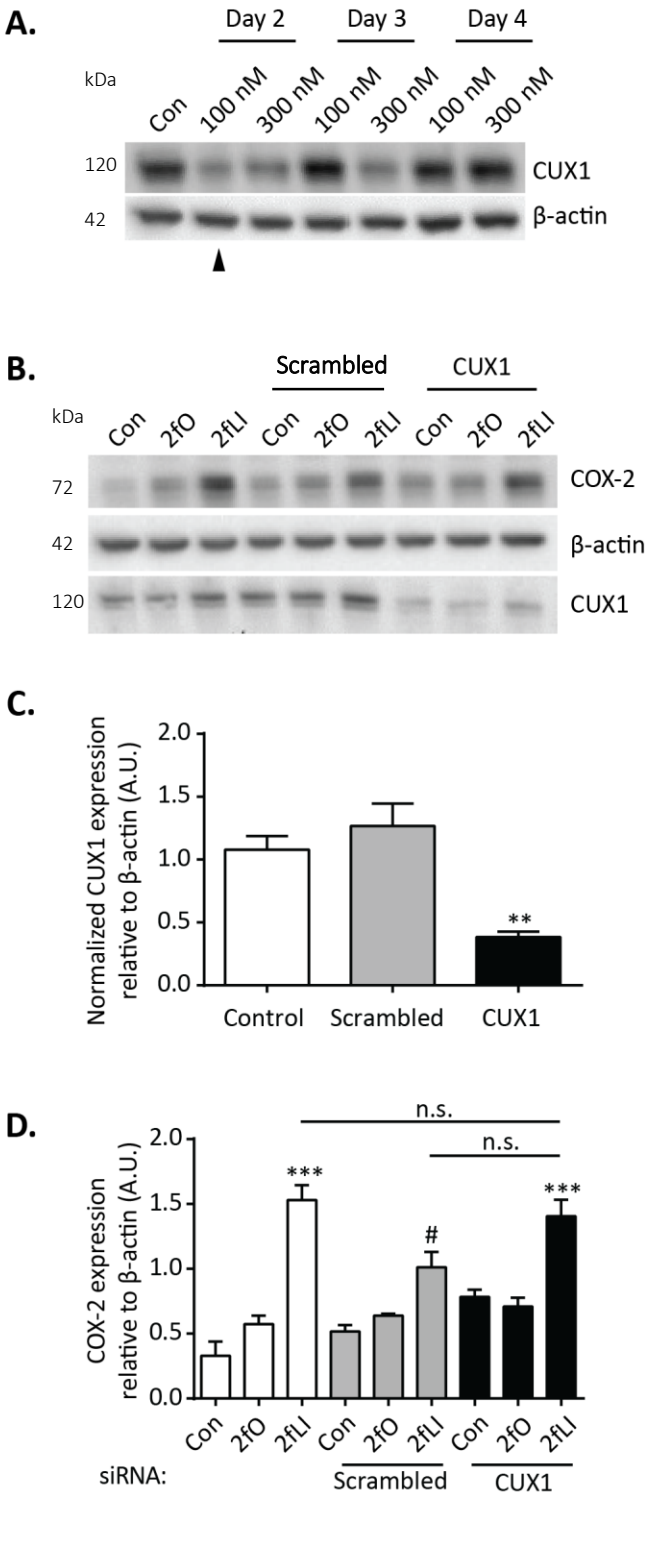
A.
Day 2
Day 3
Day 4
kDa
Con
100 nM
300 nM
100 nM
300 nM
100 nM
300 nM
120
CUX1
42
β-actin
B.
Scrambled
CUX1
kDa
Con
2fO
2fLI
Con
2fO
2fLI
Con
2fO
2fLI
72
COX-2
42
β-actin
120
CUX1
C.
Normalized CUX1 expression relative to β-actin (A.U.)
2.0
1.5
1.0
0.5
0.0
**
Control
Scrambled
CUX1
D.
n.s.
n.s.
COX-2 expression relative to β-actin (A.U.)
2.0
1.5
1.0
0.5
0.0
***
#
***
Con
2fO
2fLI
Con
2fO
2fLI
Con
2fO
2fLI
siRNA:
Scrambled
CUX1

Figure 3.7 Knock-down of CUX1 with siRNA had no effect on PAR2-induced COX-2 expression.

A: Transfection was optimized using 100 nM and 300 nM of CUX1 siRNA on day 2, 3 and 4 after plating, and analyzing the protein level on day 5. Most efficient knock-down was detected with a day 2 transfection using 100 nM siRNA (representative blot of n=2). B-D: Caco2 cells (8 x 10^4 cells/well, 12 well plate) were transfected with 100 nM CUX1 siRNA or a scrambled control siRNA 2 days after plating. On day 5, cells were serum-starved for 1 h, then treated with 2fO or 2fLI (0.5 µM) for 4 h. B: Whole-cell lysates were analyzed by western blot for COX-2, β-actin, and CUX1 expression (representative blots of n=4). C: Densitometry analysis of CUX1 expression relative to β-actin. D: Densitometry analysis of COX-2 expression relative to β-actin. *Statistics: data in C and D were analyzed using a one-way ANOVA with Tukey's post-hoc test. (** p<0.01, *** p<0.001 - significantly different from control and 2fO; # p<0.05 – significantly different from scrambled control and 2fO)*

3.2 PAR2-mediated inhibition of wound healing in Caco2 cells

Rationale: Both PAR2 activation and COX-2 expression have been shown to have pro-wound healing effects including increased proliferation and migration in many cell types (Darmoul et al. 2004; Zhou et al. 2011; Guo et al. 2015; Zhu, Zhu, and Lance 2013). However, there have not been any studies linking the potential role of COX-2 as a mediator of PAR2-induced wound healing. In order to test the hypothesis that COX-2-derived lipid mediators function downstream of PAR2 activation to induce wound healing, the wound healing response in Caco2 cells was first characterized.

3.2.1 PAR2 activation inhibited wound healing in Caco2 cells

Caco2 cells were plated and wounded according to the standard wound healing protocol, and individual circular wounds were followed over 48 h for each condition (control, 2fO, and 2fLI). Surprisingly, in the presence of full-serum media, PAR2 activation (2fLI, 10 μM) significantly inhibited wound healing compared to control and 2fO (Figure 3.8 A). In order to further characterize the effect of PAR2 activation on Caco2 wound healing, circular wound healing was performed in low-serum (0.5%, Figure 3.8 B), with cells grown on Transwells (to ensure polarization, Figure 3.8 C), and with cells grown for 21 days (differentiated, Figure 3.8 D). In each case, PAR2 activation was able to significantly inhibit wound healing. As a positive control to show increased wound healing in Caco2 cells, EGF was used in the presence of 10% serum (5 or 20 ng/mL, Figure 3.8 E).

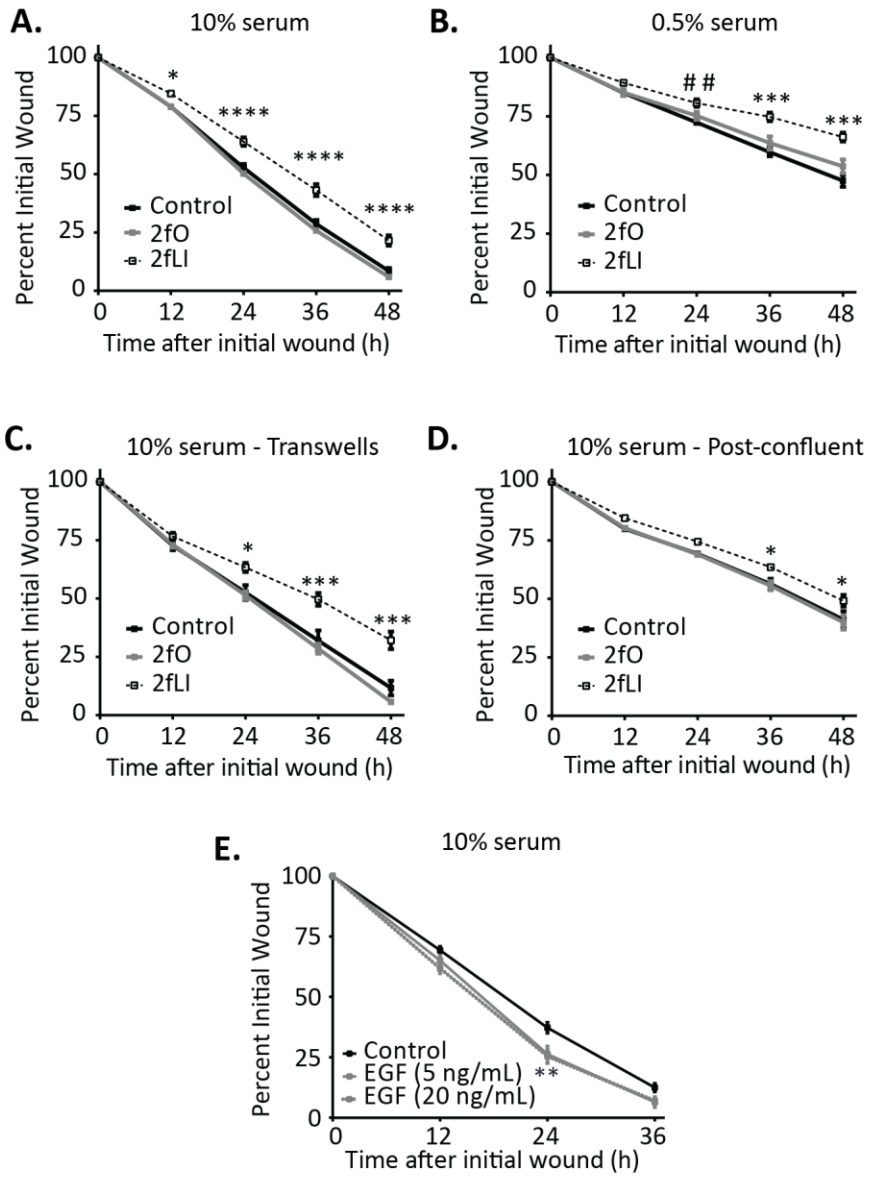
A.
10% serum
Percent Initial Wound
Time after initial wound (h)
Control
2fO
2fLI
*
****
****
****
B.
0.5% serum
Percent Initial Wound
Time after initial wound (h)
Control
2fO
2fLI
##
***
***
C.
10% serum - Transwells
Percent Initial Wound
Time after initial wound (h)
Control
2fO
2fLI
*
***
***
D.
10% serum - Post-confluent
Percent Initial Wound
Time after initial wound (h)
Control
2fO
2fLI
*
*
E.
10% serum
Percent Initial Wound
Time after initial wound (h)
Control
EGF (5 ng/mL) **
EGF (20 ng/mL)

Figure 3.8 PAR2 activation inhibited circular wound healing in Caco2 cells.

Caco2 cells were grown in several conditions (detailed in methods) including standard (A, B, E), polarized (C), and post-confluent (D). Circular wounds were made in monolayers of Caco2 cells with a pipette tip attached to the end of an aspirator, and images of the entire wound were taken every 12 h for 48 h. 2fO or 2fLI (10 μM) were added every 12 h. The areas of the remaining wound at 12 h – 48 h were compared to the area at 0 h to determine the Percent Initial Wound (plotted). A, B: After the cells were wounded, media was replaced with fresh media containing either 10% serum (A, n=6-9) or 0.5% serum (B, n=3-5). C, D: Caco2 cells were polarized on Transwells (C, n=5), and Caco2 cells were differentiated by growing for 21 days (D, n=4). E: As a positive control, following the addition of media containing 10% serum, EGF (5 and 20 ng/mL added at 0 h and 24 h) was added to Caco2 cells (n=8). *Statistics: data were analyzed using a two-way ANOVA with Bonferroni's multiple comparisons test. (* p<0.05; ** p<0.01; *** p<0.001; **** p<0.0001 – significantly different from control and 2fO. ## p<0.01 – significantly different from control only.)*

To confirm that the PAR2-mediated inhibition of wound healing was not dependent on the type of wound created, uniform scratch wounds were created using a WoundMaker tool on Caco2 cells grown in a 96-well plate, and were monitored using the IncuCyte microscope for 24 h. PAR2-activation (2fLI, 10 µM) inhibited wound healing compared to control and 2fO (Figure 3.9 A, B), indicating the effect was not unique to circular wounds.

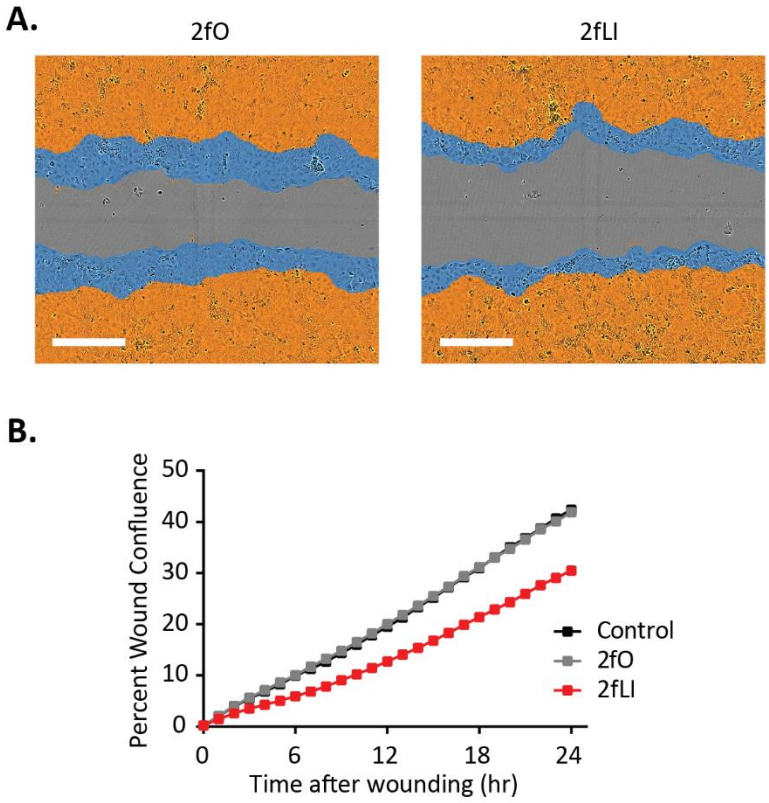

Figure 3.9 PAR2 activation inhibited scratch wound healing in Caco2 cells.

Caco2 cells (8 x 10^3 cells/well, 96 well plate) were grown for 3 days, starved overnight, and wounded with the WoundMaker™ tool. Media was replaced with media containing 10% serum, and cells were treated with 2fO or 2fLI (10 µM). A: Images (4X) were taken every hour for 24 h with the IncuCyte microscope. Representative images are shown. The IncuCyte ZOOM software was used to create a mask to highlight the initial wound (orange), the area covered in 24 h (blue), and the remaining wound area (grey). B: Data were compiled from two separate experiments (with 3-8 wounds per condition, per experiment). *Scale bar: 400 µm.*

3.2.2 COX-2 inhibition had no effect on wound healing in Caco2 cells

The initial wound healing results were contrary to the original hypothesis, that PAR2-induced COX-2-derived lipid mediators would enhance wound healing in Caco2 cells. The role of COX-2 was still investigated to determine if COX-2-derived lipid mediators were involved but had an inhibitory effect on wound healing. Caco2 cells treated with the COX-2 selective inhibitor NS398 (10 µg/mL) showed no significant difference in wound healing over 48 h compared to cells treated with DMSO as a vehicle control, in each experimental condition (control, 2fO or 2fLI; representative images Figure 3.10 A, quantification Figure 3.10 B). To confirm that NS398 inhibited COX-2 activity, NS398 was added to cells treated with 2fLI (0.5 µM) for 3 h in a single time course experiment from the first section, and the supernatants were analyzed for PGEM by ELISA (Figure 3.10 C). These data highlight that the COX-2 inhibitor was functional, and PAR2-induced COX-2 did not play a role in the PAR2-mediated inhibition of wound healing in Caco2 cells.

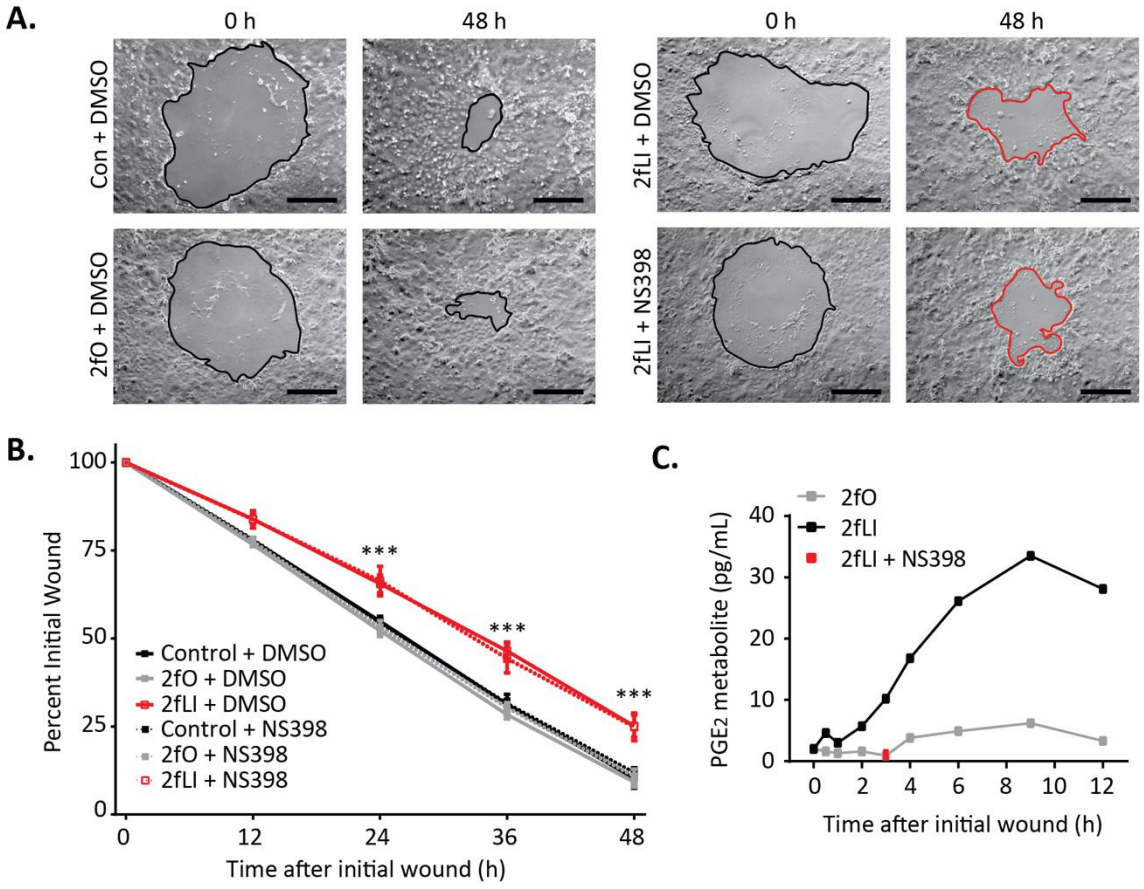

Figure 3.10 PAR2 inhibition of wound healing in Caco2 cells was not dependent on COX-2.

Caco2 cells were plated and wounded according to the standard protocol, and either DMSO or the COX-2 selective inhibitor NS398 (10 µg/mL) was added to the cells at 0 h and 24 h, in addition to 2fO or 2fLI (10 µM) every 12 h. A: Representative images of the same wound at 0 h and 48 h are shown for select conditions. B: Quantification of wound closure (n=4-5). C: During a single ELISA performed with the PAR2-induced COX-2 time course in the previous section, the ability of NS398 to inhibit COX-2 activity was confirmed. *Statistics: data in B were analyzed using a two-way ANOVA with Bonferroni's multiple comparisons test. (***p<0.001 – significantly different from control and 2fO, independent of NS398) Scale bar: 500 µm.*

3.2.3 PAR2 activation had no effect on proliferation in subconfluent or wound-edge cells, but promoted proliferation in confluent Caco2 cells

Two main facets of wound healing are proliferation and migration. In order to test if PAR2 activation reduced wound healing by affecting proliferation, Caco2 cells were grown in either low (0.5%) or high (10%) serum, with or without 2fLI or 2fO (10 μM) for 72 h, and the final cell number was indirectly measured using an XTT assay. There was no significant difference in final cell number between control, 2fO, or 2fLI in low or high serum conditions (Figure 3.11). Therefore, PAR2 activation did not have an effect on proliferation of subconfluent Caco2 cells.

Since the XTT assay indirectly measured the effect of PAR2 activation on only subconfluent cells, EdU staining was used to more thoroughly study proliferation by also assessing confluent and wound-edge cells. Caco2 cells treated with 2fO or 2fLI (10 μM) for either 12 h or 24 h were exposed to EdU for 2 h before fixation. EdU was stained to identify proliferating cells, and DAPI was used to detect total cell number. With subconfluent cells, it was confirmed that PAR2 activation had no effect compared to control and 2fO-treated cells (Figure 3.12 A, B, middle panels). With wound-edge cells, there was also no significant difference in proliferation at 12 h or 24 h with 2fLI treatment compared to 2fO or control (Figure 3.12 A, B, right panels). However, at 12 h there was a significant increase in proliferation with PAR2 activation in confluent cells (Figure 3.12 A, B, left panels). Regardless, the effect of PAR2 activation on Caco2 proliferation does not explain the inhibition of wound healing.

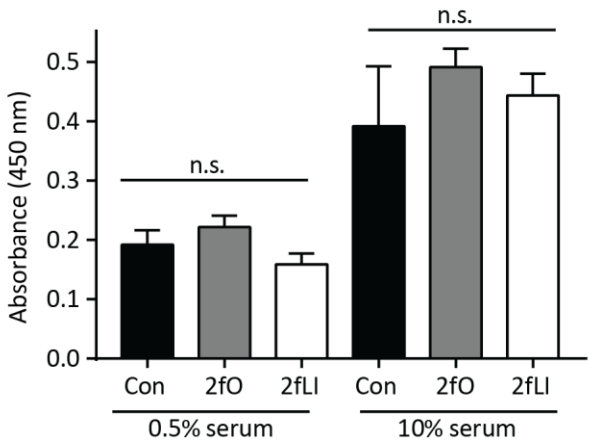

Figure 3.11 PAR2 had no effect on the proliferation of subconfluent Caco2 cells.

Caco2 cells (6 x 10^3 cells/well, 96 well plate) were plated in media containing either 0.5% serum or 10% serum. After plating, cells were treated with 2fO or 2fLI (10 µM) every 12 h for 72 h. An XTT assay was performed to indirectly measure the final cell number after 3 days of proliferation with and without PAR2 activation. *Statistics: data were analyzed using a one-way ANOVA.*

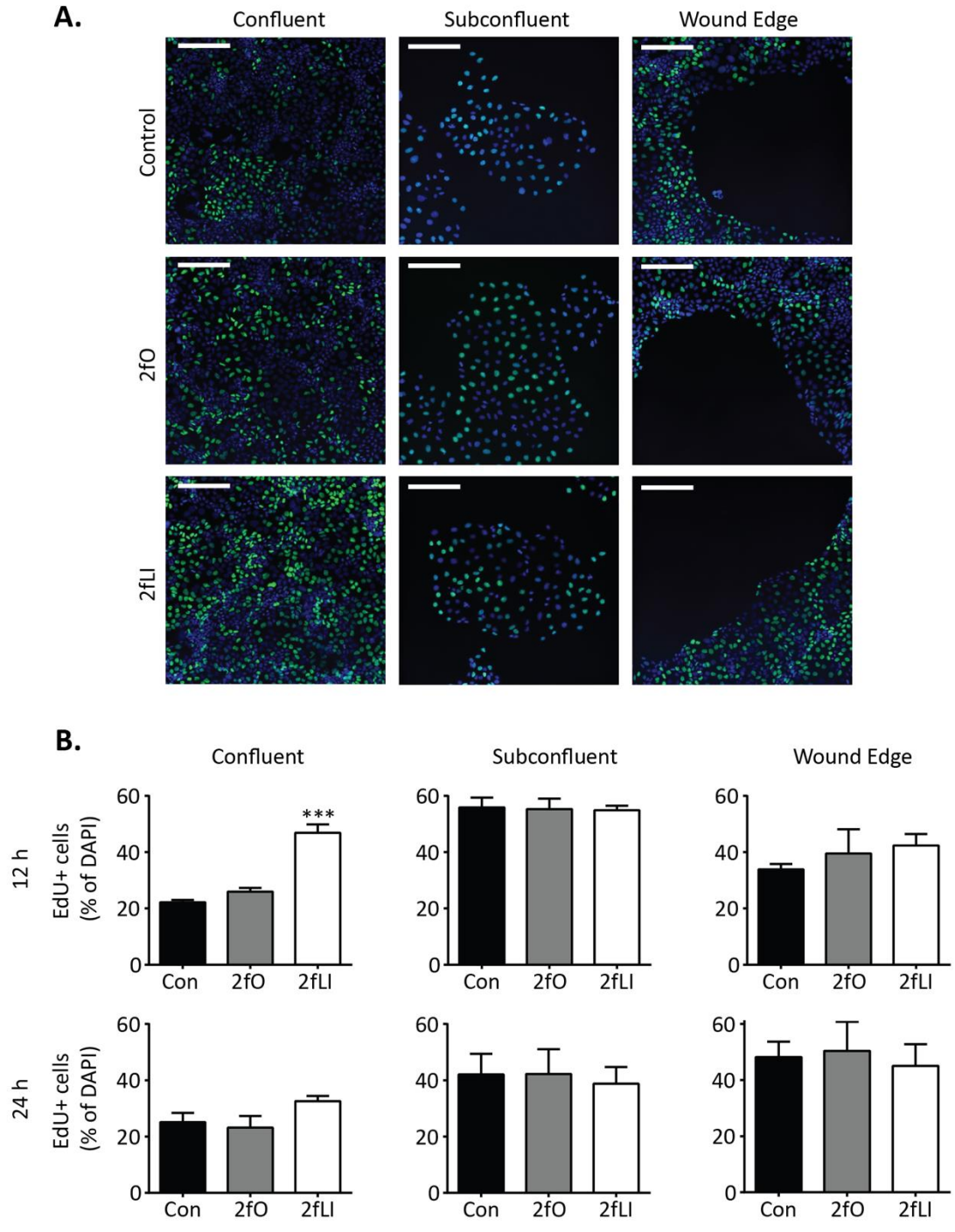
A.
Confluent
Subconfluent
Wound Edge
Control
2fO
2fLI
B.
Confluent
Subconfluent
Wound Edge
12 h
24 h
EdU+ cells (% of DAPI)
60
40
20
0
***
Con
2fO
2fLI

Figure 3.12 PAR2 activation increased proliferation in confluent Caco2 cells, but had no effect on subconfluent or wound-edge cells.

Caco2 cells were plated and wounded according to the staining protocol, and analyzed at 12 h and 24 h. For the 12 h time-point, cells were wounded, then treated with 2fO or 2fLI (10 µM) at 0 h and returned to the incubator for 12 h. From 12 – 14 h, cells were incubated with EdU and then fixed. For the 24 h time-point, cells were wounded then treated with peptides at 0 h and 12 h, and incubated with EdU from 22 h – 24 h before fixation. Wide-field images were captured, and ImageJ was used to automatically count both DAPI (blue) and EdU+ (green) cells. A: Representative images from confluent, subconfluent, and wound-edge conditions for control, 2fO and 2fLI treated cells at the 12 h time point. B: Quantification (expressed as percent EdU positive cells compared to total DAPI positive cells) of the confluent, subconfluent, and wound-edge data from the 12 h and 24 h time-points (n=4 individual experiments with 3 FOV/experiment). *Statistics: data in B were analyzed using a one-way ANOVA with Bonferroni's multiple comparisons test. (*** p<0.001 – compared to control and 2fO) Scale bar: 200 µm.*

3.2.4 Migration of Caco2 cells was reduced with PAR2 activation

Since the PAR2-mediated inhibition of wound healing could not be explained by a change in proliferation, the next step was to test the hypothesis that PAR2 activation reduced wound healing by inhibiting cell migration.

First, single cell migration was analyzed using the xCelligence system that functions as a modified Boyden-chamber assay. Caco2 cells were lifted using EDTA (without trypsin) and suspended in media, with or without 2fLI (10 μM). Cells were plated on top of the microporous membrane in the xCelligence CIM-Plate, and the electrical impedance (cell index) measured from the underside of the membrane detected the Caco2 cells that had migrated through the membrane, in the absence of a chemotactic gradient. Over 24 h, there was a linear increase in migrating cells under control conditions, but significantly fewer cells were detected with PAR2 activation (Figure 3.13), indicating that PAR2 activation inhibited single cell migration.

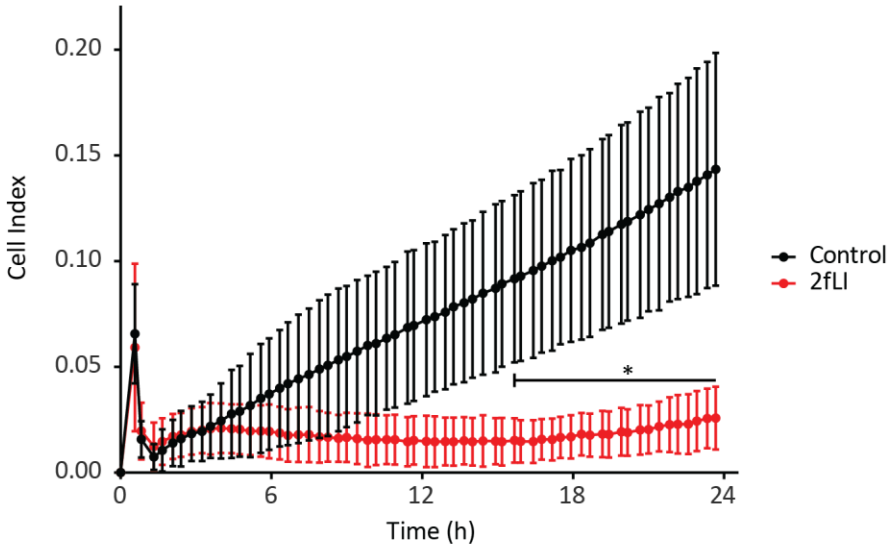

Figure 3.13 PAR2 activation inhibited Caco2 single cell migration.

Caco2 cells (1 x 10^4 cells/well, CIM-Plate 16 well) were plated to be analyzed using the xCelligence RTCA in a Boyden chamber-like assay. Cells that migrated through the chamber were sensed by electrodes on the underside of the membrane to give an impedance measurement, plotted as cell index. Impedance measurements were taken every 20 min for 24 h. Cells were treated with 2fLI (10 µM). A lower cell index indicates decreased migration (n=3 individual experiments with 3 wells per condition per experiment). *Statistics: data were analyzed using a two-way ANOVA with Bonferroni's multiple comparisons test. (* p<0.05)*

To assess the effect of PAR2 activation on Caco2 sheet migration, wound healing was measured over 48 h in the absence of proliferation by using cells pretreated with MMC (5 μg/mL) to inhibit proliferation. DMSO was used as the vehicle control. With both DMSO and MMC pretreatment, wounded Caco2 cells were able to heal, and PAR2 activation significantly inhibited wound closure compared to 2fO and control (Figure 3.14 A, B, left panels). Inhibition of proliferation was confirmed by pretreating cells with the same concentration of DMSO or MMC, and assessing proliferation using an EdU assay after 48 h (Figure 3.14 A, B, right panels). These data acquired in the absence of proliferation demonstrated that the PAR2-mediated inhibition of wound healing was through an effect on migration.

Additionally, live cell wound healing in Caco2 cells was used to directly measure the distance the wound-edge cell migration by tracking individual cells over 24 h. First, to ensure wound healing was comparable using cells within an incubator and cells within the live cell microscope chamber, wound healing of multiple wounds was measured at 0 h and 24 h in a single experiment (Figure 3.15 A). Once confirmed, live cell videos were made with control cells, and cells treated with 2fO or 2fLI (10 μM) by imaging wounds every 15 min for 24 h (Supplementary videos 1-3). In each video, 10 cells at the wound edge were tracked from 0 h to 24 h using MTrackJ (Figure 3.15 B). Cells at the wound edge with 2fLI treatment traveled a significantly shorter distance (87 μm in 24 h), compared to control cells (139 μm in 24 h) (Figure 3.15 C), further supporting the hypothesis that PAR2 activation inhibited wound healing by reducing migration.

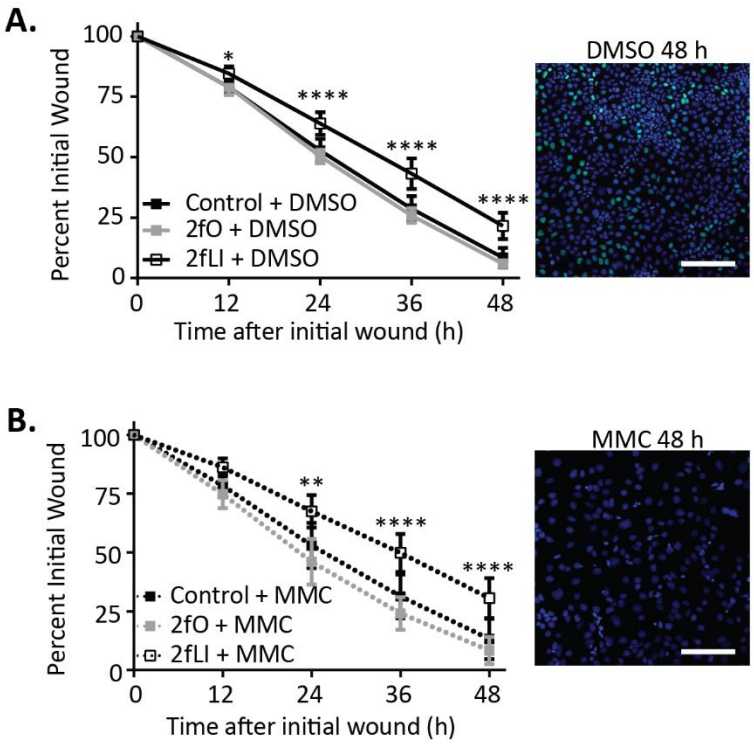

Figure 3.14 PAR2 activation inhibited wound healing in the absence of proliferation.

Caco2 cells were plated and wounded similar to the standard wounding protocol. However, 2 h prior to wounding, cells were treated with either DMSO (vehicle control) or MMC (5 µg/mL) to irreversibly inhibit proliferation. A, B: With both DMSO and MMC pretreatment, PAR2 activation with 2fLI (10 µM) was able to significantly inhibit wound healing compared to control and 2fO (n=6). In a similar experiment, cells were plated at the same density and treated for 2 h with either DMSO or MMC, washed well, and then incubated with EdU from 48 – 50 h in order to confirm that proliferation was inhibited for the entirety of the wound healing experiment (right panels in A and B). *Statistics: data were analyzed using a two-way ANOVA with Bonferroni's multiple comparisons test. (* p<0.05; ** p<0.01; **** p<0.0001 – compared to control and 2fO) Scale bar: 200 µm.*

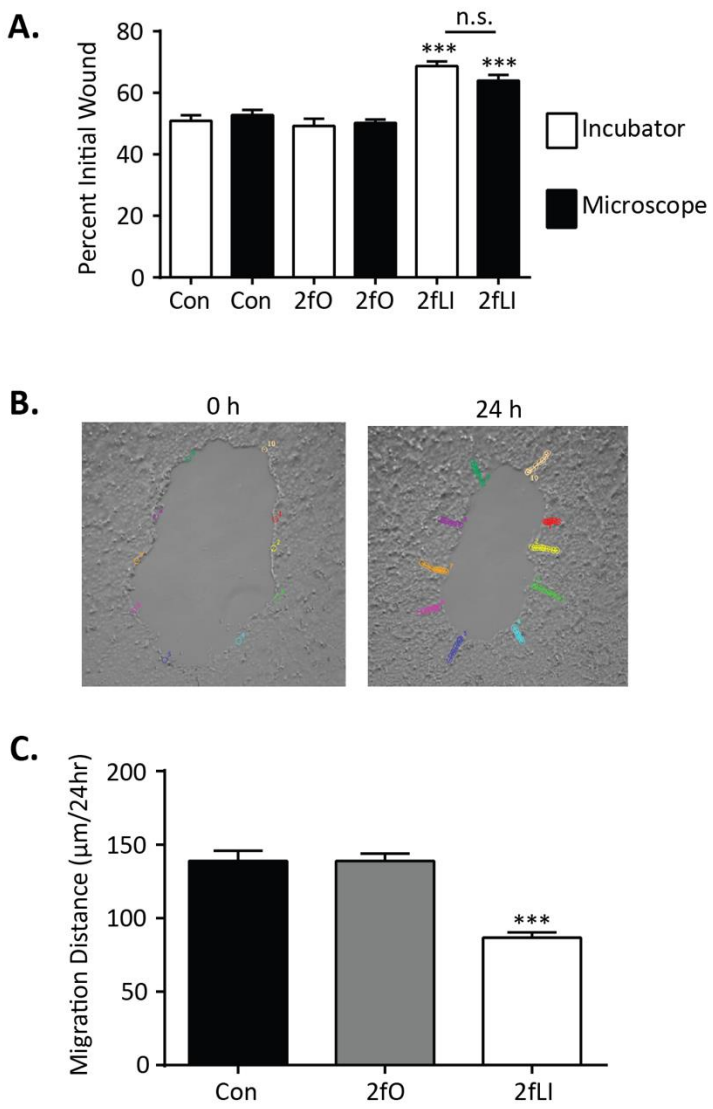

Figure 3.15 Addition of 2fLI reduced the migration distance of wound edge cells.

Caco2 cells were plated according to the live-cell wound healing protocol. A: Wound healing was compared in a single experiment (5-9 wounds per condition) between cells left in an incubator and cells within the microscope live-cell chamber. B, C: Using the images acquired from live-cell wound healing experiments, the MTrackJ plugin (ImageJ) was used to track wound-edge cells during the first 24 h following wounding. An example of 10 cells around the perimeter of a single wound tracked from 0 h to 24 h (B). PAR2 activation with 2fLI (10 µM) was able to significantly reduce the distance that the wound-edge cells travelled compared to control and 2fO (C). (n=4 separate experiments, with 3 wounds quantified per experiment, and 10 cells tracked in each wound). *Statistics: data in A and C were analyzed using a one-way ANOVA with Bonferroni's multiple comparisons test. (*** p<0.001 - compared to control and 2fO)*

3.2.5 PAR2 activation induced actin cabling surrounding the wound edge in Caco2 cells

Rationale: Cellular migration is controlled by Rho and Rac GTPases, which regulate lamellipodia and filipodia formation (Disanza et al. 2005). It was hypothesized that PAR2 activation inhibited migration in Caco2 cells by effecting lamellipodia formation at the wound edge.

Caco2 cells plated and wounded according to the staining protocol were fixed after 12 h or 24 h. Phalloidin was used to stain F-actin (green) and DAPI to visualize nuclei (blue). The entire wound border was visualized by stitching 20X widefield images. Representative images at 24 h are shown for control (Figure 3.16 A) and 2fLI (Figure 3.16 B) wounds. In control cells, there were numerous areas with lamellipodia formation at the wound edge (Figure 3.16 A inserts), whereas the wound edge in 2fLI-treated cells had very little lamellipodia, but obvious actin cabling (Figure 3.16 B inserts). Wounds at 12 h and 24 h were blindly quantified, and although there was no significant difference in actin properties at 12 h between 2fLI and control or 2fO (Figure 3.16 C, D), there was a significant increase in actin cabling and a significant decrease in lamellipodia in 2fLI-treated wounds compared to control and 2fO at 24 h (Figure 3.16 F, G).

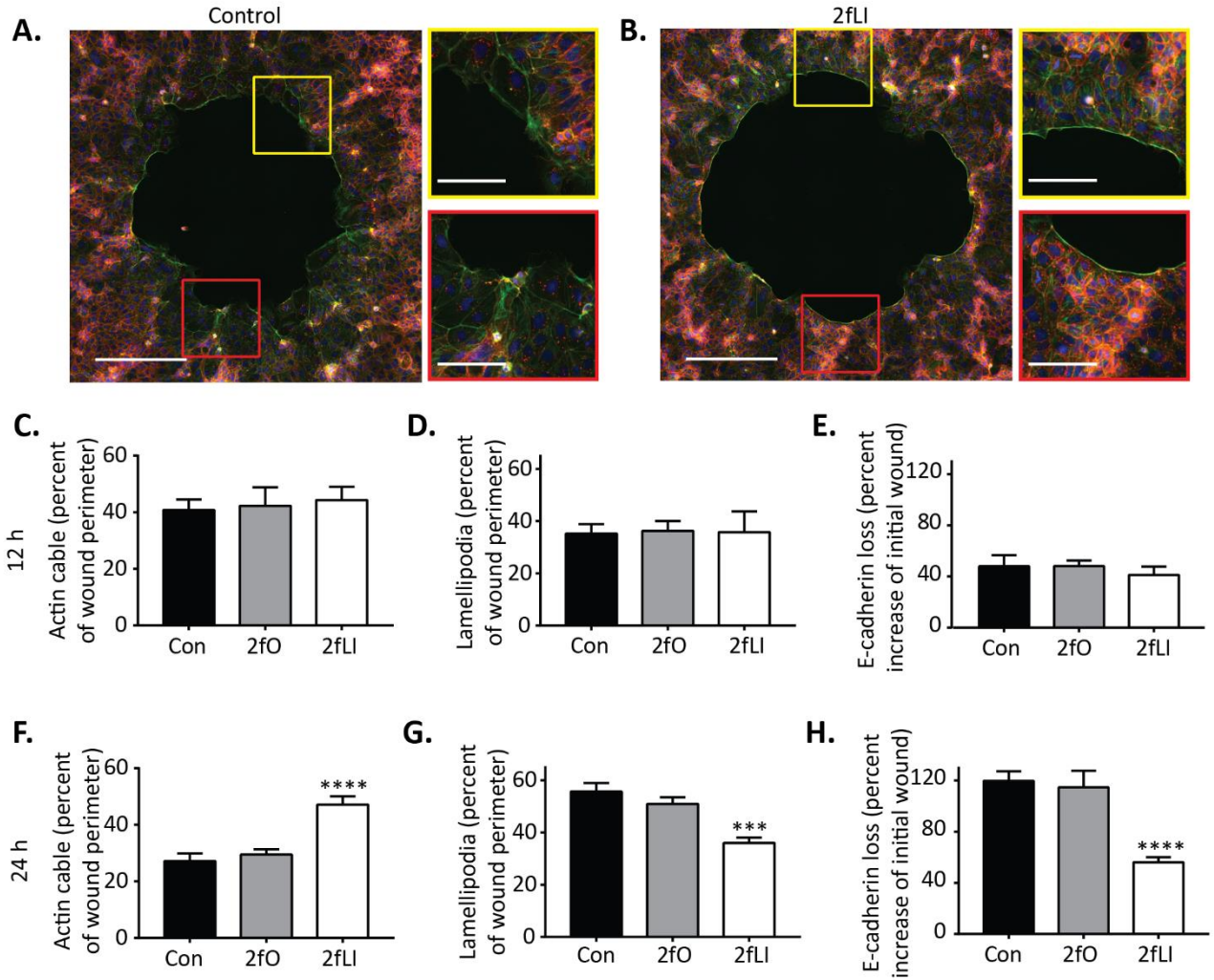
A.
Control
B.
2fLI
C.
12 h
Actin cable (percent of wound perimeter)
60
40
20
0
Con
2fO
2fLI
D.
Lamellipodia (percent of wound perimeter)
60
40
20
0
Con
2fO
2fLI
E.
E-cadherin loss (percent increase of initial wound)
120
80
40
0
Con
2fO
2fLI
F.
24 h
Actin cable (percent of wound perimeter)
60
40
20
0
****
Con
2fO
2fLI
G.
Lamellipodia (percent of wound perimeter)
60
40
20
0
***
Con
2fO
2fLI
H.
E-cadherin loss (percent increase of initial wound)
120
80
40
0
****
Con
2fO
2fLI

Figure 3.16 PAR2 activation reduced lamellipodia formation, and prevented the loss of E-cadherin at the wound edge in Caco2 cells.

Caco2 cells were plated according to the staining protocol, and were fixed at 12 h or 24 h post-wound. Cells were stained for F-actin (phalloidin, green), E-cadherin (red), and nuclei (DAPI, blue). A, B: Representative images of control and 2fLI-treated wounds, 24 h after wounding. Control cells showed lamellipodia formation and loss of E-cadherin surrounding the wound (A), whereas cells treated with 2fLI had actin cabling and E-cadherin expression remained high at the wound-edge (B). C-E: Blinded quantification of the actin cabling, lamellipodia formation, and E-cadherin loss in wounds at 12 h showed no significant difference between control/2fO and 2fLI treated cells. F-H: At 24 h after wounding, PAR2-activation resulted in increased actin cabling (F), fewer lamellipodia (G), and less E-cadherin internalization in wound-edge cells (H). *Statistics: data in C-H were analyzed using a one-way ANOVA with Bonferroni's multiple comparisons test (*** p<0.001, **** p<0.0001 – compared to control and 2fO). Scale bars – stitched image: 300 µm; 20X image: 100 µm.*

To further characterize actin cable formation at the wound edge, Caco2 cells were transfected with LifeAct-GFP to visualize actin-dynamics in live cells over 24 h. Videos were taken over 24 h (Supplementary videos 4, 5), and images are shown for cells at the edge of a control wound and a 2fLI wound every 3 h for the first 12 h (Figure 3.17 A, B). The F-actin movement was very dynamic in control cells, with initial formation of lamellipodia retracting to form a cable of actin by 6 h, and lamellipodia reforming by 9 h (Figure 3.17 A). F-actin was less dynamic in cells treated with 2fLI, with cable formation by 6 h that was maintained through 12 h (Figure 3.17 B).

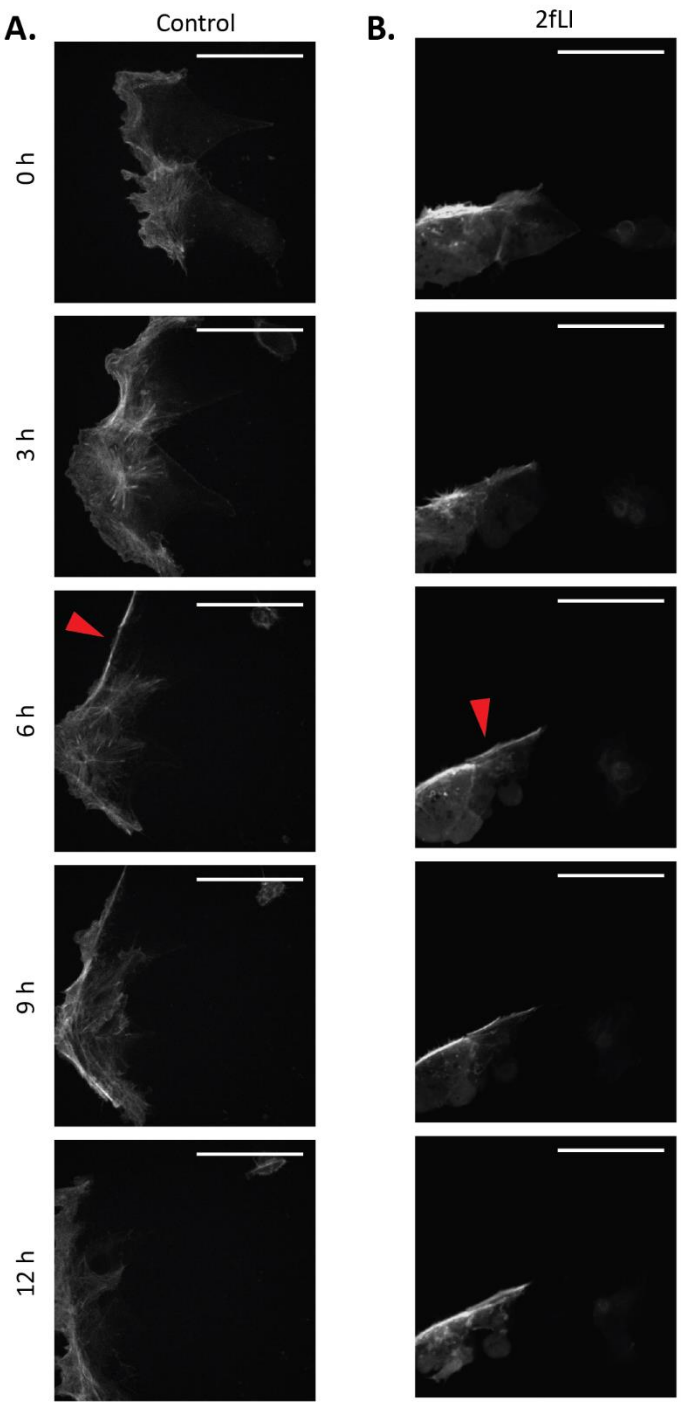
A.
Control
B.
2fLI
0 h
3 h
6 h
9 h
12 h

Figure 3.17 LifeAct imaging revealed cable formation and loss within the first 12 h in control Caco2 cells, but only cable formation in cells treated with 2fLI.

Caco2 cells (2.1 x 10^4 cells/well) were plated in an 8-well glass bottom chamber slide and transfected with LifeAct-GFP. After wounding, transfected cells at the edge of the wound were imaged on a spinning disk confocal every 15 min for 24 h. Single images are shown at 3 h intervals from 0 h to 12 h. A: In control cells, an actin cable formed by 6 h (red arrow) but lamellipodia returned by 9 h. B: Cells treated with 2fLI (10 µM) formed a cable by 6 h (red arrow), which remained through 12 h. Scale bar: 50 µm.

3.2.6 PAR2 activation affected E-cadherin internalization but not ZO-1 localization in Caco2 cells at the wound edge

Rationale: Epithelial cells undergo characteristic phenotypic changes prior to movement *in vitro*, including alterations in adherens junction and tight junction protein localization and expression (Huang, Guilford, and Thiery 2012). It was hypothesized that PAR2 activation was inhibiting migration in Caco2 cells by affecting the regulation of cell-cell junctions necessary for epithelial cells to migrate.

The adherens junction was analyzed in wounded Caco2 cells that were fixed at 12 h and 24 h post-wounding by staining E-cadherin (red) and DAPI (blue) to visualize the nuclei. The entire wound border was visualized by stitching 20X widefield images, and representative images at 24 h are shown for control (Figure 3.16 A) and 2fLI (Figure 3.16 B) wounds. In control cells, there was a distinct internalization of E-cadherin in cells surrounding the wound at 24 h (Figure 3.16 A inserts) compared to the intercellular E-cadherin expression in cells treated with 2fLI (Figure 3.16 B inserts). When the loss of E-cadherin was blindly quantified at 12 h and 24 h, there was no significant difference between control, 2fO and 2fLI at 12 h, however there was significantly more E-cadherin loss in control and 2fO wounds compared to 2fLI wounds (Figure 3.16 E, H).

The tight junction was analyzed in wounded Caco2 cells fixed 24 h after wounding, and stained for ZO-1 (green) and DAPI (blue). Representative images from 4 individual experiments are shown for control and 2fLI wounds, as well as an IgG control (Figure 3.18

A-C). ZO-1 expression was even throughout the monolayer up to the edge of the wound, with no differences between control, 2fO (not shown) and 2fLI wounds.

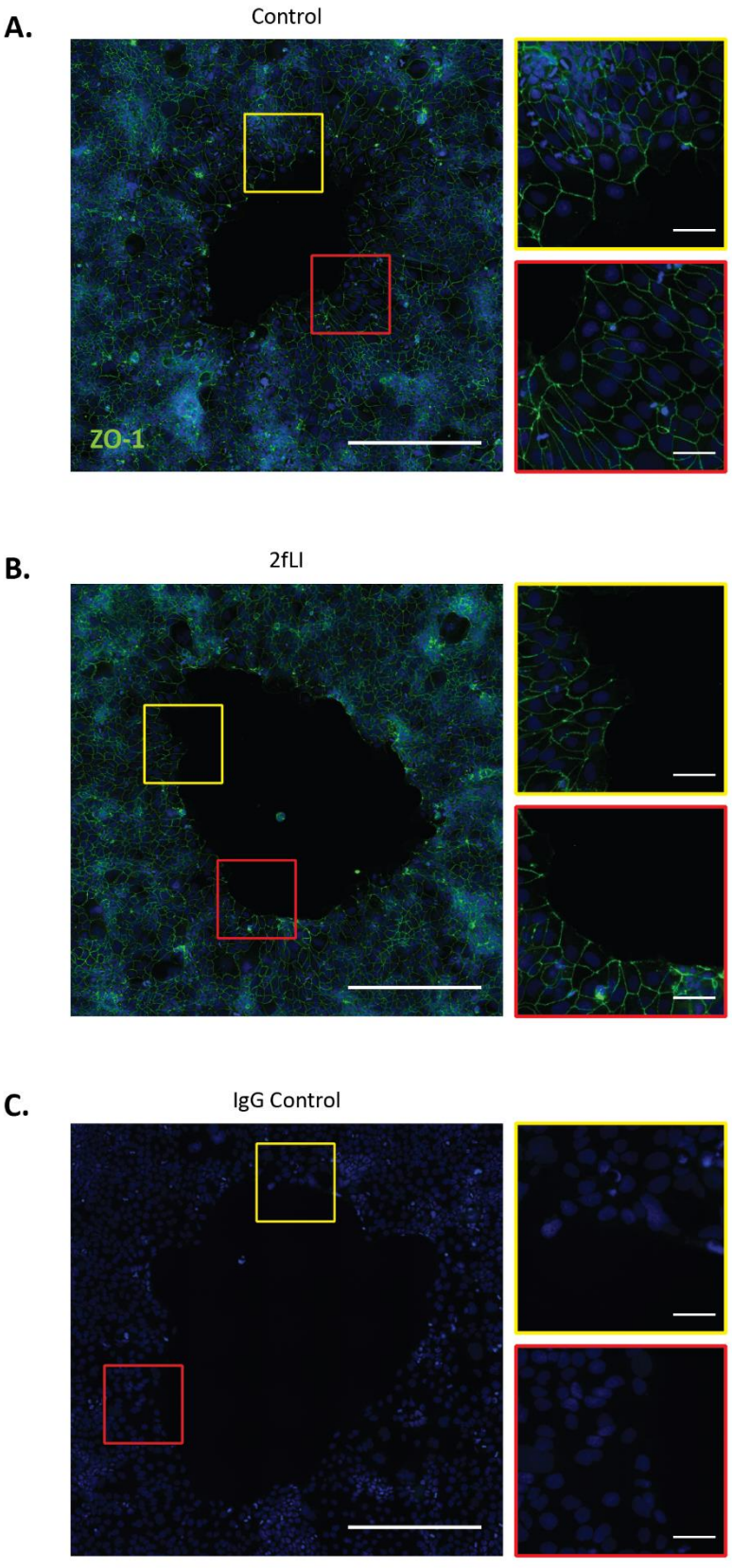
A.
Control
ZO-1
B.
2fLI
C.
IgG Control

Figure 3.18 ZO-1 is maintained during wound healing in Caco2 cells independently of PAR2 activation.

Caco2 cells were plated and wounded according to the staining protocol, and were fixed 24 h post-wound. A, B: Both control and 2fLI wounds showed similar ZO-1 expression throughout the monolayer, without any loss in cells surrounding the wound edge (representative images from n=4 independent experiments with 2 wounds per condition per experiment). C: Mouse IgG control. *Scale bars – stitched image: 400 µm; 20X image: 50 µm.*

3.2.7 No evidence of typical EMT was found at the wound edge in Caco2 cells

With the changes observed in E-cadherin at the wound-edge, and knowing that E-cadherin internalization is associated with EMT (Huang, Guilford, and Thiery 2012), it was hypothesized that PAR2 activation could inhibit wound healing-associated EMT in Caco2 cells.

First, in order to determine if Caco2 cells undergo EMT changes at the wound edge to facilitate wound healing, cells were wounded and fixed after 24 h, then stained for three typical markers of EMT: SNAIL (Figure 3.19), N-cadherin (Figure 3.20), and vimentin (Figure 3.21). Caco2 cells had very low expression of all three markers, and the expression was not changed near the wound edge. PAR2 activation had no effect on protein expression or localization.

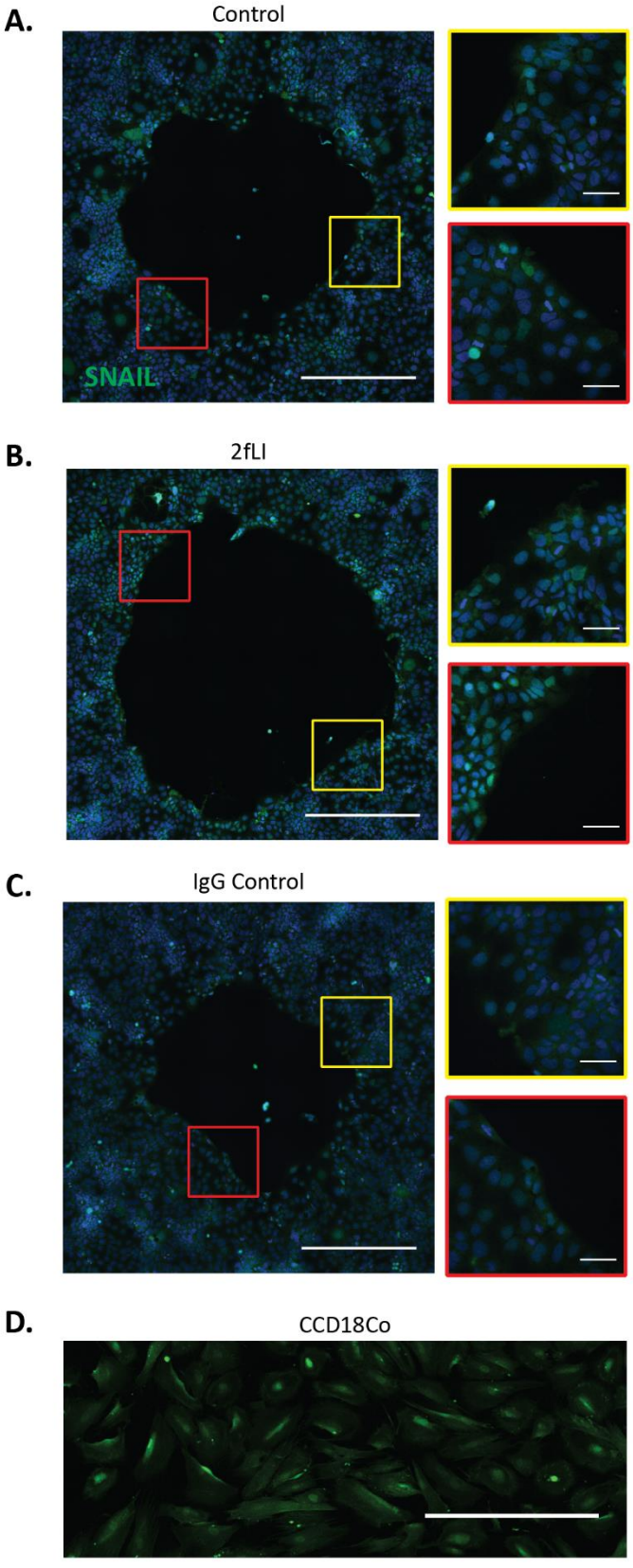
A.
Control
SNAIL
B.
2fLI
C.
IgG Control
D.
CCD18Co

Figure 3.19 SNAIL expression does not change with PAR2 activation or during wound healing.

Caco2 cells were plated and wounded according to the staining protocol, and were fixed 24 h post-wound. A, B: Both control and 2fLI wounds showed a very low level of SNAIL expression throughout the monolayer, without any change in cells surrounding the wound edge (representative images from n=4 independent experiments with 2 wounds per condition per experiment). C: Mouse IgG control. D: SNAIL expression in CCD18Co fibroblasts as a positive control. *Scale bars – stitched image: 400 µm; 20X image: 50 µm.*

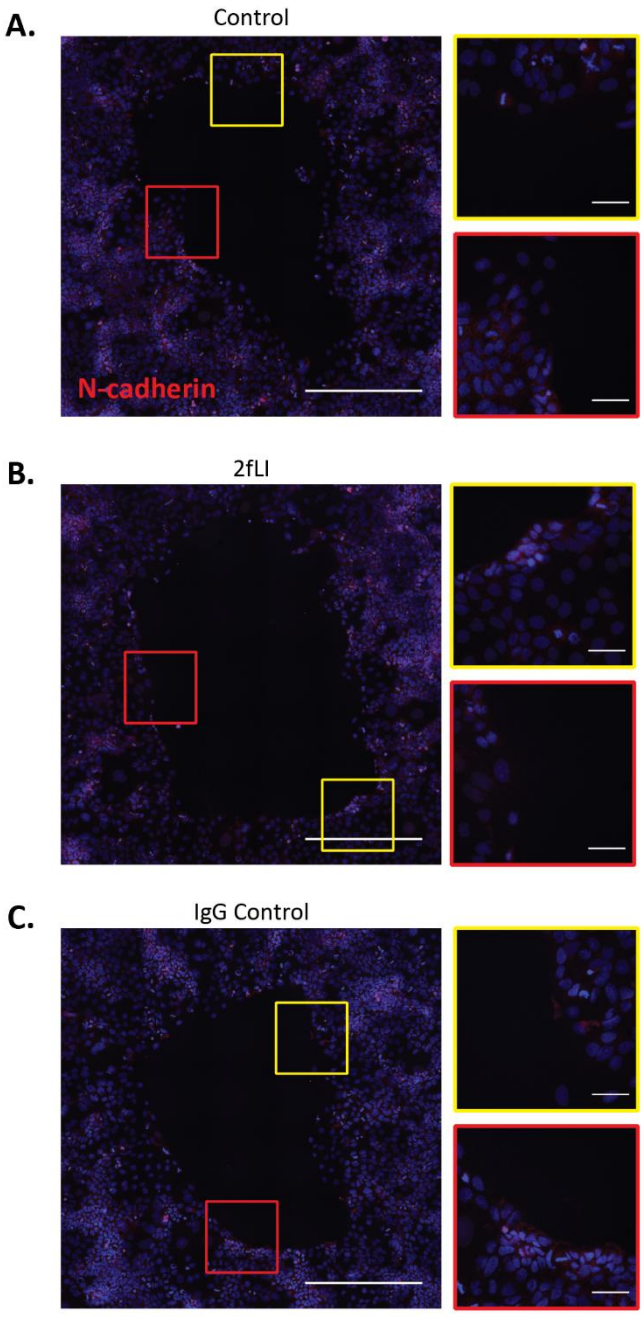

Figure 3.20 N-cadherin expression does not change with PAR2 activation or during wound healing.

Caco2 cells were plated and wounded according to the staining protocol, and were fixed 24 h post-wound. A, B: Both control and 2fLI wounds showed a very low level of N-cadherin expression throughout the monolayer, without any change in cells surrounding the wound edge (representative images from n=4 independent experiments with 2 wounds per condition per experiment). C: Mouse IgG control. *Scale bars – stitched image: 400 µm; 20X image: 50 µm.*

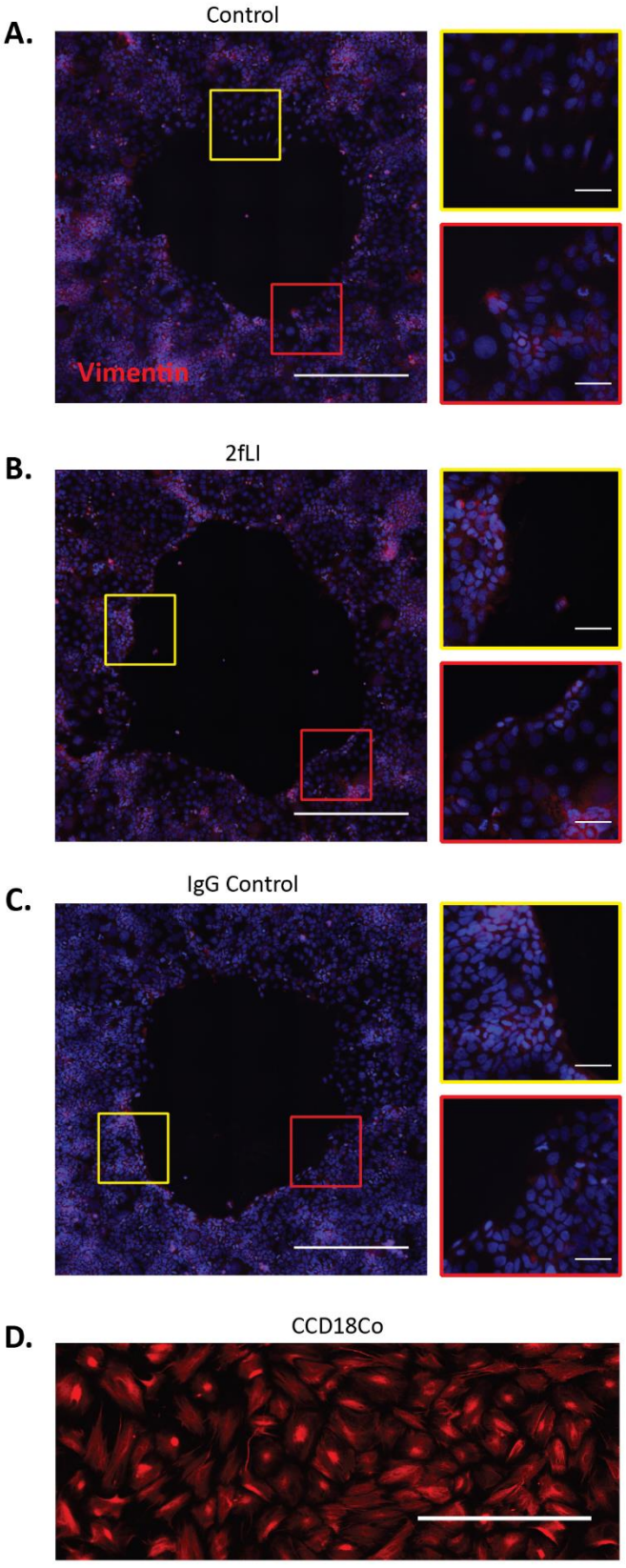
A.
Control
Vimentin
B.
2fLI
C.
IgG Control
D.
CCD18Co

Figure 3.21 Vimentin expression does not change with PAR2 activation or during wound healing.

Caco2 cells were plated and wounded according to the staining protocol, and were fixed 24 h post-wound. A, B: Both control and 2fLI wounds showed a very low level of vimentin expression throughout the monolayer, without any change in cells surrounding the wound edge (representative images from n=4 independent experiments with 2 wounds per condition per experiment). C: Mouse IgG control. D: Vimentin expression in CCD18Co fibroblasts as a positive control. *Scale bars – stitched image: 400 µm; 20X image: 50 µm.*

3.2.8 Wound healing in Caco2 cells was dependent on transcription

With a known association between transcriptional activity and cell motility (Olson and Nordheim 2010), the contribution of transcription to Caco2 wound healing was assessed.

When Caco2 cells were treated with actinomycin D (5 μg/mL) to inhibit transcription during a standard wound healing experiment for 48 h, the ability of the wounds to heal was almost entirely prevented (control wound healed 14% at 48 h) compared to cells treated with an equivalent volume of DMSO as control (control wound healed 94% at 48 h) (Figure 3.22). PAR2 activation did not have a significant effect on wound healing in the absence of transcription.

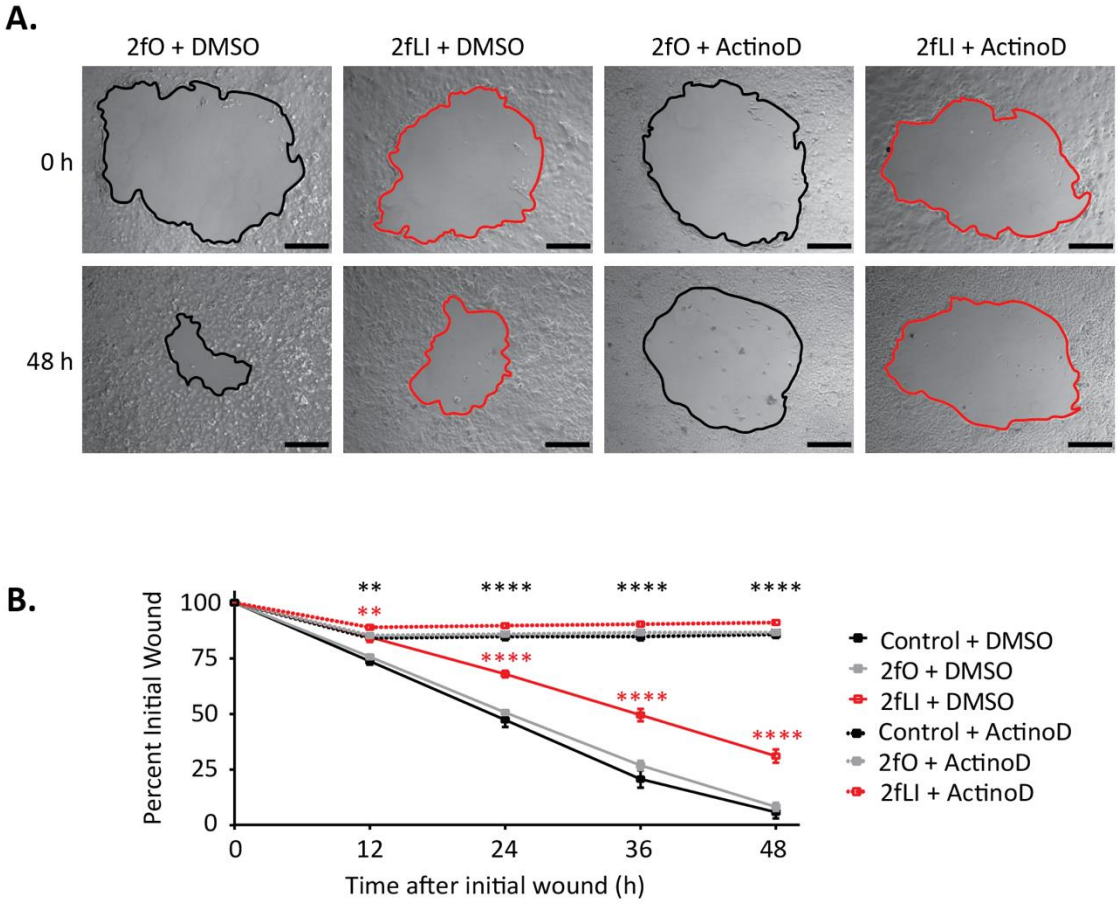

Figure 3.22 Wound healing in Caco2 cells was dependent on transcription.

Caco2 cells were plated and wounded according to the standard protocol, and treated with either actinomycin D (5 μg/mL) or an equivalent volume of DMSO (1:200) prior to the addition of 2fO or 2fLI (10 μM at 0 h). A: Representative images of the same wound at 0 h and 48 h, with either 2fO or 2fLI, and DMSO or actinomycin D (n=4). Cells treated with actinomycin D were unable to heal. B: PAR2 activation significantly inhibited wound healing when cells were exposed to DMSO alone. All cells exposed to actinomycin D had significantly inhibited wound healing compared to DMSO, with no significant difference between control, 2fO, and 2fLI. *Statistics: data in B were analyzed using a two-way ANOVA with Bonferroni's multiple comparisons test. (** p<0.01; **** p<0.0001. Red: 2fLI + DMSO significantly different than 2fO and control + DMSO. Black: Actinomycin D significantly different than DMSO.) Scale bar: 400 μm.*

3.2.9 PAR2 activation induced a pro-wound-healing transcriptional program in Caco2 cells

Caco2 cells were wounded in a grid pattern to maximize the number of wounded cells, and after 3 h, RNA was isolated and sent for RNA sequencing. The aligned files returned were run through CuffDiff, and gene lists were compiled based on two comparisons: non-wounded control (NW-C) vs wounded control (W-C), and NW-C vs non-wounded PAR2 activated (NW-PAR2). These data illustrated genes that were more than 2-fold increased or decreased when cells were either wounded, or when PAR2 was activated. As an initial comparison, the gene lists were compared with Venn diagrams in order to visualize the overlap in gene expression (Figure 3.23). Surprisingly, 113/128 (88%) of genes increased with wounding were also increased when PAR2 was activated (Figure 3.23 A). Of the overlapping genes that were increased, particular genes of interest are highlighted in Table 3.1. There was also considerable overlap between genes decreased with each treatment (Figure 3.23 B). Importantly, PAR2 activation did not increase any gene that was decreased with wounding (Figure 3.23 C), or conversely did not decrease any gene that was increased with wounding (Figure 3.23 D). The detailed list of genes and specific pathway analysis is found in Appendix B.

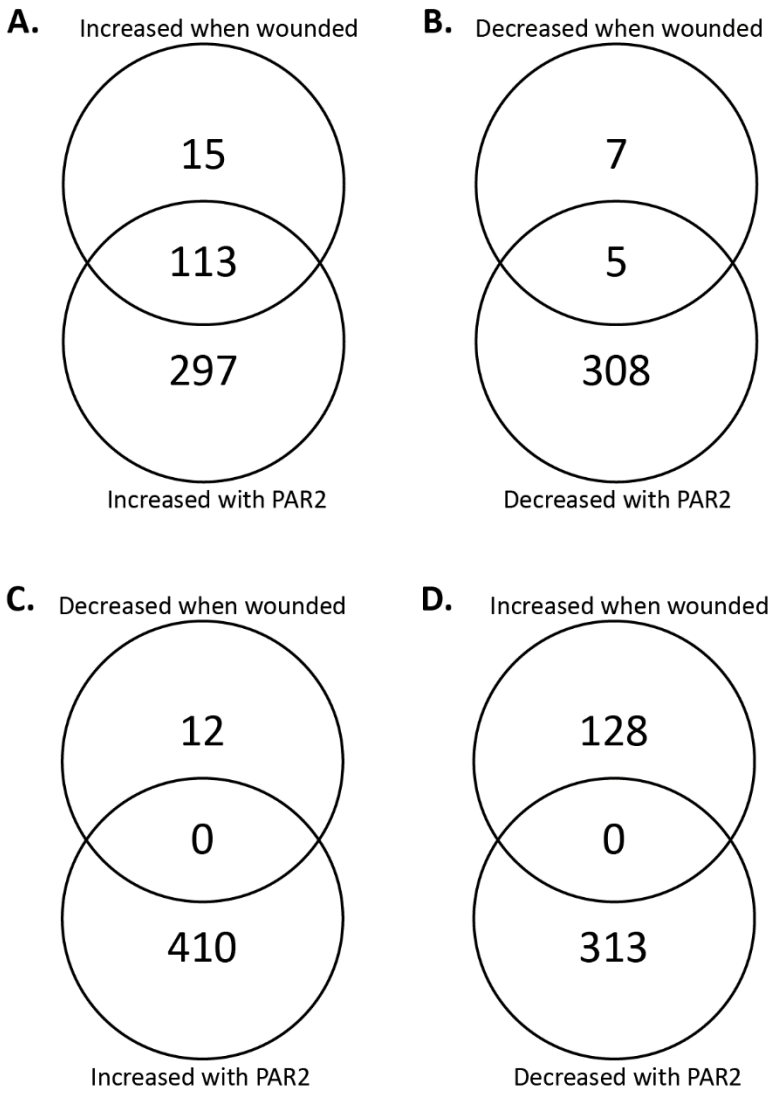

Figure 3.23 RNA sequencing figures.

Caco2 cells were either wounded, or treated with 2fLI (10 µM) for 3 h, and isolated RNA was sequenced. With CuffDiff, differential gene expression tests were created for two comparisons: NW-C vs W-C, and NW-C vs W-PAR2. Gene lists were made using a 2-fold change cut-off, and compared using Venn diagrams. A: Overlap of 113 genes that were increased with wounding and increased with PAR2 activation. B: Overlap of 5 genes that were decreased with wounding and decreased with PAR2 activation. C: No overlap of genes that were decreased with wounding and increased with PAR2 activation. D: No overlap of genes that were increased with wounding and decreased with PAR2 activation.

Table 3.1. Genes of interest increased with wounding in control cells, and increased with PAR2 activation in unwounded cells.

GENE SYMBOL	*PROTEIN NAME*
PTGS2	Prostaglandin-endoperoxide synthase 2 (also known as COX-2)
F2RL1	Coagulation factor II receptor-like 1 (also known as PAR2)
ADAMTS9	A disintegrin and metalloprotease with thrombospindin type 1 motif 9
MMP1	Matrix metalloprotease 1
MMP10	Matrix metalloprotease 10
ANXA1	Annexin A1
AREG	Amphiregulin
EREG	Epiregulin
FOS	FBJ murine osteosarcoma viral oncogene homolog (also known as AP-1 transcription factor subunit, c-Fos)
FOSB	FBJ murine osteosarcoma viral oncogene homolog B
FOSL1	FOS-like antigen 1
JUN	Jun proto-oncogene (also known as AP-1 transcription factor subunit, c-Jun)
JUNB	JunB proto-oncogene
CCL20	Chemokine (C-C motif) ligand 20
CXCR4	Chemokine (C-X-C motif) receptor 4
CXCL8	Chemokine (C-X-C motif) ligand 8 (also known as IL-8)

3.3 PAR2-mediated enhancement of wound healing in T84 cells

The original hypothesis, that COX-2 derived lipid mediators could enhance wound healing following PAR2 activation, was considered in T84 cells. Although PAR2-induced COX-2 has been described in other intestinal epithelial cell lines, including Caco2 and IEC-6 (Hirota et al. 2012), it has not been shown in T84 cells.

3.3.1 COX-2 was not detected in T84 cells

T84 cells grown for 4 days were serum-starved for 1 h, then treated for 4 h with 2fLI (0.5 – 10 μM) or 2fO (10 μM), and control cells were left untreated. Positive control cells were treated with a mix of TNFα (10 ng/mL), IFNγ (10 ng/nL) and LPS (1 μg/mL) for 4 h. Additionally, T84 whole-cell lysates were run on a western blot beside Caco2 lysates to confirm the correct COX-2 band (72 kDa). COX-2 was not detected in T84 cells with any treatment, or with either of the two primary antibodies tested (Figure 3.24).

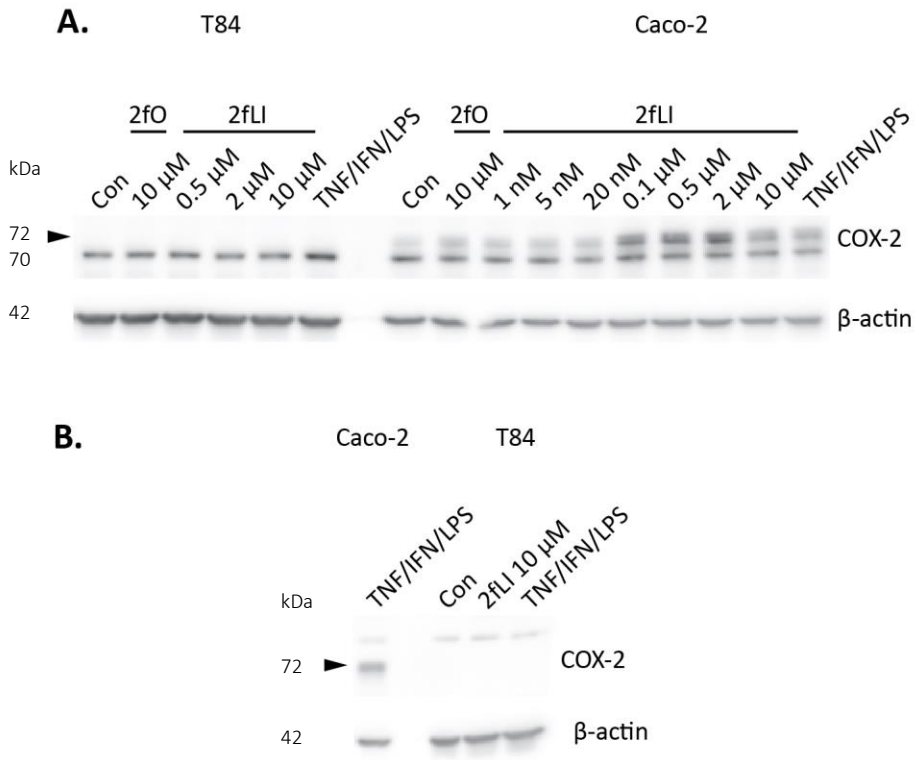

Figure 3.24 T84s did not express COX-2 in response to PAR2 activation, or to treatment with TNFα/IFNγ/LPS.

T84 cells (5 x 10^5 cells/well) were plated in a 12 well plate and grown for 4 days. Following 1 h serum starvation, cells were treated for 4 h with either 2fO (10 µM), 2fLI (0.5 – 10 µM), or a mix of TNFα (10 ng/mL), IFNγ (10 ng/nL) and LPS (1 µg/mL) as a positive control. A dose-response or a positive control with Caco2 cells is shown for comparison, and the correct COX-2 band noted with a small arrow. A: Santa Cruz COX-2 antibody sc1745. B: Cayman COX-2 antibody 160126.

3.3.2 PAR2 activation increased wound healing in T84 cells

The role of PAR2 activation in T84 wound healing was studied in order to determine if the PAR2-mediated inhibition of wound healing previously described in Caco2 cells was cell line-dependent. T84 cells were plated using the live-cell protocol, and images were captured every 15 min over 24 h (Supplementary videos 6-8). Representative images of a control wound and 2fLI-treated wound (10 µM) were traced at 0 h (black) and 24 h (white) to demonstrate the small change in wound area, and the enhanced wound healing with PAR2 activation (Figure 3.25 A). Quantification of 6 separate experiments (Figure 3.25 B) accurately reflect the healing dynamics seen in the live-cell videos, where control wounds began to heal but did not maintain movement, whereas PAR2 activation caused the cells to continuously heal over 24 h. When individual T84 cells at the edge of the wound were manually tracked using MTrackJ, PAR2 activation significantly increased cell migration (71 µm in 24 h) compared to control cells (48 µm in 24 h) (Figure 3.25 C).

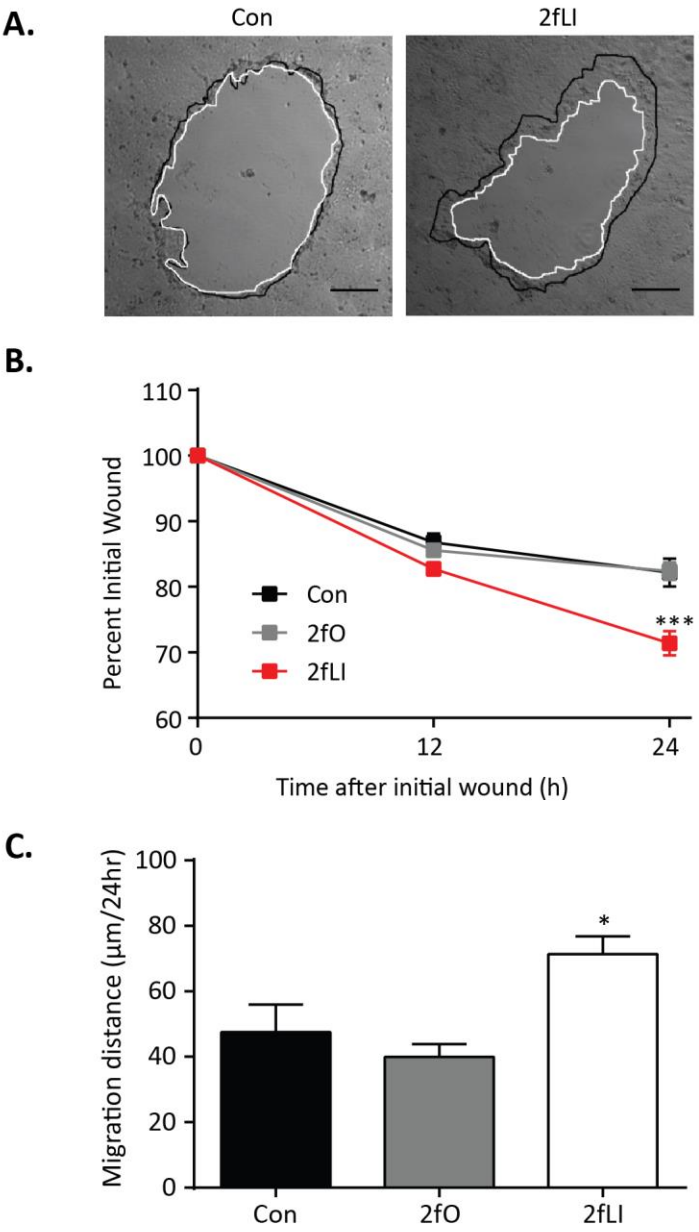
A.
Con
2fLI
B.
Percent Initial Wound
110
100
90
80
70
60
Con
2fO
2fLI
***
0
12
24
Time after initial wound (h)
C.
Migration distance (µm/24hr)
100
80
60
40
20
0
*
Con
2fO
2fLI

Figure 3.25 PAR2 activation enhanced wound healing in T84 cells.

T84 cells were plated according to the live-cell wound healing protocol. A: Representative images of control and PAR2-activated wounds (2fLI, 10 µM). The black tracing was the initial wound, and the white tracing was the same wound at 24 h. B: Quantification of the wound area at 0 h, 12 h and 24 h showed PAR2-activation significantly enhanced wound healing in T84 cells. (n=6 individual experiments with 2-3 wounds per treatment per experiment) C: The MTrackJ plugin (ImageJ) was used to track wound-edge cells during the first 24 h following wounding. PAR2 activation (2fLI, 10 µM) was able to significantly reduce the distance that the wound-edge cells travelled compared to control and 2fO. (n=6 separate experiments, with 1 wound quantified per experiment, and 10 cells tracked in each wound) *Statistics: data in B and C were analyzed using a one-way ANOVA with Bonferroni's multiple comparisons test. (*p<0.05, ***p<0.001 - compared to control and 2fO) Scale bar: 250 µm.*

3.3.3 PAR2 activation inhibited proliferation in confluent and wound-edge T84 cells, but had no effect on subconfluent cells

In order to test if PAR2 activation enhanced wound healing by affecting proliferation in addition to increasing cell migration, EdU staining was used to assess confluent, subconfluent, and wound-edge cells. T84 cells treated with 2fO or 2fLI (10 µM) for either 12 h or 24 h were exposed to EdU (thymidine analog) for 2 h before fixation. EdU was stained to identify proliferating cells, and DAPI was used to detect total cell number. The Trainable Weka Segmentation tool (FIJI) was used to automatically count cells (Appendix A). Representative images are shown for the 24 h time point (Figure 3.26 A). Although there was no significant difference in proliferation at 12 h (Figure 3.26 B top panels), there was a significant decrease in proliferation with PAR2 activation in both confluent and wound-edge cells at 24 h (Figure 3.26 B bottom panels).

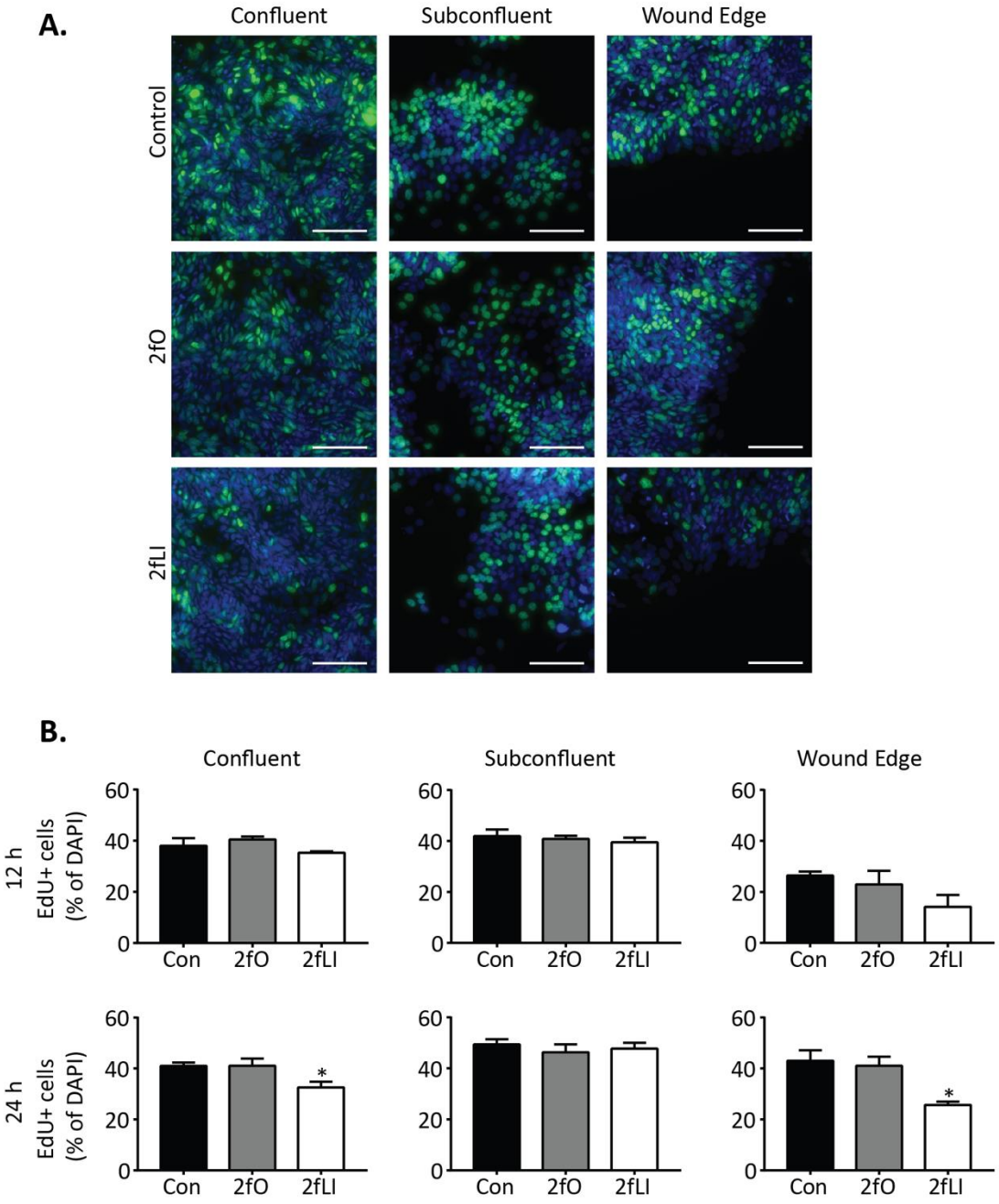
A.
Confluent
Subconfluent
Wound Edge
Control
2fO
2fLI
B.
Confluent
Subconfluent
Wound Edge
12 h
EdU+ cells
(% of DAPI)
24 h
EdU+ cells
(% of DAPI)
0
20
40
60
Con
2fO
2fLI
*

Figure 3.26 PAR2 activation decreased proliferation in confluent and wound-edge T84 cells.

T84 cells were plated and wounded according to the staining protocol, and analyzed at 12 h and 24 h. For the 12 h time-point, cells were wounded, then treated with 2fO or 2fLI (10 μM) at 0 h and returned to the incubator for 12 h. From 12 – 14 h, cells were incubated with EdU and then fixed. For the 24 h time-point, cells were wounded, treated with peptides at 0 h and 12 h, and incubated with EdU from 22 h – 24 h before fixation. Wide-field images were captured, and the Trainable Weka Segmentation tool within FIJI was used to automatically count both DAPI (blue) and EdU+ (green) cells. A: Representative images from confluent, subconfluent, and wound-edge conditions for control, 2fO and 2fLI treated cells at the 24 h time point. B: Quantification (expressed as percent positive EdU compared to total DAPI) of the confluent, subconfluent, and wound-edge data from the 12 h and 24 h time-points (n=4 individual experiments with 3 FOV/experiment), indicating PAR2 activation was able to significantly decrease proliferation in confluent and wound-edge cells at 24 h, but the effect was lost by 24 h. PAR2 activation had no effect on subconfluent cells. *Statistics: data in B were analyzed using a one-way ANOVA with Bonferroni's multiple comparisons test. (* $p<0.05$ – compared to control and 2fO) Scale bar: 100 μm.*

3.3.4 PAR2 activation enhanced lamellipodia formation and E-cadherin internalization in T84 cells at the wound edge

To further complement the findings from Caco2 cells, where PAR2 activation affected both actin dynamics and adherens junction components at the wound edge, these two important migration factors were also studied in T84 cells.

T84 cells plated and wounded according to the staining protocol were fixed after 24 h. Phalloidin was used to stain F-actin (green), E-cadherin for the adherens junction (red), and DAPI to visualize nuclei (blue). The entire wound border was visualized by stitching 20X widefield images. Representative images are shown for control (Figure 3.27 A), 2fO (Figure 3.27 B) and 2fLI (Figure 3.27 C) wounds. In control and 2fO wounds, there was some lamellipodia formation at the wound edge (Figure 3.27 A, B inserts), but the wound edge in 2fLI-treated cells had more lamellipodia (Figure 3.27 C inserts). In contrast to Caco2 cells, there was no actin cabling observed in T84 cells.

With the adherens junction, there was minor E-cadherin loss surrounding the wound in control and 2fO cells (Figure 3.27 A, B inserts) compared to the E-cadherin loss from cells treated with 2fLI (Figure 3.27 C inserts).

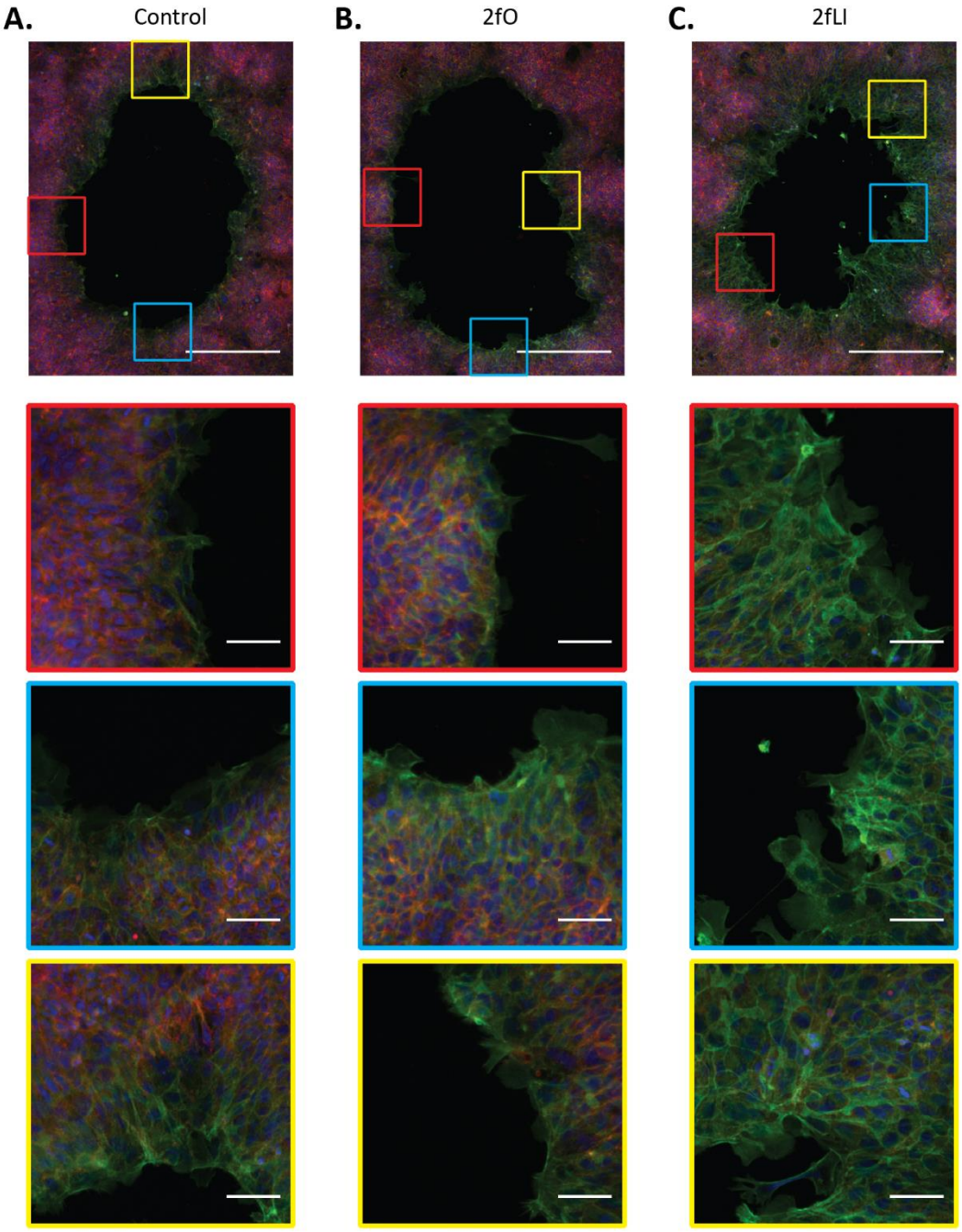
A.
Control
B.
2fO
C.
2fLI

Figure 3.27 PAR2 activation increased lamellipodia projections, and increased loss of E-cadherin surrounding the wound edge in T84 cells.

T84 cells were plated according to the staining wound healing protocol, and were fixed at 24 h post-wound. Cells were stained for E-cadherin (red), F-actin (phalloidin, green), and nuceli (DAPI, blue). A, B, C: Representative images of control, 2fO and 2fLI treated wounds. Control and 2fO cells showed limited lamellipodia formation and limited loss of E-cadherin surrounding the wound (A, B), whereas cells treated with 2fLI had greatly increased lamellipodia formation at the wound edge, as well as an increased loss of E-cadherin surrounding the wound (C). *Scale bars – stitched image: 400 µm; 20X image: 50 µm.*

CHAPTER 4

Discussion

4.1 Summary of findings

The results of this study were as unexpected as they were interesting. The original hypothesis, that PAR2-induced COX-2-derived lipid mediators would drive a pro-wound healing response in intestinal epithelial cells, had strong rationale. However, not only was COX-2 not involved in wound healing, but PAR2 activation inhibited Caco2 wound healing by reducing cell migration. Interestingly, the reduced migration was in the presence of increased cell proliferation in confluent Caco2 cells. When the actin dynamics and cell-cell junctions were investigated as potential mechanisms for decreased migration, PAR2 activation was found to affect both by inducing actin-cabling and preventing the internalization of E-cadherin. Due to the differences in E-cadherin, the role of EMT at the wound edge was investigated but was not found to play a role in Caco2 wound healing at the time points analyzed. To further investigate the effect of PAR2 on transcriptionally-dependent wound healing, RNA sequencing was performed which revealed that PAR2-activation, in the absence of wounding, induced a similar transcriptional profile compared to wounding alone. In order to determine if the effect observed was cell-line specific, wound healing was also investigated in T84 cells. PAR2 activation in T84s had the exact opposite effect compared to Caco2 cells, with enhanced wound healing through enhanced migration, decreased proliferation, and increased loss of E-cadherin at the wound edge. In addition to a detailed discussion of these results, future directions will also be proposed.

4.2 COX-2 expression in intestinal epithelial cells

The potential contribution of PAR2 activation to wound healing has been well described in the literature, and includes increased epithelial cell proliferation and migration in many cell types, including colon (Darmoul et al. 2004; Zhou et al. 2011), pancreas (Shimamoto et al. 2004; Shi et al. 2013), prostate (Mize, Wang, and Takayama 2008), and breast (Ge et al. 2004; Morris et al. 2006). PAR2-induced COX-2 expression was studied in Caco2 intestinal epithelial cells to determine if COX-2-derived lipid mediators were required for PAR2-mediated wound healing. In gastric mucosal lesions, COX-2 expression is increased early and most strongly at the edges of ulcerated regions, and the inhibition of COX-2 can delay ulcer healing (Schmassmann et al. 1998; Mizuno et al. 1997; Halter et al. 2001), indicating that COX-2 plays an important role in epithelial wound healing.

4.2.1 PAR2-induced COX-2 expression

PAR2 activation can induce the expression of COX-2 in many cell types, including the endothelium (Houliston et al. 2002), pancreas (Yada et al. 2005), airway (Kawao et al. 2005; Wang et al. 2008), bladder (Eguchi et al. 2011), and stomach (Zhang et al. 2012). The previous study that laid the groundwork for this project was the first to demonstrate that PAR2 activation induced COX-2 expression in intestinal epithelial cells (Hirota et al. 2012). The first point of discussion is the difference found between the Caco2 cells used in this previous work, and the Caco2 cells used here. In the previous study, using the same plating

protocol, PAR2-induced COX-2 was detected in post-confluent Caco2 cells (~day 8), but not in cells that had just reached confluence (~day 5). However, in the current study, PAR2 activation was able to increase COX-2 expression on day 5, but not day 8. Although these differences were not specifically investigated in this project, it is likely due to the fact that the Caco2 cells used in this project came from a different lab than the cells used in the previous study. Caco2 cells exhibit considerable variability from lab to lab, and their phenotype and differentiation is extremely sensitive to seeding density, passage number, filter support, matrix composition, media change frequency, and media composition (Volpe 2008; Vachon and Beaulieu 1992; Sambuy et al. 2005; Bestwick and Milne 2001). In an attempt to control for the Caco2 cell variability, the cells used here were de-differentiated according to a published Caco2 cell culture protocol (Natoli et al. 2012). Cells were passaged at less than 50% confluence for 10 passages, and multiple vials were saved in order to have a stable starting stock of Caco2 cells for this project.

Due to the difference in experimental day used, the day 5 response was further characterized with time course and dose response experiments. The time course showed a peak protein expression at 4 h, and peak COX-2 activity at 6 h. These results fit with COX-2 acting as an early response gene (Crofford 1997). With the dose response, 2fLI was found to have an EC_{50} of 48 nM for COX-2 expression. PAR2-induced COX-2 was also found to be dependent on transcription in Caco2 cells, which adds to the literature of transcriptional regulation of COX-2 by PAR2 activation in other cell types (Wang et al. 2008; Eguchi et al. 2011).

Components of the PAR2-COX-2 signaling pathway in Caco2 cells that were previously identified include Src tyrosine kinase, PI3K, and Rho-associated kinase (Hirota et al. 2012). In an attempt to further characterize the signaling pathway, Rac1 and CUX1 were investigated. The rationale behind investigating Rac1 includes its role in COX-2 expression (Chang et al. 2005), as well as its role downstream of EGFR activation (Zhu et al. 2015; Wu et al. 2007). Two pharmacological inhibitors were first used to target the activation of Rac1 by inhibiting different GEFs: NSC23766 to inhibit TrioN and Tiam1 (Gao et al. 2004), and EHOP-016 to inhibit Vav2 (Montalvo-Ortiz et al. 2012). EHOP-016 had no effect on PAR2-induced COX-2, and while not reaching significance, the few experiments performed with NSC23766 appeared to inhibit COX-2 expression. However, the possible inhibition was only seen with high concentrations (100 – 200 μM). It has since been shown in platelets that NSC23766 acts non-specifically above 100 μM, by demonstrating Rac-independent inhibition of PAK1 and PAK2, which are targets for Rac as well as Cdc42 (Dutting et al. 2015). In addition, siRNA was used to more specifically target Rac1. A significant knock down of 73% was achieved, but PAR2-induced COX-2 expression was not affected. The second signaling component investigated was CUX1, which is ubiquitous transcription factor that was previously shown to be necessary in PAR2-induced COX-2 expression in fibroblasts (Wilson et al. 2009). Using siRNA, a significant knock-down of 65% was achieved, but this had no effect on PAR2-induced COX-2. Although the simple conclusion from these data could be that Rac1 and CUX1 are not involved in the PAR2-COX-2 signaling pathway, it cannot be completely ruled out that a greater knock-down

efficiency is required. In order to ensure these data are real, a technique such as the CRISPR/Cas9 system could be used to achieve complete knock-out of the genes of interest.

4.2.2 Future directions for PAR2-induced COX-2 expression

Many transcription factors have been found to interact with the COX-2 promoter to induce its expression, including NF-κB, C/EBP, CREB, NFAT, AP-1, PPAR, and HIFα (Wu et al. 2010). A promising method to identify additional components of the PAR2-COX-2 signaling pathway may be to first determine the required transcription factors for this particular pathway. Experimentally this can be done by using a luciferase-expressing plasmid driven by the COX-2 promoter, and manipulating the promoter by truncation or site-directed mutagenesis. Identifying the transcription factors would allow for a more targeted approach to discovering important upstream signaling molecules and pathways.

Additionally, it would be interesting to investigate the effect of PAR2 activation on other factors influencing lipid mediator production in Caco2 cells, including the expression of PLA_2, as well as PG synthases and PG receptors. This would provide more insight into how PAR2 activation tailors the environment of lipid mediator signaling. It was also shown that PAR2 activation does not have an effect on COX-1 expression (Hirota et al. 2012), but other enzymes that process AA, an ω-6 FA, have not been investigated. By expanding these future directions to include analysis of ω-3 FA processing (EPA and DHA), a complete picture could be generated for the effect of PAR2 activation on pro-resolving lipid

mediators including lipoxin A_4, resolvins, protectins, and maresins (Serhan 2007; Buckley, Gilroy, and Serhan 2014).

The functional consequence of PAR2-induced COX-2 in Caco2 cells was not found in this project, since COX-2 did not play a role in wound healing. In canine intestinal epithelial cells (SCBNs), COX-1 and COX-2 regulated PAR2-mediated chloride secretion, which would be a possible mechanism to explore in Caco2 cells (van der Merwe et al. 2009). An additional mechanism to explore includes the role of epithelially-derived PAR2-induced lipid mediators on other cell types. An ideal candidate is the intestinal subepithelial myofibroblast, due to their close proximity and intricate interaction with epithelial cells to regulate intestinal homeostasis (Kedinger et al. 1998; Le Guen et al. 2015).

4.3 Wound healing in intestinal epithelial cells

The single layer of epithelial cells lining the intestines needs to act as a selectively permeable barrier for proper homeostasis and host health. When the barrier becomes damaged, passage of luminal contents into the body becomes unregulated and can result in intestinal inflammation. The barrier needs to heal in order to eliminate the inflammatory trigger and for inflammation to resolve. The focus on this project was specifically on the mechanisms of epithelial restitution.

There are multiple methods that can be used *in vitro* to model epithelial restitution (Iizuka and Konno 2011; Hulkower and Herber 2011). These can be divided into wound-based models, and non-wound based models. Wound based models involve growing a

monolayer of epithelial cells, and then removing a portion of cells to create a wound which damages some cells, more accurately mimicking the *in vivo* scenario. Cells can be removed with either a razor blade to clear a large area of the monolayer and study the forward movement of a single wound edge, or with a pipette tip attached to an aspirator used to create a straight scratch wound or circular wound. These wounds can be used to study full wound closure. There are also non-wound based models of epithelial restitution called cell exclusion zone assays, which attempt to create wounds without damaging cells. Instead of wounding a monolayer, an obstruction is placed on the plate surface prior to adding cells. The cells then grow around the obstruction, and upon removal of the object a wound is created. These objects include ibidi culture inserts (Nalleweg et al. 2015) that result in line wounds, or Oris cell seeding stoppers (Hulkower and Herber 2011) that result in circular wounds. There are also unique methods of letting agarose droplets solidify on the surface prior to cell plating, and once cells are confluent, digesting the agarose to create cell-free regions (Klarlund 2012). For the majority of this project, circular wounds were created using a pipette tip. This method allowed for the entire wound edge to be considered in each method of analysis. Being able to visualize the entire wound border was a strength of the circular wound model compared to scratch wound model, especially when the same wound area needed to be identified manually at many time points.

4.3.1 PAR2-mediated inhibition of wound healing in Caco2 cells

There is strong evidence in the literature that PAR2 activation enhances epithelial proliferation and migration (Darmoul et al. 2004; Zhou et al. 2011; Mize, Wang, and Takayama 2008; Ge et al. 2004; Wu et al. 2014), which would suggest that PAR2 activation could mediate enhanced wound healing. In contrast to the original hypothesis, PAR2 activation in Caco2 intestinal epithelial cells inhibited circular wound healing. The original observation was made in cells that were serum-starved overnight (0% FBS), and then allowed to heal in the presence of full serum (10% FBS). In order to confirm these data in different conditions, wound healing was also performed in low serum (0.5% FBS), with cells grown on Transwells to ensure polarization, and with post-confluent differentiated Caco2 cells. In each situation, PAR2 activation resulted in a significant inhibition of wound healing. The type of wound was also considered, and when wound healing of scratch wounds was assessed, PAR2 activation was still able to inhibit wound closure. Interestingly, although PAR2 activation has been shown to transactivate EGFR (Chung et al. 2013; Hirota et al. 2012; Abdallah et al. 2010; van der Merwe, Hollenberg, and MacNaughton 2008; Darmoul et al. 2004), circular wound healing was enhanced with EGF treatment compared to control, suggesting that the primary PAR2 signaling pathway resulting in the inhibition of wound healing is not through EGFR transactivation. This could be confirmed with future studies using inhibitors of EGFR that either target the extracellular domain (monoclonal antibodies) or intracellular catalytic domain (small molecule tyrosine kinase inhibitors).

Next, the individual components of wound healing, proliferation and migration, were investigated in order to determine the mechanism of wound healing inhibition by PAR2 activation. Although both proliferation and migration have important roles in epithelial wound healing, there is an interesting model in the cancer literature referred to as the Go or Grow Hypothesis that could also be explored in wound healing. This hypothesis was generated following the observation that proliferation and migration are temporally, mutually exclusive phenotypes (Xie, Mittal, and Berens 2014). Although this is not true for all types of cancer, and others have found that highly invasive tumors tend to also be highly proliferative (Garay et al. 2013), it is an interesting concept to consider during wound healing.

Proliferation was first measured in subconfluent Caco2 cells using an XTT assay, which did not show significant differences in either low or high serum following PAR2 activation. However, there were two main pitfalls of using the XTT assay. First, it is only considered an indirect measurement of proliferation since it depends on mitochondrial function, so if the treatment affects the mitochondrial activity, the read out will not accurately reflect cell number. Although there was no significant difference found with PAR2 activation in Caco2 cells, it has been previously reported that PAR2 activation can increase mitochondrial activity (Sevigny et al. 2011). Second, the XTT assay was only able to assess proliferation in subconfluent cells, which does not accurately reflect the state of the cells during wound healing. Due to these issues, proliferation was also assessed using an EdU assay. Since EdU is a thymidine analog, it directly measures proliferation by

identifying cells that are actively synthesizing DNA, and with an imaging end-point, it allowed for analysis of confluent and wound-edge cells. Using this method, the proliferation in subconfluent cells was confirmed to be unchanged with PAR2 activation, and proliferation at the wound edge was also not significantly different between groups. However, a significant increase in proliferation was detected with PAR2 activation in confluent cells. These data support the literature that described PAR2 activation promoted proliferation (Darmoul et al. 2004; Zhou et al. 2011; Shimamoto et al. 2004; Mize, Wang, and Takayama 2008), but it does not directly explain the effect of PAR2 activation on Caco2 wound healing. It could be speculated that the increased proliferation following PAR2 activation applies to the go or grow hypothesis. If PAR2 signaling was overwhelming the cells with a pro-proliferative signal, it might have been preventing the cells from developing the necessary migratory phenotype required to move.

Next, cell migration was characterized using multiple methods. Single cell migration was analyzed using a sensitive Boyden-like chamber technique with the xCelligence system. Where the Boyden chamber is labor intensive and only applies to a single time point, the xCelligence system allows for quick and multiple real-time measurements. When cells were plated on the top membrane in the presence of 2fLI, fewer cells were detected on the underside of the membrane within 24 h compared to control. These data suggested that PAR2 activation was able to inhibit single cell migration. However, it is important to note that cell attachment was not measured in the presence of 2fLI compared to control, and therefore these data could also suggest decreased attachment with PAR2 activation

that could be responsible for the reduced appearance of cells on the underside of the membrane. Importantly, the effect of 2fLI on cell attachment could provide an additional mechanism whereby PAR2 activation could regulate cell migration, and should be explored in future studies.

In addition to single cell migration, it was important to assess sheet migration to directly relate the data to wound healing. First, the migration component of wound healing was isolated by performing a standard wound healing experiment in the absence of proliferation. When proliferation was irreversibly inhibited using MMC, Caco2 cells were still able to heal, and PAR2 activation was still able to significantly inhibit wound healing. To complement these data, live-cell images were captured to create videos in order to track the migration distance of individual wound-edge cells, and it was found that PAR2 activation significantly limited the distance that cells travelled. Although the majority of PAR2 literature suggests that it has a pro-migratory effect (Zhou et al. 2011; Shi et al. 2013; Ge et al. 2004; Morris et al. 2006), there was a single study where PAR2-deficient mice had decreased metastasis in a melanoma model (Olejar et al. 2014), which supports these data showing PAR2 activation can inhibit cell migration.

Considering that PAR2 activation was able to inhibit both single cell migration and epithelial sheet migration, it was speculated that the mechanism of inhibition might be shared. Due to the necessity of dynamic actin regulation during any type of cell migration, it was the first potential mechanism studied.

For an initial analysis of actin, wounds in the process of healing were fixed and stained with phalloidin in order to visualize F-actin. Although there was no significant difference at 12 h, when wound healing was established at 24 h there were significantly fewer lamellipodia and significantly more actin cabling with PAR2 activation. Actin dynamics were also analyzed following transfection with a LifeAct plasmid that labelled F-actin without interfering with its function (Riedl et al. 2008), allowing for live-cell imaging of the actin regulation. The videos captured of wound edge cells showed that although actin cabling also forms in control cells, it was dynamic and transformed into lamellipodia. However, with PAR2 activation, there was cable formation at the wound edge that was long-lasting. These data indicate that PAR2 activation is able to affect the regulation of actin, which could potentially be a shared mechanism for PAR2-mediated inhibition of single-cell and sheet migration.

An interesting aspect of actin cabling during sheet migration is its role in leader cell formation. It was previously shown that as long as the actin forms a cable at the wound edge, the leader cells that drive sheet migration cannot develop (Reffay et al. 2014). Due to the importance of leader cells during sheet migration, it was hypothesized that PAR2 activation prevented the formation of leader cells due to the presence of actin cabling. Using a marker of leader cells that was identified in mammary epithelial cells (Riahi et al. 2015), Delta-like ligand (Dll)4 staining was performed on fixed Caco2 wounds (Appendix C). Unfortunately, the staining with the isotype control was very similar to the primary antibody, and in areas where leader cell formation would be expected, there was no

positive staining with the Dll4 antibody. It is possible that a different Dll4 antibody would be able to detect leader cells, but in the original paper, the antibody staining was not as clear as their use of double stranded locked nucleic acid (dsLNA) probes in single-cell gene expression analysis (Riahi et al. 2015). It is also possible that Dll4 is not a marker of leader cells in intestinal epithelial cells.

A second mechanism investigated as a method of PAR2-mediated inhibition of wound healing was the role of cell-cell junction regulation. It is well described that E-cadherin internalization is required for epithelial cell migration (Haeger et al. 2015; Peglion, Llense, and Etienne-Manneville 2014). Therefore, it was hypothesized that PAR2 activation would prevent the internalization of E-cadherin at the wound edge. Similar to the actin analysis, cells were fixed during the wound healing process and stained for E-cadherin. At 24 h, there was considerable loss of E-cadherin in cells surrounding control wounds, but E-cadherin expression was maintained in wounds treated with 2fLI. These data showing increased E-cadherin expression could result in decreased migration due to wound edge cells being held back by follower cells through maintained AJ strength. On the other hand, it has also been described that E-cadherin expression and relocalization is required for collective cell migration, and interestingly E-cadherin relocalization is dependent on F-actin reorganization (Li et al. 2012; Hwang et al. 2012), which could potentially link these two observations made in Caco2 cells.

With the changes found in the AJ structure, it was hypothesized that wound healing-associated EMT might play a role. In addition to E-cadherin internalization, other

canonical changes associated with EMT include changes to the TJ structure, as well as increased expression of mesenchymal markers such as SNAIL, vimentin, and N-cadherin (Huang, Guilford, and Thiery 2012; Peglion, Llense, and Etienne-Manneville 2014). The TJ was studied by staining for the scaffolding protein ZO-1 in order to determine if TJ integrity was lost, but no changes were found at the wound edge in control cells, or with PAR2 activation. Similarly, there were no differences in any of the mesenchymal markers stained, either at the wound edge or with PAR2 activation. It is possible that the time-point studied (24 h) was too early for wound-healing associated EMT to establish, since EMT is normally characterized over days or weeks (Maeda, Johnson, and Wheelock 2005).

There were multiple topics that could have been investigated in order to explore the mechanism of wound healing inhibition, including the specifics of actin regulation and cable formation, cell-cell communication and adhesion, cell-matrix interactions, as well as studying leader cell and follower cell characteristics. It was first considered to perform a migration/wound healing specific PCR array that would address many of these potential mechanisms. However, due to the cost and relatively limited data acquired with an array, RNA sequencing was chosen as an optimal method to un-biasedly investigate the mechanism of PAR2-mediated inhibition of Caco2 wound healing. Importantly, it has been shown that cytoskeletal dynamics are intricately related to genome activity (Olson and Nordheim 2010).

First, the role of transcription during Caco2 wound healing was investigated by performing a standard wound healing experiment in the presence of actinomycin D to

inhibit transcription. Wound healing in Caco2 cells was almost entirely shut off in the absence of transcription. These data provided a good rationale to move forward with RNA sequencing of wounded Caco2 cells, to study the effect of PAR2 activation on transcriptionally-dependent wound healing.

Analysis of RNA sequencing data proved to be a challenge. Due to a lack of computer programming expertise within the lab, the only available methods of analysis were those modified to function as web-based platforms. The ACHRI genomic facility uploaded the aligned datasets to Galaxy web-interface, which was used for data processing. Triplicates within each experimental condition were grouped, and two conditions were compared using CuffDiff.

Four experimental conditions were sequenced: non-wounded control, wounded control, non-wounded with PAR2 activation, and wounded with PAR2 activation. The comparisons analyzed in this project were non-wounded control vs wounded control, and non-wounded control vs non-wounded PAR2-activated. These comparisons were prioritized in order to compare the transcriptome induced by wounding to the transcriptome induced following PAR2 activation. Interestingly, 88% of the genes that were increased (>2-fold) when the control cells were wounded, were also increased with PAR2 activation. For any obvious gene targets to pursue, genes that were increased with wounding were compared to genes decreased with PAR2-activation, but none were identified. Similarly, no genes decreased with wounding that were increased with PAR2-activation. Although we attempted pathway analysis using these gene lists (Appendix B),

there was considerable variability in the data based on the analysis tool used, and we were unable to conclusively identify prominent signaling pathways. In order to have confidence in the pathway analysis data, additional studies would need to be performed to investigate each signaling pathway, which was beyond the scope of this project. However, it is interesting to focus on the unexpected overlap of genes increased with both PAR2-activation and wound healing. Included in this overlap are genes that change their expression at the wound edge during sheet migration, including claudin-2 (Ikari et al. 2011), CXCR4 (Ghosh et al. 2012), as well as c-FOS, FOSB, and FOSL1 (Renaud et al. 2014). In addition, COX-2 was increased with PAR2 activation, which served as a good internal control, since it was previously shown that PAR2 activation induced COX-2 expression in a transcriptionally-dependent manner. COX-2 was also increased with wounding, which could suggest that COX-2 plays a role in the wound healing response. However, use of a COX-2 selective inhibitor had no effect on the rate of wound healing. Additional genes of interest that were upregulated with both wounding and PAR2 activation, and have previously been shown to modulate wound healing, include regulators of ECM components (ADAMTS9, MMP1, MMP10) (Rohani and Parks 2015), annexin A1 (Leoni et al. 2015; Leoni et al. 2013), EGFR ligands (amphiregulin, epiregulin) (Yamaoka et al. 2011), as well as chemokines and chemokine receptors (CCL20, CXCR4, and IL-8) (Vongsa, Zimmerman, and Dwinell 2009; Ghosh et al. 2012; Wilson, Byron, and Gibson 1999). Due to their strong association with epithelial wound healing in the literature, these select genes of interest all have strong rationale for potential future investigation.

It has also been shown that ERK1/2 is persistently activated at the leading edge during sheet migration (Block et al. 2010). In relation to ERK1/2, it has also been shown that when ERK1/2 is universally activated across the entire monolayer, rather than specifically at the wound edge, there is no organized sheet migration and cells do not move in a coordinated direction (Chapnick and Liu 2014). Therefore, expression and activation of specific proteins at the wound edge likely plays a large role in communicating the direction of movement that is needed. Since PAR2 activation signals through ERK1/2, and increases the expression of other wound edge-associated factors, it is possible that activation of PAR2 is creating a universal increase in components that are required solely at the wound edge. This would explain how PAR2 activation could inhibit Caco2 wound healing even in the presence of the pro-wound healing transcriptional profile.

4.3.2 PAR2-mediated enhancement of wound healing in T84 cells

With the novel findings in Caco2 cells, PAR2-mediated wound healing was also studied in a second cell line in order to determine if the effect characterized was cell-line specific. T84 cells were chosen since they are phenotypically different than Caco2 cells, but still form complete monolayers in culture. More in line with the literature, PAR2 activation increased wound healing in T84 cells, that was associated with increased migration. When proliferation was analyzed with EdU staining, PAR2 activation was found to decrease proliferation in confluent and wound-edge T84 cells. These data, similar to the increased proliferation in Caco2 cells, could also relate to the go or grow hypothesis, where PAR2

activation in T84 cells might program the cells toward a migratory phenotype rather than a proliferative phenotype.

When the actin dynamics and E-cadherin localization were visualized in the T84 cells, PAR2 activation increased lamellipodia formation and increased the loss of E-cadherin surrounding the wound. Actin cabling was not observed in T84 cells.

These data raise the obvious question of the differences between Caco2 cells and T84 cells, and the cell line-specific mutations are important to consider. The COSMIC project, which developed a curated database with information on human cancer cell line mutations (Forbes et al. 2011), identified 409 mutations in Caco2 cells, and 428 mutations in T84 cells. When the lists of these mutations were entered into an online Venn diagram tool, only 20 mutations were shared between the cell lines, indicating considerable variability between the two cell types. Future studies could analyse these differences to mine for underlying pathway variations that could explain the difference in response to PAR2 activation in these cell lines.

4.3.3 Future directions for wound healing in intestinal epithelial cells

To further analyze the mechanism of PAR2-mediated wound healing, would be useful to investigate the opposing responses to PAR2 activation seen in Caco2 and T84 cells. Although it was beyond the scope of this thesis, a deeper investigation into specific mutations in Caco2 cells and T84 cells that are associated with wound healing responses and actin regulation might provide important insight. It was also interesting to observe the

phenotypic differences in Caco2 and T84 cells during passaging and as they grew to confluence. Caco2 cells were easy to lift with trypsin-EDTA, and easy to disperse into single cells with repeated pipetting, whereas T84 cells took at least twice as long to lift, and were very difficult to disperse. After plating, Caco2 cells became large by spreading out on the plate bottom, and became smaller after reaching confluence to pack together more closely. Conversely, T84 cells did not spread out immediately after plating, and tended to form tightly packed islands of cells that reached confluence through proliferation, and not cell-spreading. These observations relate closely to a paper that describes in detail the effect of extra-cellular matrix composition and cell-cell adhesion components on cell spreading (Ravasio et al. 2015). In this paper, the type of matrix (collagen vs fibronectin), the concentration of fibronectin, and the cadherin levels were each manipulated to study cell spreading. With either collagen, low concentrations of fibronectin, or high levels of E-cadherin, cells displayed low adhesion (to the matrix) and high cohesion (to other cells), which looked strikingly similar to the T84 cell phenotype. When higher concentrations of fibronectin were used, or E-cadherin levels were reduced, cells displayed high adhesion and low cohesion that was phenotypically similar to Caco2 cells. Therefore, it addition to exploring the differences in cell line-specific mutations, it would be interesting to characterize differences in ECM protein expression and E-cadherin levels in Caco2 cells and T84 cells.

In order to relate these mechanisms of wound healing to conditions such as IBD, it would also be interesting to perform wound healing experiments in the presence of pro-

inflammatory mediators such as TNFα and IFNγ that are commonly up regulated during IBD.

The translational application of these data is the ultimate goal, in order to understand intestinal epithelial wound healing as it pertains to human health. The cell lines used for this project were tools to model a normal intestinal epithelial cell, but there are significant draw backs to using cancer cells to model normal cell wound healing, due to the inherent differences that cause cells to become cancerous. The development and commercialization of products used in the growth of primary intestinal epithelial cells is rapidly expanding, and making these techniques accessible to many labs that previously did not have access to the necessary materials. As such, the MacNaughton lab has recently developed a modified protocol to take organoids grown from the mouse colon, and plate them into a 2D culture. The method to culture mouse colonoids and grow the 2D cultures, as well as preliminary data acquired with these primary intestinal epithelial cells, is found in Appendix D.

4.4 Significance

During IBD, there is an increased level of proteases (Raithel et al. 2001) and increased expression of PAR2 on epithelial cells (Maeda et al. 2014). These findings are significant in that they could implicate the activation of PAR2 in either the disease pathogenesis, or the host response to resolve inflammation. While at first glance the data in this thesis are contradictory, the fact that a biological system can have opposite effects

in the same tissue has precedents. For example, prostanoids derived from COX-2 can be inflammatory in the early phases of inflammation, but have clear pro-resolution characteristics later in the response. The key is in the timing of expression and the tissue microenvironment in which the response occurs. These are vital factors to consider as researchers in academia and industry work to target the PAR2 pathway in the development of new drugs.

In this thesis, we focused on the previous work showing that PAR2 activation in intestinal epithelial cells could increase the expression of COX-2 (Hirota et al. 2012), and the protective role of COX-2 in the GI tract (Wallace and Devchand 2005), generating the hypothesis that PAR2 activation could enhance epithelial wound healing through lipid-derived mediators. When PAR2 activation was found to inhibit wound healing in Caco2 cells, independently of COX-2 activity, we decided to further characterize these novel and unexpected data. PAR2-dependent inhibition of wound healing was correlated with decreased migration, alterations in actin dynamics, and increased E-cadherin expression at the wound edge. Interestingly, the transcriptome profile induced by PAR2 activation in Caco2 cells was comparable to a profile induced in control cells during wound healing, and further analysis showed similarities in pro-migratory pathways.

When T84 cells were used, in contrast to the data acquired with Caco2 cells, PAR2 activation enhanced wound healing. These contrasting data highlight an important limitation in using cell lines to model normal epithelial cells, and emphasize not only the importance of using multiple cell lines to repeat observations, but also that culturing

primary epithelial cells should be prioritized to avoid cell line-specific effects. While cell lines have been the backbone of intestinal epithelial research for decades, results such as ours demonstrate the danger of using data derived from these systems to predict drug responses or disease outcomes in patients. By perpetuating the use of these models, are we actually slowing the generation of accurate knowledge, to the detriment of patients? Questions such as these should fuel the development of primary cell cultures and human tissue-based experimental systems in discovery-based research and therapeutic development.

Finally, our work has broader implications beyond IBD. Proteases, PARs, and cell migration have been implicated in cancer cell migration and invasion. Our results, therefore, provide a strong rationale to study the effect of PAR2 activation on EMT in colitis-associated cancer as a future direction. Indeed, out work has demonstrated the importance for future, targeted research into the role of proteases and the proteome in disease and drug development.

REFERENCES

Abdallah, R. T., J. S. Keum, H. M. El-Shewy, M. H. Lee, B. Wang, M. Gooz, D. K. Luttrell, L. M. Luttrell, and A. A. Jaffa. 2010. 'Plasma kallikrein promotes epidermal growth factor receptor transactivation and signaling in vascular smooth muscle through direct activation of protease-activated receptors', *J Biol Chem*, 285: 35206-15.

Ajuebor, M. N., A. Singh, and J. L. Wallace. 2000. 'Cyclooxygenase-2-derived prostaglandin D(2) is an early anti-inflammatory signal in experimental colitis', *Am J Physiol Gastrointest Liver Physiol*, 279: G238-44.

Allison, M. C., A. G. Howatson, C. J. Torrance, F. D. Lee, and R. I. Russell. 1992. 'Gastrointestinal damage associated with the use of nonsteroidal antiinflammatory drugs', *N Engl J Med*, 327: 749-54.

Antalis, Toni M., Terez Shea-Donohue, Stefanie N. Vogel, Cynthia Sears, and Alessio Fasano. 2007. 'Mechanisms of Disease: protease functions in intestinal mucosal pathobiology', *Nature clinical practice. Gastroenterology & hepatology*, 4: 393-402.

Asfaha, S., W. K. MacNaughton, C. B. Appleyard, K. Chadee, and J. L. Wallace. 2001. 'Persistent epithelial dysfunction and bacterial translocation after resolution of intestinal inflammation', *Am J Physiol Gastrointest Liver Physiol*, 281: G635-44.

Barker, N., J. H. van Es, J. Kuipers, P. Kujala, M. van den Born, M. Cozijnsen, A. Haegebarth, J. Korving, H. Begthel, P. J. Peters, and H. Clevers. 2007. 'Identification of stem cells in small intestine and colon by marker gene Lgr5', *Nature*, 449: 1003-7.

Barrett, K. E., and S. J. Keely. 2000. 'Chloride secretion by the intestinal epithelium: molecular basis and regulatory aspects', *Annu Rev Physiol*, 62: 535-72.

Beck, I. T., and P. K. Dinda. 1981. 'Acute exposure of small intestine to ethanol: effects on morphology and function', *Dig Dis Sci*, 26: 817-38.

Beck, P. L., I. M. Rosenberg, R. J. Xavier, T. Koh, J. F. Wong, and D. K. Podolsky. 2003. 'Transforming growth factor-beta mediates intestinal healing and susceptibility to injury in vitro and in vivo through epithelial cells', *Am J Pathol*, 162: 597-608.

Bestwick, C. S., and L. Milne. 2001. 'Alteration of culture regime modifies antioxidant defenses independent of intracellular reactive oxygen levels and resistance to severe oxidative stress within confluent Caco-2 "intestinal cells"', *Dig Dis Sci*, 46: 417-23.

Block, Ethan R., Michael A. Tolino, Jennifer S. Lozano, Kira L. Lathrop, Rebecca S. Sullenberger, Abigail R. Mazie, and Jes K. Klarlund. 2010. 'Free Edges in Epithelial Cell Sheets Stimulate Epidermal Growth Factor Receptor Signaling', *Mol Biol Cell*, 21: 2172-81.

Brand, S. 2009. 'Crohn's disease: Th1, Th17 or both? The change of a paradigm: new immunological and genetic insights implicate Th17 cells in the pathogenesis of Crohn's disease', *Gut*, 58: 1152-67.

Buckley, C. D., D. W. Gilroy, and C. N. Serhan. 2014. 'Proresolving lipid mediators and mechanisms in the resolution of acute inflammation', *Immunity*, 40: 315-27.

Camerer, E., W. Huang, and S. R. Coughlin. 2000. 'Tissue factor- and factor X-dependent activation of protease-activated receptor 2 by factor VIIa', *Proc Natl Acad Sci U S A*, 97: 5255-60.

Canada, Crohn's and Colitis. 2012. 'The Impact of Inflammatory Bowel Disease in Canada'.

Cenac, N., A. M. Coelho, C. Nguyen, S. Compton, P. Andrade-Gordon, W. K. MacNaughton, J. L. Wallace, M. D. Hollenberg, N. W. Bunnett, R. Garcia-Villar, L. Bueno, and N. Vergnolle. 2002. 'Induction of intestinal inflammation in mouse by activation of proteinase-activated receptor-2', *Am J Pathol*, 161: 1903-15.

Chang, Y. W., K. Putzer, L. Ren, B. Kaboord, T. W. Chance, M. W. Qoronfleh, and R. Jakobi. 2005. 'Differential regulation of cyclooxygenase 2 expression by small GTPases Ras, Rac1, and RhoA', *J Cell Biochem*, 96: 314-29.

Chapnick, D. A., and X. Liu. 2014. 'Leader cell positioning drives wound-directed collective migration in TGFbeta-stimulated epithelial sheets', *Mol Biol Cell*, 25: 1586-93.

Chen, Edward Y., Christopher M. Tan, Yan Kou, Qiaonan Duan, Zichen Wang, Gabriela Vaz Meirelles, Neil R. Clark, and Avi Ma'ayan. 2013. 'Enrichr: interactive and collaborative HTML5 gene list enrichment analysis tool', *BMC Bioinformatics*, 14: 1-14.

Chen, G. Y., and G. Nunez. 2010. 'Sterile inflammation: sensing and reacting to damage', *Nature Reviews Immunology*, 10: 826-37.

Chung, H., R. Ramachandran, M. D. Hollenberg, and D. A. Muruve. 2013. 'Proteinase-activated receptor-2 transactivation of epidermal growth factor receptor and transforming growth factor-beta receptor signaling pathways contributes to renal fibrosis', *J Biol Chem*, 288: 37319-31.

Clevers, H. C., and C. L. Bevins. 2013. 'Paneth cells: maestros of the small intestinal crypts', *Annu Rev Physiol*, 75: 289-311.

Crofford, L. J. 1997. 'COX-1 and COX-2 tissue expression: implications and predictions', *J Rheumatol Suppl*, 49: 15-9.

Darmoul, D., V. Gratio, H. Devaud, and M. Laburthe. 2004. 'Protease-activated receptor 2 in colon cancer: trypsin-induced MAPK phosphorylation and cell proliferation are mediated by epidermal growth factor receptor transactivation', *J Biol Chem*, 279: 20927-34.

de Beco, S., F. Amblard, and S. Coscoy. 2012. 'New insights into the regulation of E-cadherin distribution by endocytosis', *Int Rev Cell Mol Biol*, 295: 63-108.

DeFea, K. A., J. Zalevsky, M. S. Thoma, O. Déry, R. D. Mullins, and N. W. Bunnett. 2000. 'β-Arrestin–Dependent Endocytosis of Proteinase-Activated Receptor 2 Is Required for Intracellular Targeting of Activated Erk1/2', *J Cell Biol*, 148: 1267-82.

Dignass, A., K. Lynch-Devaney, H. Kindon, L. Thim, and D. K. Podolsky. 1994. 'Trefoil peptides promote epithelial migration through a transforming growth factor beta-independent pathway', *J Clin Invest*, 94: 376-83.

Dignass, A. U., and D. K. Podolsky. 1993. 'Cytokine modulation of intestinal epithelial cell restitution: central role of transforming growth factor beta', *Gastroenterology*, 105: 1323-32.

Disanza, A., A. Steffen, M. Hertzog, E. Frittoli, K. Rottner, and G. Scita. 2005. 'Actin polymerization machinery: the finish line of signaling networks, the starting point of cellular movement', *Cell Mol Life Sci*, 62: 955-70.

Dona, E., J. D. Barry, G. Valentin, C. Quirin, A. Khmelinskii, A. Kunze, S. Durdu, L. R. Newton, A. Fernandez-Minan, W. Huber, M. Knop, and D. Gilmour. 2013. 'Directional tissue migration through a self-generated chemokine gradient', *Nature*, 503: 285-9.

Dutting, S., J. Heidenreich, D. Cherpokova, E. Amin, S. C. Zhang, M. R. Ahmadian, C. Brakebusch, and B. Nieswandt. 2015. 'Critical off-target effects of the widely used Rac1 inhibitors NSC23766 and EHT1864 in mouse platelets', *J Thromb Haemost*, 13: 827-38.

Eguchi, H., K. Iwaki, K. Shibata, T. Ogawa, M. Ohta, and S. Kitano. 2011. 'Protease-activated receptor-2 regulates cyclooxygenase-2 expression in human bile duct cancer via the pathways of mitogen-activated protein kinases and nuclear factor kappa B', *J Hepatobiliary Pancreat Sci*, 18: 147-53.

Firat-Karalar, Elif Nur, and Matthew D. Welch. 2011. 'New mechanisms and functions of actin nucleation', *Curr Opin Cell Biol*, 23: 4-13.

Forbes, S. A., N. Bindal, S. Bamford, C. Cole, C. Y. Kok, D. Beare, M. Jia, R. Shepherd, K. Leung, A. Menzies, J. W. Teague, P. J. Campbell, M. R. Stratton, and P. A. Futreal. 2011. 'COSMIC: mining complete cancer genomes in the Catalogue of Somatic Mutations in Cancer', *Nucleic Acids Res*, 39: D945-50.

Fordtran, J. S. 2006. 'Colitis due to Clostridium difficile toxins: underdiagnosed, highly virulent, and nosocomial', *Proc (Bayl Univ Med Cent)*, 19: 3-12.

Gao, X., S. Hao, H. Yan, W. Ding, K. Li, and J. Li. 2015. 'Neutrophil extracellular traps contribute to the intestine damage in endotoxemic rats', *J Surg Res*, 195: 211-8.

Gao, Y., J. B. Dickerson, F. Guo, J. Zheng, and Y. Zheng. 2004. 'Rational design and characterization of a Rac GTPase-specific small molecule inhibitor', *Proc Natl Acad Sci U S A*, 101: 7618-23.

Garay, T., E. Juhasz, E. Molnar, M. Eisenbauer, A. Czirok, B. Dekan, V. Laszlo, M. A. Hoda, B. Dome, J. Timar, W. Klepetko, W. Berger, and B. Hegedus. 2013. 'Cell migration or cytokinesis and proliferation?--revisiting the "go or grow" hypothesis in cancer cells in vitro', *Exp Cell Res*, 319: 3094-103.

Ge, L., S. K. Shenoy, R. J. Lefkowitz, and K. DeFea. 2004. 'Constitutive protease-activated receptor-2-mediated migration of MDA MB-231 breast cancer cells requires both beta-arrestin-1 and -2', *J Biol Chem*, 279: 55419-24.

Ghosh, Manik C., Patrudu S. Makena, Vijay Gorantla, Scott E. Sinclair, and Christopher M. Waters. 2012. 'CXCR4 regulates migration of lung alveolar epithelial cells through activation of Rac1 and matrix metalloproteinase-2', *American Journal of Physiology - Lung Cellular and Molecular Physiology*, 302: L846-L56.

Gilroy, D. W., P. R. Colville-Nash, D. Willis, J. Chivers, M. J. Paul-Clark, and D. A. Willoughby. 1999. 'Inducible cyclooxygenase may have anti-inflammatory properties', *Nat Med*, 5: 698-701.

Gould, S. R., A. R. Brash, and M. E. Conolly. 1977. 'Increased prostaglandin production in ulcerative colitis', *Lancet*, 2: 98.

Graham, D. Y., A. R. Opekun, F. F. Willingham, and W. A. Qureshi. 2005. 'Visible small-intestinal mucosal injury in chronic NSAID users', *Clinical Gastroenterology and Hepatology*, 3: 55-59.

Grisham, M. B., and D. N. Granger. 1988. 'Neutrophil-mediated mucosal injury. Role of reactive oxygen metabolites', *Dig Dis Sci*, 33: 6s-15s.

Groschwitz, K. R., and S. P. Hogan. 2009. 'Intestinal barrier function: molecular regulation and disease pathogenesis', *J Allergy Clin Immunol*, 124: 3-20; quiz 21-2.

Gunawardene, Ashok R., Bernard M. Corfe, and Carolyn A. Staton. 2011. 'Classification and functions of enteroendocrine cells of the lower gastrointestinal tract', *International Journal of Experimental Pathology*, 92: 219-31.

Guo, Z., J. H. Jiang, J. Zhang, H. J. Yang, F. Q. Yang, Y. P. Qi, Y. P. Zhong, J. Su, R. R. Yang, L. Q. Li, and B. D. Xiang. 2015. 'COX-2 Promotes Migration and Invasion by the Side Population of Cancer Stem Cell-Like Hepatocellular Carcinoma Cells', *Medicine (Baltimore)*, 94: e1806.

Haeger, A., K. Wolf, M. M. Zegers, and P. Friedl. 2015. 'Collective cell migration: guidance principles and hierarchies', *Trends in Cell Biology*, 25: 556-66.

Halter, F., A. S. Tarnawski, A. Schmassmann, and B. M. Peskar. 2001. 'Cyclooxygenase 2-implications on maintenance of gastric mucosal integrity and ulcer healing: controversial issues and perspectives', *Gut*, 49: 443-53.

Harris, Tony J. C., and Ulrich Tepass. 2010. 'Adherens junctions: from molecules to morphogenesis', *Nat Rev Mol Cell Biol*, 11: 502-14.

Helander, Herbert F., and Lars Fändriks. 2014. 'Surface area of the digestive tract – revisited', *Scandinavian Journal of Gastroenterology*, 49: 681-89.

Heller, F., P. Florian, C. Bojarski, J. Richter, M. Christ, B. Hillenbrand, J. Mankertz, A. H. Gitter, N. Burgel, M. Fromm, M. Zeitz, I. Fuss, W. Strober, and J. D. Schulzke. 2005. 'Interleukin-13 is the key effector Th2 cytokine in ulcerative colitis that affects epithelial tight junctions, apoptosis, and cell restitution', *Gastroenterology*, 129: 550-64.

Hendel, J., and O. H. Nielsen. 1997. 'Expression of cyclooxygenase-2 mRNA in active inflammatory bowel disease', *Am J Gastroenterol*, 92: 1170-3.

Hirota, C. L., F. Moreau, V. Iablokov, M. Dicay, B. Renaux, M. D. Hollenberg, and W. K. MacNaughton. 2012. 'Epidermal growth factor receptor transactivation is required for proteinase-activated receptor-2-induced COX-2 expression in intestinal epithelial cells', *Am J Physiol Gastrointest Liver Physiol*, 303: G111-9.

Hollenberg, M. D., B. Renaux, E. Hyun, S. Houle, N. Vergnolle, M. Saifeddine, and R. Ramachandran. 2008. 'Derivatized 2-furoyl-LIGRLO-amide, a versatile and selective probe for proteinase-activated receptor 2: binding and visualization', *J Pharmacol Exp Ther*, 326: 453-62.

Houliston, R. A., R. J. Keogh, D. Sugden, J. Dudhia, T. D. Carter, and C. P. Wheeler-Jones. 2002. 'Protease-activated receptors upregulate cyclooxygenase-2 expression in human endothelial cells', *Thromb Haemost*, 88: 321-8.

Huang, Ruby Yun-Ju, Parry Guilford, and Jean Paul Thiery. 2012. 'Early events in cell adhesion and polarity during epithelial-mesenchymal transition', *Journal of Cell Science*, 125: 4417-22.

Hulkower, Keren I., and Renee L. Herber. 2011. 'Cell Migration and Invasion Assays as Tools for Drug Discovery', *Pharmaceutics*, 3: 107-24.

Hunter, M. V., D. M. Lee, T. J. Harris, and R. Fernandez-Gonzalez. 2015. 'Polarized E-cadherin endocytosis directs actomyosin remodeling during embryonic wound repair', *J Cell Biol*, 210: 801-16.

Hwang, Soonyean, Noah P. Zimmerman, Kimberle A. Agle, Jerrold R. Turner, Suresh N. Kumar, and Michael B. Dwinell. 2012. 'E-cadherin Is Critical for Collective Sheet Migration and Is Regulated by the Chemokine CXCL12 Protein During Restitution', *J Biol Chem*, 287: 22227-40.

Hyun, E., P. Andrade-Gordon, M. Steinhoff, and N. Vergnolle. 2008. 'Protease-activated receptor-2 activation: a major actor in intestinal inflammation', *Gut*, 57: 1222-9.

Iizuka, Masahiro, and Shiho Konno. 2011. 'Wound healing of intestinal epithelial cells', *World Journal of Gastroenterology : WJG*, 17: 2161-71.

Ikari, A., A. Takiguchi, K. Atomi, T. Sato, and J. Sugatani. 2011. 'Decrease in claudin-2 expression enhances cell migration in renal epithelial Madin-Darby canine kidney cells', *J Cell Physiol*, 226: 1471-8.

Ishihara, H., A. J. Connolly, D. Zeng, M. L. Kahn, Y. W. Zheng, C. Timmons, T. Tram, and S. R. Coughlin. 1997. 'Protease-activated receptor 3 is a second thrombin receptor in humans', *Nature*, 386: 502-6.

Ito, S., E. R. Lacy, M. J. Rutten, J. Critchlow, and W. Silen. 1984. 'Rapid repair of injured gastric mucosa', *Scand J Gastroenterol Suppl*, 101: 87-95.

Jiang, G. L., A. Nieves, W. B. Im, D. W. Old, D. T. Dinh, and L. Wheeler. 2007. 'The prevention of colitis by E Prostanoid receptor 4 agonist through enhancement of epithelium survival and regeneration', *J Pharmacol Exp Ther*, 320: 22-8.

Johansson, M. E., D. Ambort, T. Pelaseyed, A. Schutte, J. K. Gustafsson, A. Ermund, D. B. Subramani, J. M. Holmen-Larsson, K. A. Thomsson, J. H. Bergstrom, S. van der Post, A. M. Rodriguez-Pineiro, H. Sjovall, M. Backstrom, and G. C. Hansson. 2011. 'Composition and functional role of the mucus layers in the intestine', *Cell Mol Life Sci*, 68: 3635-41.

Johansson, Malin E. V., Henrik Sjövall, and Gunnar C. Hansson. 2013. 'The gastrointestinal mucus system in health and disease', *Nature reviews. Gastroenterology & hepatology*, 10: 352-61.

Jostins, L., S. Ripke, R. K. Weersma, R. H. Duerr, D. P. McGovern, K. Y. Hui, J. C. Lee, L. P. Schumm, Y. Sharma, C. A. Anderson, J. Essers, M. Mitrovic, K. Ning, I. Cleynen, E. Theatre, S. L. Spain, S. Raychaudhuri, P. Goyette, Z. Wei, C. Abraham, J. P. Achkar, T. Ahmad, L. Amininejad, A. N. Ananthakrishnan, V. Andersen, J. M. Andrews, L. Baidoo, T. Balschun, P. A. Bampton, A. Bitton, G. Boucher, S. Brand, C. Buning, A. Cohain, S. Cichon, M. D'Amato, D. De Jong, K. L. Devaney, M. Dubinsky, C. Edwards, D. Ellinghaus, L. R. Ferguson, D. Franchimont, K. Fransen, R. Gearry, M. Georges, C. Gieger, J. Glas, T. Haritunians, A. Hart, C. Hawkey, M. Hedl, X. Hu, T. H. Karlsen, L. Kupcinskas, S. Kugathasan, A. Latiano, D. Laukens, I. C. Lawrance, C. W. Lees, E. Louis, G. Mahy, J. Mansfield, A. R. Morgan, C. Mowat, W. Newman, O. Palmieri, C. Y. Ponsioen, U. Potocnik, N. J. Prescott, M. Regueiro, J. I. Rotter, R. K. Russell, J. D. Sanderson, M. Sans, J. Satsangi, S. Schreiber, L. A. Simms, J. Sventoraityte, S. R. Targan, K. D. Taylor, M. Tremelling, H. W. Verspaget, M. De Vos, C. Wijmenga, D. C. Wilson, J. Winkelmann, R. J. Xavier, S. Zeissig, B. Zhang, C. K. Zhang, H. Zhao, M. S. Silverberg, V. Annese, H. Hakonarson, S. R. Brant, G. Radford-Smith, C. G. Mathew, J. D. Rioux, E. E. Schadt, M. J. Daly, A. Franke, M. Parkes, S. Vermeire, J. C. Barrett,

and J. H. Cho. 2012. 'Host-microbe interactions have shaped the genetic architecture of inflammatory bowel disease', *Nature*, 491: 119-24.

Kahn, M. L., Y. W. Zheng, W. Huang, V. Bigornia, D. Zeng, S. Moff, R. V. Farese, Jr., C. Tam, and S. R. Coughlin. 1998. 'A dual thrombin receptor system for platelet activation', *Nature*, 394: 690-4.

Kaplan, M. J., and M. Radic. 2012. 'Neutrophil extracellular traps: double-edged swords of innate immunity', *J Immunol*, 189: 2689-95.

Kapoor, M., F. Kojima, L. Yang, and L. J. Crofford. 2007. 'Sequential induction of pro- and anti-inflammatory prostaglandins and peroxisome proliferators-activated receptor-gamma during normal wound healing: a time course study', *Prostaglandins Leukot Essent Fatty Acids*, 76: 103-12.

Kaser, A., S. Zeissig, and R. S. Blumberg. 2010. 'Inflammatory bowel disease', *Annu Rev Immunol*, 28: 573-621.

Kawao, N., M. Nagataki, K. Nagasawa, S. Kubo, K. Cushing, T. Wada, F. Sekiguchi, S. Ichida, M. D. Hollenberg, W. K. MacNaughton, H. Nishikawa, and A. Kawabata. 2005. 'Signal transduction for proteinase-activated receptor-2-triggered prostaglandin E2 formation in human lung epithelial cells', *J Pharmacol Exp Ther*, 315: 576-89.

Kedinger, M., I. Duluc, C. Fritsch, O. Lorentz, M. Plateroti, and J. N. Freund. 1998. 'Intestinal epithelial-mesenchymal cell interactions', *Ann N Y Acad Sci*, 859: 1-17.

Kelly, J. P., D. W. Kaufman, R. S. Koff, A. Laszlo, B. E. Wiholm, and S. Shapiro. 1995. 'Alcohol consumption and the risk of major upper gastrointestinal bleeding', *Am J Gastroenterol*, 90: 1058-64.

Kim, Y. S., and S. B. Ho. 2010. 'Intestinal goblet cells and mucins in health and disease: recent insights and progress', *Curr Gastroenterol Rep*, 12: 319-30.

Klarlund, J. K. 2012. 'Dual modes of motility at the leading edge of migrating epithelial cell sheets', *Proc Natl Acad Sci U S A*, 109: 15799-804.

Kohyama, T., X. D. Liu, F. Q. Wen, H. J. Kim, H. Takizawa, and S. I. Rennard. 2002. 'Prostaglandin D2 inhibits fibroblast migration', *Eur Respir J*, 19: 684-9.

Kowalczyk, Andrew P., and Kathleen J. Green. 2013. 'Structure, Function and Regulation of Desmosomes', *Prog Mol Biol Transl Sci*, 116: 95-118.

Kuhn, K. A., N. A. Manieri, T. C. Liu, and T. S. Stappenbeck. 2014. 'IL-6 stimulates intestinal epithelial proliferation and repair after injury', *PLoS One*, 9: e114195.

Lacy, E. R. 1988. 'Epithelial restitution in the gastrointestinal tract', *J Clin Gastroenterol*, 10 Suppl 1: S72-7.

Ladwein, M., and K. Rottner. 2008. 'On the Rho'd: the regulation of membrane protrusions by Rho-GTPases', *FEBS Lett*, 582: 2066-74.

Le Guen, L., S. Marchal, S. Faure, and P. de Santa Barbara. 2015. 'Mesenchymal-epithelial interactions during digestive tract development and epithelial stem cell regeneration', *Cell Mol Life Sci*, 72: 3883-96.

Leoni, G., A. Alam, P. A. Neumann, J. D. Lambeth, G. Cheng, J. McCoy, R. S. Hilgarth, K. Kundu, N. Murthy, D. Kusters, C. Reutelingsperger, M. Perretti, C. A. Parkos, A. S. Neish, and A. Nusrat. 2013. 'Annexin A1, formyl peptide receptor, and NOX1 orchestrate epithelial repair', *J Clin Invest*, 123: 443-54.

Leoni, G., P. A. Neumann, N. Kamaly, M. Quiros, H. Nishio, H. R. Jones, R. Sumagin, R. S. Hilgarth, A. Alam, G. Fredman, I. Argyris, E. Rijcken, D. Kusters, C. Reutelingsperger, M. Perretti, C. A. Parkos, O. C. Farokhzad, A. S. Neish, and A. Nusrat. 2015. 'Annexin A1-containing extracellular vesicles and polymeric nanoparticles promote epithelial wound repair', *J Clin Invest*, 125: 1215-27.

Ley, K., C. Laudanna, M. I. Cybulsky, and S. Nourshargh. 2007. 'Getting to the site of inflammation: the leukocyte adhesion cascade updated', *Nat Rev Immunol*, 7: 678-89.

Li, L., R. Hartley, B. Reiss, Y. Sun, J. Pu, and D. Wu. 2012. 'E-cadherin plays an essential role in collective directional migration of large epithelial sheets', *Cell Mol Life Sci*, 69.

Li, Y. J., N. Kanaji, X. Q. Wang, T. Sato, M. Nakanishi, M. Kim, J. Michalski, A. J. Nelson, M. Farid, H. Basma, A. Patil, M. L. Toews, X. Liu, and S. I. Rennard. 2015. 'Prostaglandin E2 switches from a stimulator to an inhibitor of cell migration after epithelial-to-mesenchymal transition', *Prostaglandins Other Lipid Mediat*, 116-117: 1-9.

Liu, J. Z., S. van Sommeren, H. Huang, S. C. Ng, R. Alberts, A. Takahashi, S. Ripke, J. C. Lee, L. Jostins, T. Shah, S. Abedian, J. H. Cheon, J. Cho, N. E. Daryani, L. Franke, Y. Fuyuno, A. Hart, R. C. Juyal, G. Juyal, W. H. Kim, A. P. Morris, H. Poustchi, W. G. Newman, V. Midha, T. R. Orchard, H. Vahedi, A. Sood, J. J. Sung, R. Malekzadeh, H. J. Westra, K. Yamazaki, S. K. Yang, J. C. Barrett, A. Franke, B. Z. Alizadeh, M. Parkes, K. T. B, M. J. Daly, M. Kubo, C. A. Anderson, and R. K. Weersma. 2015. 'Association analyses identify 38 susceptibility loci for inflammatory bowel disease and highlight shared genetic risk across populations', *Nat Genet*, 47: 979-86.

Lohman, R. J., A. J. Cotterell, J. Suen, L. Liu, A. T. Do, D. A. Vesey, and D. P. Fairlie. 2012. 'Antagonism of protease-activated receptor 2 protects against experimental colitis', *J Pharmacol Exp Ther*, 340: 256-65.

Maeda, Masato, Keith R. Johnson, and Margaret J. Wheelock. 2005. 'Cadherin switching: essential for behavioral but not morphological changes during an epithelium-to-mesenchyme transition', *Journal of Cell Science*, 118: 873-87.

Maeda, S., K. Ohno, K. Uchida, H. Igarashi, Y. Goto-Koshino, Y. Fujino, and H. Tsujimoto. 2014. 'Intestinal protease-activated receptor-2 and fecal serine protease activity are increased in canine inflammatory bowel disease and may contribute to intestinal cytokine expression', *J Vet Med Sci*, 76: 1119-27.

Majumdar, R., M. Sixt, and C. A. Parent. 2014. 'New paradigms in the establishment and maintenance of gradients during directed cell migration', *Curr Opin Cell Biol*, 30: 33-40.

Manieri, N. A., M. R. Drylewicz, H. Miyoshi, and T. S. Stappenbeck. 2012. 'Igf2bp1 is required for full induction of Ptgs2 mRNA in colonic mesenchymal stem cells in mice', *Gastroenterology*, 143: 110-21.e10.

Marshman, E., C. Booth, and C. S. Potten. 2002. 'The intestinal epithelial stem cell', *Bioessays*, 24: 91-8.

McCarty, S. M., C. A. Cochrane, P. D. Clegg, and S. L. Percival. 2012. 'The role of endogenous and exogenous enzymes in chronic wounds: a focus on the implications of aberrant levels of both host and bacterial proteases in wound healing', *Wound Repair Regen*, 20: 125-36.

McCoy, K. L., S. F. Traynelis, and J. R. Hepler. 2010. 'PAR1 and PAR2 couple to overlapping and distinct sets of G proteins and linked signaling pathways to differentially regulate cell physiology', *Mol Pharmacol*, 77: 1005-15.

McGrath, James L., Eric A. Osborn, Yanik S. Tardy, C. Forbes Dewey, and John H. Hartwig. 2000. 'Regulation of the actin cycle in vivo by actin filament severing', *Proc Natl Acad Sci U S A*, 97: 6532-37.

Mihara, K., R. Ramachandran, M. Saifeddine, K. K. Hansen, B. Renaux, D. Polley, S. Gibson, C. Vanderboor, and M. D. Hollenberg. 2016. 'Thrombin-Mediated Direct Activation of Proteinase-Activated Receptor-2: Another Target for Thrombin Signaling', *Mol Pharmacol*, 89: 606-14.

Miyoshi, H., R. Ajima, C. T. Luo, T. P. Yamaguchi, and T. S. Stappenbeck. 2012. 'Wnt5a potentiates TGF-beta signaling to promote colonic crypt regeneration after tissue injury', *Science*, 338: 108-13.

Miyoshi, H., K. L. VanDussen, N. P. Malvin, S. H. Ryu, Y. Wang, N. M. Sonnek, C. W. Lai, and T. S. Stappenbeck. 2016. 'Prostaglandin E2 promotes intestinal repair through an adaptive cellular response of the epithelium', *Embo j*.

Mize, G. J., W. Wang, and T. K. Takayama. 2008. 'Prostate-specific kallikreins-2 and -4 enhance the proliferation of DU-145 prostate cancer cells through protease-activated receptors-1 and -2', *Mol Cancer Res*, 6: 1043-51.

Mizuno, H., C. Sakamoto, K. Matsuda, K. Wada, T. Uchida, H. Noguchi, T. Akamatsu, and M. Kasuga. 1997. 'Induction of cyclooxygenase 2 in gastric mucosal lesions and its inhibition by the specific antagonist delays healing in mice', *Gastroenterology*, 112: 387-97.

Molino, M., E. S. Barnathan, R. Numerof, J. Clark, M. Dreyer, A. Cumashi, J. A. Hoxie, N. Schechter, M. Woolkalis, and L. F. Brass. 1997. 'Interactions of mast cell tryptase with thrombin receptors and PAR-2', *J Biol Chem*, 272: 4043-9.

Molodecky, N. A., I. S. Soon, D. M. Rabi, W. A. Ghali, M. Ferris, G. Chernoff, E. I. Benchimol, R. Panaccione, S. Ghosh, H. W. Barkema, and G. G. Kaplan. 2012. 'Increasing incidence and prevalence of the inflammatory bowel diseases with time, based on systematic review', *Gastroenterology*, 142: 46-54.e42; quiz e30.

Montalvo-Ortiz, B. L., L. Castillo-Pichardo, E. Hernandez, T. Humphries-Bickley, A. De la Mota-Peynado, L. A. Cubano, C. P. Vlaar, and S. Dharmawardhane. 2012. 'Characterization of EHop-016, novel small molecule inhibitor of Rac GTPase', *J Biol Chem*, 287: 13228-38.

Morris, D. R., Y. Ding, T. K. Ricks, A. Gullapalli, B. L. Wolfe, and J. Trejo. 2006. 'Protease-activated receptor-2 is essential for factor VIIa and Xa-induced signaling, migration, and invasion of breast cancer cells', *Cancer Res*, 66: 307-14.

Nalleweg, Nancy, Mircea Teodor Chiriac, Eva Podstawa, Christian Lehmann, Tilman T Rau, Raja Atreya, Ekaterina Krauss, Gheorghe Hundorfean, Stefan Fichtner-Feigl, Arndt Hartmann, Christoph Becker, and Jonas Mudter. 2015. 'IL-9 and its receptor are predominantly involved in the pathogenesis of UC', *Gut*, 64: 743-55.

Natoli, M., B. D. Leoni, I. D'Agnano, F. Zucco, and A. Felsani. 2012. 'Good Caco-2 cell culture practices', *Toxicol In Vitro*, 26: 1243-6.

Nystedt, S., K. Emilsson, C. Wahlestedt, and J. Sundelin. 1994. 'Molecular cloning of a potential proteinase activated receptor', *Proc Natl Acad Sci U S A*, 91: 9208-12.

Olejar, T., D. Vetvicka, M. Zadinova, P. Pouckova, J. Kukal, P. Jezek, and R. Matej. 2014. 'Dual role of host Par2 in a murine model of spontaneous metastatic B16 melanoma', *Anticancer Res*, 34: 3511-5.

Olson, Eric N., and Alfred Nordheim. 2010. 'Linking actin dynamics and gene transcription to drive cellular motile functions', *Nat Rev Mol Cell Biol*, 11: 353-65.

Pabst, O., V. Cerovic, and M. Hornef. 2016. 'Secretory IgA in the Coordination of Establishment and Maintenance of the Microbiota', *Trends Immunol*, 37: 287-96.

Papaconstantinou, Harry T., and J. Scott Thomas. 2007. 'Bacterial Colitis', *Clinics in Colon and Rectal Surgery*, 20: 18-27.

Pastorelli, L., C. De Salvo, J. R. Mercado, M. Vecchi, and T. T. Pizarro. 2013. 'Central role of the gut epithelial barrier in the pathogenesis of chronic intestinal inflammation: lessons learned from animal models and human genetics', *Front Immunol*, 4: 280.

Patel, S., R. Behara, G. R. Swanson, C. B. Forsyth, R. M. Voigt, and A. Keshavarzian. 2015. 'Alcohol and the Intestine', *Biomolecules*, 5: 2573-88.

Peglion, Florent, Flora Llense, and Sandrine Etienne-Manneville. 2014. 'Adherens junction treadmilling during collective migration', *Nat Cell Biol*, 16: 639-51.

Pineton de Chambrun, G., P. Blanc, and L. Peyrin-Biroulet. 2016. 'Current evidence supporting mucosal healing and deep remission as important treatment goals for inflammatory bowel disease', *Expert Rev Gastroenterol Hepatol*, 10: 915-27.

Pinto, D., and H. Clevers. 2005. 'Wnt control of stem cells and differentiation in the intestinal epithelium', *Exp Cell Res*, 306: 357-63.

Poujade, M., E. Grasland-Mongrain, A. Hertzog, J. Jouanneau, P. Chavrier, and B. Ladoux. 2007. 'Collective migration of an epithelial monolayer in response to a model wound', *Proc Natl Acad Sci U S A*, 104.

Raithel, M., S. Winterkamp, A. Pacurar, P. Ulrich, J. Hochberger, and E. G. Hahn. 2001. 'Release of mast cell tryptase from human colorectal mucosa in inflammatory bowel disease', *Scand J Gastroenterol*, 36: 174-9.

Ramachandran, R., K. Mihara, H. Chung, B. Renaux, C. S. Lau, D. A. Muruve, K. A. DeFea, M. Bouvier, and M. D. Hollenberg. 2011. 'Neutrophil elastase acts as a biased agonist for proteinase-activated receptor-2 (PAR2)', *J Biol Chem*, 286: 24638-48.

Rasmussen, U. B., V. Vouret-Craviari, S. Jallat, Y. Schlesinger, G. Pages, A. Pavirani, J. P. Lecocq, J. Pouyssegur, and E. Van Obberghen-Schilling. 1991. 'cDNA cloning and expression of a hamster alpha-thrombin receptor coupled to Ca2+ mobilization', *FEBS Lett*, 288: 123-8.

Ravasio, A., A. P. Le, T. B. Saw, V. Tarle, H. T. Ong, C. Bertocchi, R. M. Mege, C. T. Lim, N. S. Gov, and B. Ladoux. 2015. 'Regulation of epithelial cell organization by tuning cell-substrate adhesion', *Integr Biol (Camb)*, 7: 1228-41.

Reffay, M., M. C. Parrini, O. Cochet-Escartin, B. Ladoux, A. Buguin, S. Coscoy, F. Amblard, J. Camonis, and P. Silberzan. 2014. 'Interplay of RhoA and mechanical forces in collective cell migration driven by leader cells', *Nat Cell Biol*, 16: 217-23.

Reinecker, H. C., E. Y. Loh, D. J. Ringler, A. Mehta, J. L. Rombeau, and R. P. MacDermott. 1995. 'Monocyte-chemoattractant protein 1 gene expression in intestinal epithelial cells and inflammatory bowel disease mucosa', *Gastroenterology*, 108: 40-50.

Renaud, S. J., K. Kubota, M. A. Rumi, and M. J. Soares. 2014. 'The FOS transcription factor family differentially controls trophoblast migration and invasion', *J Biol Chem*, 289: 5025-39.

Reuter, B. K., S. Asfaha, A. Buret, K. A. Sharkey, and J. L. Wallace. 1996. 'Exacerbation of inflammation-associated colonic injury in rat through inhibition of cyclooxygenase-2', *J Clin Invest*, 98: 2076-85.

Riahi, R., J. Sun, S. Wang, M. Long, D. D. Zhang, and P. K. Wong. 2015. 'Notch1-Dll4 signalling and mechanical force regulate leader cell formation during collective cell migration', *Nat Commun*, 6: 6556.

Riedl, J., A. H. Crevenna, K. Kessenbrock, J. H. Yu, D. Neukirchen, M. Bista, F. Bradke, D. Jenne, T. A. Holak, Z. Werb, M. Sixt, and R. Wedlich-Soldner. 2008. 'Lifeact: a versatile marker to visualize F-actin', *Nat Methods*, 5: 605-7.

Riegler, M., R. Sedivy, C. Pothoulakis, G. Hamilton, J. Zacherl, G. Bischof, E. Cosentini, W. Feil, R. Schiessel, J. T. LaMont, and et al. 1995. 'Clostridium difficile toxin B is more potent than toxin A in damaging human colonic epithelium in vitro', *J Clin Invest*, 95: 2004-11.

Riewald, M., and W. Ruf. 2001. 'Mechanistic coupling of protease signaling and initiation of coagulation by tissue factor', *Proc Natl Acad Sci U S A*, 98: 7742-7.

Robinson, K., Z. Deng, Y. Hou, and G. Zhang. 2015. 'Regulation of the Intestinal Barrier Function by Host Defense Peptides', *Front Vet Sci*, 2: 57.

Rohani, M. G., and W. C. Parks. 2015. 'Matrix remodeling by MMPs during wound repair', *Matrix Biol*, 44-46: 113-21.

Russo, J. M., P. Florian, L. Shen, W. V. Graham, M. S. Tretiakova, A. H. Gitter, R. J. Mrsny, and J. R. Turner. 2005. 'Distinct temporal-spatial roles for rho kinase and myosin light chain kinase in epithelial purse-string wound closure', *Gastroenterology*, 128: 987-1001.

Sadok, A., and C. J. Marshall. 2014. 'Rho GTPases: masters of cell migration', *Small GTPases*, 5: e29710.

Sambuy, Y., I. De Angelis, G. Ranaldi, M. L. Scarino, A. Stammati, and F. Zucco. 2005. 'The Caco-2 cell line as a model of the intestinal barrier: influence of cell and culture-related factors on Caco-2 cell functional characteristics', *Cell Biol Toxicol*, 21: 1-26.

Sansregret, L., and A. Nepveu. 2008. 'The multiple roles of CUX1: insights from mouse models and cell-based assays', *Gene*, 412: 84-94.

Savla, U., H. J. Appel, P. H. Sporn, and C. M. Waters. 2001. 'Prostaglandin E(2) regulates wound closure in airway epithelium', *Am J Physiol Lung Cell Mol Physiol*, 280: L421-31.

Schaus, Thomas E., Edwin W. Taylor, and Gary G. Borisy. 2007. 'Self-organization of actin filament orientation in the dendritic-nucleation/array-treadmilling model', *Proc Natl Acad Sci U S A*, 104: 7086-91.

Schenk, M., and C. Mueller. 2008. 'The mucosal immune system at the gastrointestinal barrier', *Best Pract Res Clin Gastroenterol*, 22: 391-409.

Scher, J. U., and M. H. Pillinger. 2005. '15d-PGJ2: the anti-inflammatory prostaglandin?', *Clin Immunol*, 114: 100-9.

Schmassmann, A., B. M. Peskar, C. Stettler, P. Netzer, T. Stroff, B. Flogerzi, and F. Halter. 1998. 'Effects of inhibition of prostaglandin endoperoxide synthase-2 in chronic gastro-intestinal ulcer models in rats', *Br J Pharmacol*, 123: 795-804.

Sears, C. L. 2001. 'The toxins of Bacteroides fragilis', *Toxicon*, 39: 1737-46.

Sekirov, Inna, Shannon L. Russell, L. Caetano M. Antunes, and B. Brett Finlay. 2010. 'Gut Microbiota in Health and Disease', *Physiological Reviews*, 90: 859-904.

Sender, R., S. Fuchs, and R. Milo. 2016. 'Are We Really Vastly Outnumbered? Revisiting the Ratio of Bacterial to Host Cells in Humans', *Cell*, 164: 337-40.

Serhan, C. N. 2007. 'Resolution phase of inflammation: novel endogenous anti-inflammatory and proresolving lipid mediators and pathways', *Annu Rev Immunol*, 25: 101-37.

Serhan, C. N., and J. Savill. 2005. 'Resolution of inflammation: the beginning programs the end', *Nat Immunol*, 6: 1191-7.

Serhan, Charles N., Sue D. Brain, Christopher D. Buckley, Derek W. Gilroy, Christopher Haslett, Luke A. J. O'Neill, Mauro Perretti, Adriano G. Rossi, and John L. Wallace. 2007. 'Resolution of inflammation: state of the art, definitions and terms', *Faseb j*, 21: 325-32.

Sevigny, Leila M., Karyn M. Austin, Ping Zhang, Shogo Kasuda, Georgios Koukos, Sheida Sharifi, Lidija Covic, and Athan Kuliopulos. 2011. 'Protease-Activated Receptor-2 Modulates Protease-Activated Receptor-1–Driven Neointimal Hyperplasia', *Arteriosclerosis, Thrombosis, and Vascular Biology*, 31: e100-e06.

Shafran, I., W. Maurer, and F. B. Thomas. 1977. 'Prostaglandins and Crohn's disease', *N Engl J Med*, 296: 694.

Sheibanie, A. F., J. H. Yen, T. Khayrullina, F. Emig, M. Zhang, R. Tuma, and D. Ganea. 2007. 'The proinflammatory effect of prostaglandin E2 in experimental inflammatory bowel disease is mediated through the IL-23-->IL-17 axis', *J Immunol*, 178: 8138-47.

Shelley-Fraser, G., N. R. Borley, B. F. Warren, and N. A. Shepherd. 2012. 'The connective tissue changes of Crohn's disease', *Histopathology*, 60: 1034-44.

Shi, K., K. C. Queiroz, J. Stap, D. J. Richel, and C. A. Spek. 2013. 'Protease-activated receptor-2 induces migration of pancreatic cancer cells in an extracellular ATP-dependent manner', *J Thromb Haemost*, 11: 1892-902.

Shimamoto, R., T. Sawada, Y. Uchima, M. Inoue, K. Kimura, Y. Yamashita, N. Yamada, T. Nishihara, M. Ohira, and K. Hirakawa. 2004. 'A role for protease-activated receptor-2 in pancreatic cancer cell proliferation', *Int J Oncol*, 24: 1401-6.

Singer, Irwin I., Douglas W. Kawka, Suzanne Schloemann‡, Teresa Tessner‡, Terrence Riehl‡, and William F. Stenson‡. 1998. 'Cyclooxygenase 2 is induced in colonic epithelial cells in inflammatory bowel disease', *Gastroenterology*, 115: 297-306.

Smith, W. L., Y. Urade, and P. J. Jakobsson. 2011. 'Enzymes of the cyclooxygenase pathways of prostanoid biosynthesis', *Chem Rev*, 111: 5821-65.

Soh, Unice J. K., Michael R. Dores, Buxin Chen, and JoAnn Trejo. 2010. 'Signal transduction by protease-activated receptors', *British Journal of Pharmacology*, 160: 191-203.

Spencer, J., and L. M. Sollid. 2016. 'The human intestinal B-cell response', *Mucosal Immunol*, 9: 1113-24.

Stables, M. J., and D. W. Gilroy. 2011. 'Old and new generation lipid mediators in acute inflammation and resolution', *Prog Lipid Res*, 50: 35-51.

Swaminathan, Sunita. 2004. 'The Role of PAR-1 & PAR-2 in the Modulation of Intestinal Epithelial Wound Repair in vitro (Masters Dissertation)', *University of Calgary, Calgary AB*.

Takeuchi, O., and S. Akira. 2010. 'Pattern Recognition Receptors and Inflammation', *Cell*, 140: 805-20.

Turner, J. R. 2009. 'Intestinal mucosal barrier function in health and disease', *Nat Rev Immunol*, 9: 799-809.

Vachon, P. H., and J. F. Beaulieu. 1992. 'Transient mosaic patterns of morphological and functional differentiation in the Caco-2 cell line', *Gastroenterology*, 103: 414-23.

van der Merwe, J. Q., M. D. Hollenberg, and W. K. MacNaughton. 2008. 'EGF receptor transactivation and MAP kinase mediate proteinase-activated receptor-2-induced chloride secretion in intestinal epithelial cells', *Am J Physiol Gastrointest Liver Physiol*, 294: G441-51.

van der Merwe, J. Q., C. L. Ohland, C. L. Hirota, and W. K. MacNaughton. 2009. 'Prostaglandin E2 derived from cyclooxygenases 1 and 2 mediates intestinal epithelial ion transport stimulated by the activation of protease-activated receptor 2', *J Pharmacol Exp Ther*, 329: 747-52.

Volpe, D. A. 2008. 'Variability in Caco-2 and MDCK cell-based intestinal permeability assays', *J Pharm Sci*, 97: 712-25.

Vong, L., J. G. Ferraz, R. Panaccione, P. L. Beck, and J. L. Wallace. 2010. 'A pro-resolution mediator, prostaglandin D(2), is specifically up-regulated in individuals in long-term remission from ulcerative colitis', *Proc Natl Acad Sci U S A*, 107: 12023-7.

Vongsa, R. A., N. P. Zimmerman, and M. B. Dwinell. 2009. 'CCR6 regulation of the actin cytoskeleton orchestrates human beta defensin-2- and CCL20-mediated restitution of colonic epithelial cells', *J Biol Chem*, 284: 10034-45.

Vu, T. K., D. T. Hung, V. I. Wheaton, and S. R. Coughlin. 1991. 'Molecular cloning of a functional thrombin receptor reveals a novel proteolytic mechanism of receptor activation', *Cell*, 64: 1057-68.

Wallace, John L., and Pallavi R. Devchand. 2005. 'Emerging roles for cyclooxygenase-2 in gastrointestinal mucosal defense', *British Journal of Pharmacology*, 145: 275-82.

Wang, H., S. Wen, N. W. Bunnett, R. Leduc, M. D. Hollenberg, and W. K. MacNaughton. 2008. 'Proteinase-activated receptor-2 induces cyclooxygenase-2 expression through beta-catenin and cyclic AMP-response element-binding protein', *J Biol Chem*, 283: 809-15.

Weinberger, T., E. Feuille, C. Thompson, and A. Nowak-Wegrzyn. 2016. 'Chronic food protein-induced enterocolitis syndrome: Characterization of clinical phenotype and literature review', *Ann Allergy Asthma Immunol*, 117: 227-33.

Wilson, A. J., K. Byron, and P. R. Gibson. 1999. 'Interleukin-8 stimulates the migration of human colonic epithelial cells in vitro', *Clin Sci (Lond)*, 97: 385-90.

Wilson, B. J., R. Harada, L. LeDuy, M. D. Hollenberg, and A. Nepveu. 2009. 'CUX1 transcription factor is a downstream effector of the proteinase-activated receptor 2 (PAR2)', *J Biol Chem*, 284: 36-45.

Wu, R., S. J. Coniglio, A. Chan, M. H. Symons, and B. M. Steinberg. 2007. 'Up-regulation of Rac1 by epidermal growth factor mediates COX-2 expression in recurrent respiratory papillomas', *Mol Med*, 13: 143-50.

Wu, W. K., J. J. Sung, C. W. Lee, J. Yu, and C. H. Cho. 2010. 'Cyclooxygenase-2 in tumorigenesis of gastrointestinal cancers: an update on the molecular mechanisms', *Cancer Lett*, 295: 7-16.

Wu, Y., J. Wang, H. Zhou, X. Yu, L. Hu, F. Meng, and S. Jiang. 2014. 'Effects of calcium signaling on coagulation factor VIIa-induced proliferation and migration of the SW620 colon cancer cell line', *Mol Med Rep*, 10: 3021-6.

Xavier, R. J., and D. K. Podolsky. 2007. 'Unravelling the pathogenesis of inflammatory bowel disease', *Nature*, 448: 427-34.

Xie, Q., S. Mittal, and M. E. Berens. 2014. 'Targeting adaptive glioblastoma: an overview of proliferation and invasion', *Neuro Oncol*, 16: 1575-84.

Xu, W. F., H. Andersen, T. E. Whitmore, S. R. Presnell, D. P. Yee, A. Ching, T. Gilbert, E. W. Davie, and D. C. Foster. 1998. 'Cloning and characterization of human protease-activated receptor 4', *Proc Natl Acad Sci U S A*, 95: 6642-6.

Yada, K., K. Shibata, T. Matsumoto, M. Ohta, S. Yokoyama, and S. Kitano. 2005. 'Protease-activated receptor-2 regulates cell proliferation and enhances cyclooxygenase-2 mRNA expression in human pancreatic cancer cells', *J Surg Oncol*, 89: 79-85.

Yamaguchi, N., T. Mizutani, K. Kawabata, and H. Haga. 2015. 'Leader cells regulate collective cell migration via Rac activation in the downstream signaling of integrin beta1 and PI3K', *Sci Rep*, 5: 7656.

Yamaoka, T., M. R. Frey, R. S. Dise, J. K. Bernard, and D. B. Polk. 2011. 'Specific epidermal growth factor receptor autophosphorylation sites promote mouse colon epithelial

cell chemotaxis and restitution', *Am J Physiol Gastrointest Liver Physiol*, 301: G368-76.

Yang, S. K., L. Eckmann, A. Panja, and M. F. Kagnoff. 1997. 'Differential and regulated expression of C-X-C, C-C, and C-chemokines by human colon epithelial cells', *Gastroenterology*, 113: 1214-23.

Zamuner, S. R., N. Warrier, A. G. Buret, W. K. MacNaughton, and J. L. Wallace. 2003. 'Cyclooxygenase 2 mediates post-inflammatory colonic secretory and barrier dysfunction', *Gut*, 52: 1714-20.

Zeeh, F., D. Witte, T. Gadeken, B. H. Rauch, E. Grage-Griebenow, N. Leinung, S. J. Fromm, S. Stolting, K. Mihara, R. Kaufmann, U. Settmacher, H. Lehnert, M. D. Hollenberg, and H. Ungefroren. 2016. 'Proteinase-activated receptor 2 promotes TGF-beta-dependent cell motility in pancreatic cancer cells by sustaining expression of the TGF-beta type I receptor ALK5', *Oncotarget*.

Zegers, Mirjam M., and Peter Friedl. 2014. 'Rho GTPases in collective cell migration', *Small GTPases*, 5: e28997.

Zhang, C., G. R. Gao, C. G. Lv, B. L. Zhang, Z. L. Zhang, and X. F. Zhang. 2012. 'Protease-activated receptor-2 induces expression of vascular endothelial growth factor and cyclooxygenase-2 via the mitogen-activated protein kinase pathway in gastric cancer cells', *Oncol Rep*, 28: 1917-23.

Zhao, Min, Bing Song, Jin Pu, Teiji Wada, Brian Reid, Guangping Tai, Fei Wang, Aihua Guo, Petr Walczysko, Yu Gu, Takehiko Sasaki, Akira Suzuki, John V. Forrester, Henry R. Bourne, Peter N. Devreotes, Colin D. McCaig, and Josef M. Penninger. 2006. 'Electrical signals control wound healing through phosphatidylinositol-3-OH kinase-[gamma] and PTEN', *Nature*, 442: 457-60.

Zhou, B., H. Zhou, S. Ling, D. Guo, Y. Yan, F. Zhou, and Y. Wu. 2011. 'Activation of PAR2 or/and TLR4 promotes SW620 cell proliferation and migration via phosphorylation of ERK1/2', *Oncol Rep*, 25: 503-11.

Zhu, G., Z. Fan, M. Ding, H. Zhang, L. Mu, Y. Ding, Y. Zhang, B. Jia, L. Chen, Z. Chang, and W. Wu. 2015. 'An EGFR/PI3K/AKT axis promotes accumulation of the Rac1-GEF Tiam1 that is critical in EGFR-driven tumorigenesis', *Oncogene*, 34: 5971-82.

Zhu, M., Y. Zhu, and P. Lance. 2013. 'TNFalpha-activated stromal COX-2 signalling promotes proliferative and invasive potential of colon cancer epithelial cells', *Cell Prolif*, 46: 374-81.

Zygmunt, B., and M. Veldhoen. 2011. 'T helper cell differentiation more than just cytokines', *Adv Immunol*, 109: 159-96.

APPENDIX A

Details of Image Analysis and Quantification

A.1 Cell counting for Caco2 EdU analysis

The following cell counting protocol was performed separately on both captured channels (DAPI 405 nm, and EdU 488 nm), in order to express data as percent EdU+ cells relative to total DAPI cell number.

With an individual image to be analyzed open in ImageJ:

1. Process – Subtract background (Rolling ball radius: 50 px)
2. Image – Adjust – Threshold (Default, B&W, Dark background)
3. Process – Binary – Make Binary
4. Process – Binary – Watershed (added a 1 px white line through objects that were likely distinct)
5. Analyze – Analyze particles (Size: 300 - ∞; Circularity 0 – 1; Exclude on edges; Summarize)

Figure A.1 details the process in confluent (A), subconfluent (B), and wound edge cells (C). An additional step was performed for the wound edge cells in order to isolate an area surrounding the wound that was 2-3 cells deep (Figure A.1 C). The edge of the wound on the DAPI image was manually traced, and the size of the selection was increased by 30 px. The selection was then copied to the EdU image in order to ensure the same area was analyzed. Next, the area surrounding the enlarged selection was deleted, and the above protocol was performed on only the cells surrounding the wound.

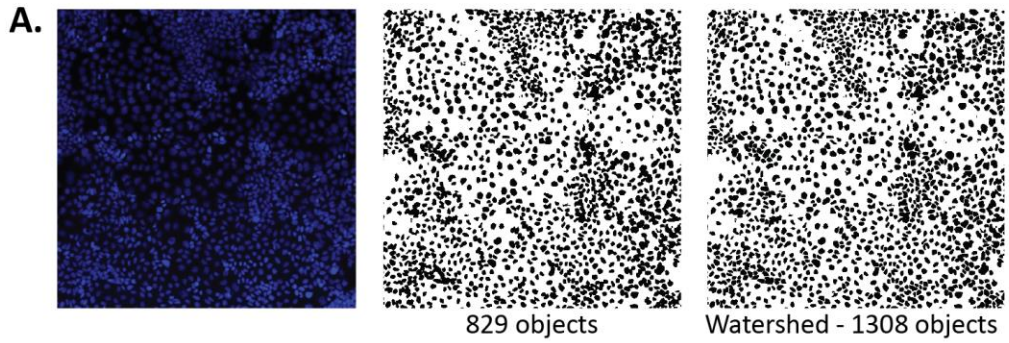
A.
829 objects
Watershed - 1308 objects
B.
C.

Figure A.1 Caco2 cell counting for EdU analysis using ImageJ.

The DAPI and EdU images were analyzed with the following protocol in order to count the cells. Examples are provided for DAPI images for confluent (A), subconfluent (B) and wound edge (C) cells. A: Images of confluent cells had the background subtracted (left), and had a threshold applied in order to turn the image into black and white (middle). If the objects were counted at this step, there were only 829. The next important step of applying the watershed function, which added a 1 px line to separate predicted objects (right), resulted in the count increasing to 1308 objects. B, C: Subconfluent and wound edge cells were counted using the same protocol.

A.2 Cell counting for T84 EdU analysis

Compared to the Caco2 cells, the T84 cells were more tightly packed and the protocol for Caco2 cell counting did not accurately identify cell numbers in either the DAPI or EdU T84 images. Instead, the Trainable Weka Segmentation tool within FIJI was used to create "classifiers". A classifier was created by opening a single image, manually tracing a number of nuclei, and sorting those traces to Class 1. Next, areas of the background and areas between the cells were manually traced and sorted to Class 2. The classifier was "trained", and the above process of manually tracing areas was repeated, followed by repeatedly training the classifier, until it accurately identified individual nuclei within the entire image (Figure A.2). One classifier was created for DAPI images, and one for EdU images. Once the classifiers were created, they were applied to folders of images in order to batch process the T84 cell counting.

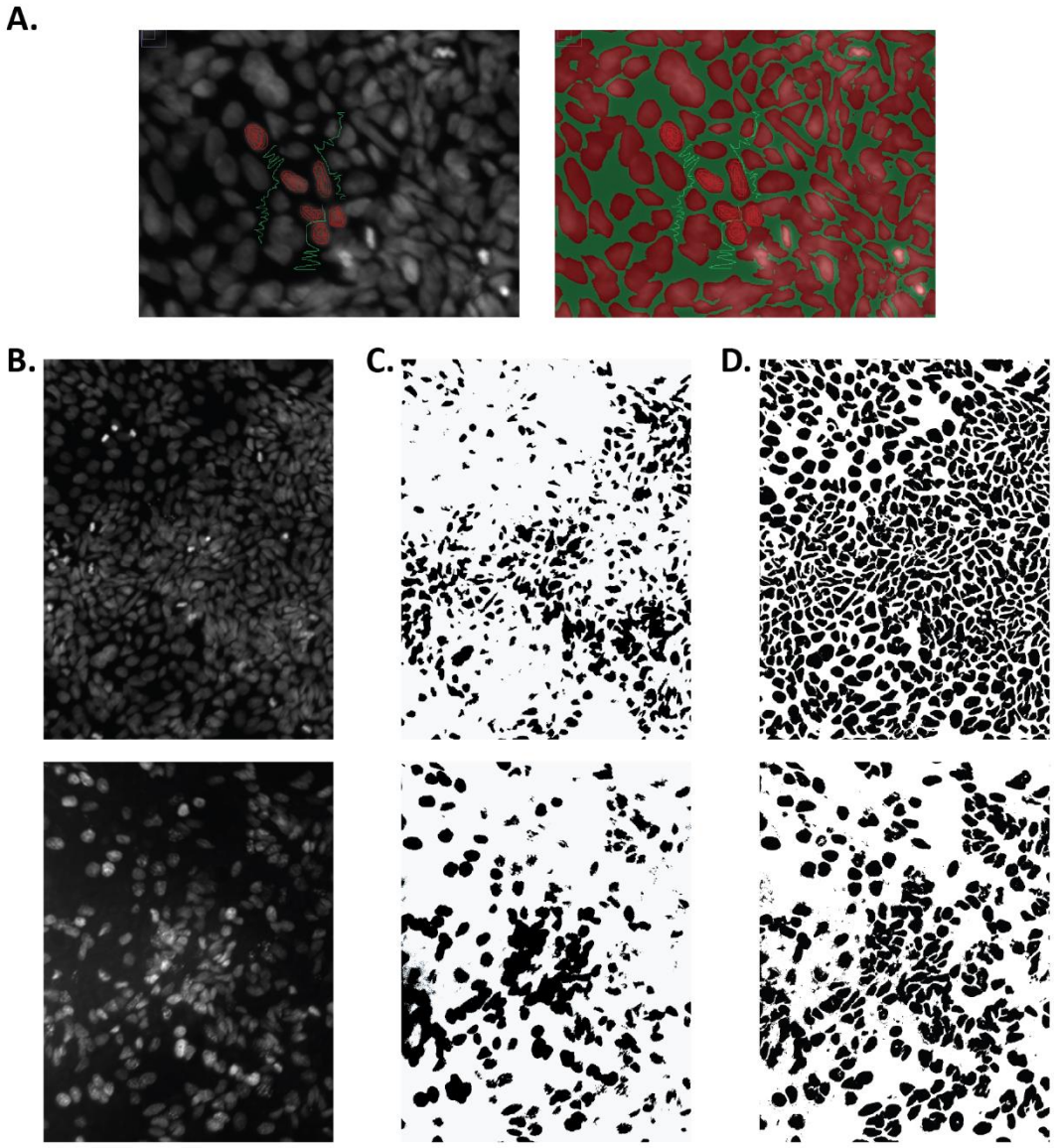

Figure A.2 T84 cell counting for EdU analysis using Trainable Weka Segmentation in FIJI.

A: An example of the tracings to identify Class 1 (nuclei, red) and Class 2 (background, green). B: Starting T84 images, DAPI (top) and EdU (bottom). C: Using the Caco2 cell counting protocol, all of the T84 cells were not accurately identified. D: The Trainable Weka Segmentation tool allowed for a more accurate automated count of T84 cells.

A.3 Quantification of actin cabling and E-cadherin in Caco2 cells

In order to quantify the actin properties (cable, lamellipodia) and E-cadherin loss surrounding the wounds, stitched Caco2 wound images were randomized and given to 4 individuals for blinded quantification, and the 4 values were averaged.

For actin properties, individuals were asked to manually trace the distance surrounding the wound that had apparent actin cable (Figure A.3 A), and apparent lamellipodia. The cable and lamellipodia distance was compared to the total wound perimeter, and data were expressed as a percent of wound perimeter.

For E-cadherin loss, individuals were asked to manually trace the area surrounding the wound that had apparent E-cadherin loss/internalization (Figure A.3 B). The area was compared to the wound area, and data were expressed as percent increase of initial wound.

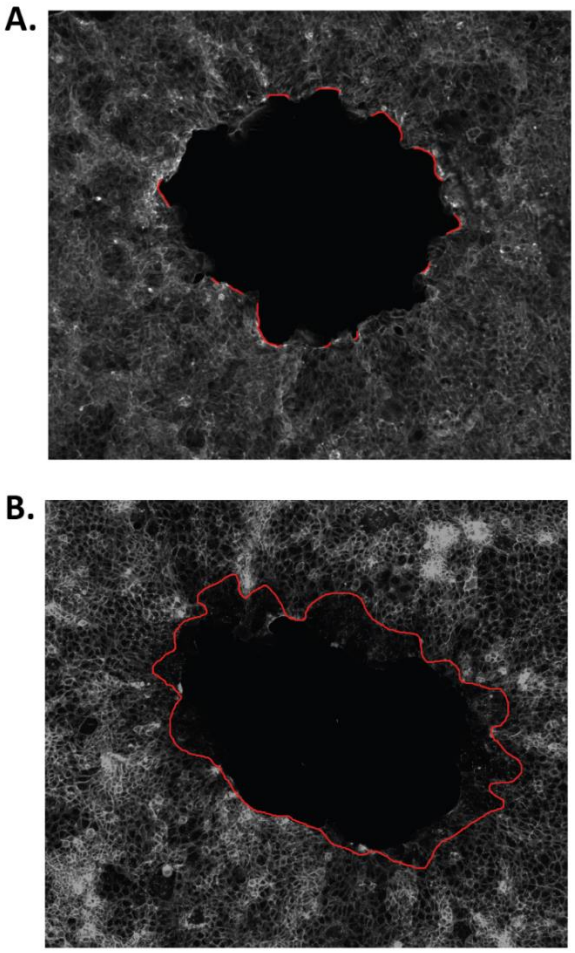

Figure A.3 Examples of quantification for actin cable and E-cadherin loss.

The actin properties and E-cadherin loss were quantified by 4 blinded individuals and averaged. A: Example of actin cable tracing. B: Example of E-cadherin tracing.

APPENDIX B

RNA sequencing of wounded Caco2 cells

B.1 Venn diagrams with gene lists

Complimentary to the data in the body of the thesis, the Venn diagrams are reproduced with gene lists included.

B.2 Top pathways identified using EnrichR

EnrichR is a web-based platform that can run a list of genes through multiple pathway analyses, and output the top hits from each database. To give a representation of the data acquired using this method, tables are provided for the top 5 pathways identified from three databases commonly used for RNA sequencing pathway analysis (Kyoto Encyclopedia of Genes and Genomes (KEGG), WikiPathways, and Reactome). (Table B.1 NW-C vs W-C and Table B.2 NW-C vs NW-PAR2)

B.3 Gene Ontology terms identified using EnrichR

Similar to the pathway analysis, the top 5 hits for the thee gene ontology categories (biological processes, cellular components, molecular function) are shown as representative data acquired. (Table B.3 NW-C vs W-C and Table B.4 NW-C vs NW-PAR2)

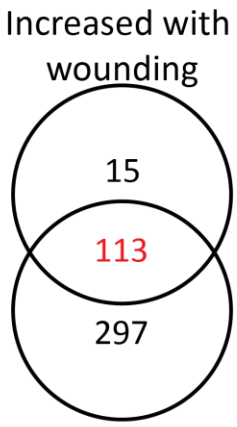

ATF3	CXCL3	HLA-C	LARP4	PRR7
CHAC1	FLNC	INHBA	NDRG2	TRIM47
CRIP2	FZD9	IRAK2	NEIL2	WNT9A

ADAMTS9	BIRC3	CXCR4	EMP3	GPRC5A	L1CAM	MYADM	PLAUR	SDCCAG3	TAL2	VGF
AK3	C8orf4	DLX2	EPHA2	HK2	LAMC2	MYC	PLEC	SFN	TM4SF1	VSIG1
ALDH1A3	CBARP	DUSP4	EREG	ID1	LDLR	N4BP3	PLK2	SGMS2	TMCC2	ZFP36
ANKRD1	CCL20	DUSP5	F2RL1	IER2	LIF	NCOA7	PLK3	SH2B3	TMEM158	ZIC5
ANXA1	CCL20	DUSP6	FAM81A	IL11	LIG4	NPPB	PMAIP1	SKIL	TN-	ZNF239
AREG	CDKN1A	EDN1	FOS	ITGA2	MAFF	NR4A1	PTGS2	SLC25A25	FRSF11B	
ARHGEF3	CEACAM6	EGR1	FOSB	JUN	MAP3K14	NUAK2	PTPRH	SLC2A1	TN-	
ARL14	CLCF1	EGR3	FOSL1	JUNB	METTL21A	PHLDA1	RELB	SOX8	FRSF12A	
ATF3	CLDN2	EGR4	GCNT3	KIAA1462	MFSD2A	PHLDA2	RGS2	SPRY2	TNFRSF21	
BHLHA15	CSRP1	EIF5A2	GDF15	KLF6	MMP1	PIP5K1A	RGS20	SPRY4	TRIB1	
BHLHE40	CXCL8	EMP1	GPR3	KRT20	MMP10	PLAU	S100A3	TAGLN	UBASH3B	

ADGRG6	CBFB	CTPS1	FERMT2	ICOSLG	KLF16	MCM10	NOP2	RABEPK	SLC7A1	TFRC	VGLL3
ADORA2B	CBFB	CYP2S1	FFAR4	ID1	KLF4	MESDC1	NOX1	RASA2	SLC7A5	TGFBR2	WDR4
AEN	CCDC86	CYP51A1	FGFR1	IFRD1	KRT17	METTL1	NR1D1	RASSF9	SLCO4A1	TGIF1	WT1
AHR	CCND1	CYR61	FGFRL1	IL2RG	KRT18	MICAL2	NR4A1	RDX	SMG7	TGIF1	YRDC
AKR1B10	CCND2	DDX21	FHL2	INPP1	LAD1	MIR205HG	NT5DC3	RELT	SNAI1	THBS1	YWHAZ
ANKRD13B	CCNE1	DKK1	FJX1	ISM1	LAMC2	MMD	ODC1	RGCC	SOWAHC	TIGAR	ZBTB16
ANKRD33B	CCNE2	DOT1L	FKBP4	ISM2	LARP1B	MORC4	OSBPL3	RGS16	SOX9	TMC7	ZC3H12A
ARAP2	CCNYL1	DUSP1	FKBP5	ITGA6	LIMCH1	MORC4	OSGIN2	RHOB	SPAG1	TMEM151	ZFYVE27
ARHGAP42	CD3EAP	DUSP2	FLNC	ITPRIPL1	LONRF1	MPP3	PAK1IP1	RNF24	SPATS2L	A	ZIC2
ARL5B	CDC25A	DUSP7	FLRT3	JAG1	LRCH1	MTMR3	PEA15	RP2	SPHK1	TMEM2	ZNF317
ATG101	CDC25A	DZANK1	FOXF2	JMJD6	LRIG3	MYL12B	PLD6	S1PR3	SPRED1	TNC	ZNF367
AXL	CDCA7	EBI3	FOXQ1	KAZN	LRIG3	NAB2	PLEKHO1	SAMD5	SPRED2	TNFAIP8	ZNF410
B4GALT4	CDCP1	EEPD1	GAD1	KCNF1	LRP8	NABP1	PLEKHO2	SAT1	SPRY1	TN-	ZNF473
B4GALT6	CDK5R1	EGLN3	GAL	KCNN4	LRP8	NCR3LG1	PLPP2	SCN1B	SRXN1	FRSF10A	ZNF655
BATF3	CEACAM5	EN2	GBX2	KCTD1	LRRC8A	NDEL1	PLXNA2	SEPT5	SSTR2	TN-	ZYX
BAZ1A	CEP83	ENC1	GEM	KCTD1	LRRC8B	NDOR1	PNO1	SERTAD4	SSX2IP	FRSF10D	
BCL3	CFAP45	EPB41L1	GJA1	KCTD15	LRRC8E	NDRG4	POP1	SGMS2	ST3GAL5	TNFRSF1B	
BDNF	CHRM4	EPHB6	GNL3L	KCTD5	LYAR	NDUFAF4	PPFIBP1	SH2D3A	STARD4	TNPO2	
BMP2	CLIC5	ERRFI1	GPAT3	KCTD9	MAFK	NES	PPRC1	SH2D5	SUCO	TPBGL	
C10orf2	COA6	ETS2	GPRIN1	KDM6B	MAK16	NFATC3	PRRG1	SHC1	SYNCRIP	TRAF3	
C10orf2	CREB3L1	ETV4	HBEGF	KIAA1191	MANEAL	NIP7	PRSS22	SHH	TAF1A	ULBP2	
C10orf54	CSF1	ETV5	HCAR3	KIF1A	MAP6D1	NIPAL4	PRSS23	SIK1	TCEB1	UPP1	
C11orf86	CSGALN-	F3	HIGD1A	KIFC3	MARS2	NKPD1	PSAPL1	SLC20A1	TCOF1	URB2	
C17orf96	ACT1	FAM111B	HNRNPAB	KISS1	MAT2A	NOCT	PXDC1	SLC25A32	TDO2	USP31	
C5orf30	CSRNP1	FAM155B	HOMER1	KLF10	MB21D1	NOL6	PYGO1	SLC35G2	TESC	VCAN	
CAPN8	CSRP1	FAM83G	HOXB9	KLF13	MCL1	NOP16	RAB31	SLC4A7	TFF1	VCL	

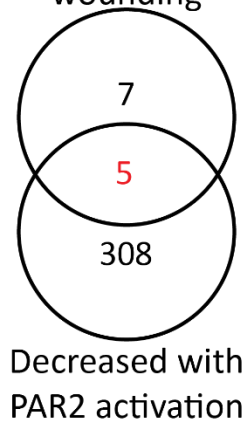

ANKZF1	JDP2
BCL2L11	SETDB2
FOXP1	TRAPPC13
FZD6	
FAM63A	SPATS2L
NEDD4L	STUM
PAM	

ABTB1	BMF	CLDN3	FAM26D	HE-	KAT5	MYCL	PDGFRL	RBBP8NL	SOWAHD	TREX1	ZNF181
ACACB	BMF	CPT1B	FAM63A	PACAM2	KIAA0141	MYO18A	PDZD3	RDH5	SPACA9	TRIM24	ZNF233
ACBD4	BORCS6	CREB3L4	FAXDC2	HEXIM2	KIF12	NATD1	PHEX	RHBG	SPTLC3	TRIM3	ZNF33A
ACCS	BRD8	CREBRF	FBXO27	HIST1H2AC	KIZ	NBR1	PIFO	RTN4RL2	SSBP2	TRPV3	ZNF33B
ACOT12	BRE	CYP4V2	FBXO8	HIST1H2A	KLHDC7A	NCK2	PIGZ	RWDD2A	ST5	TSC22D1	ZNF446
ADGRG1	C10orf10	CYSRT1	FEZ2	G	KLHDC9	NET1	PITX2	SALL2	STARD13	TSPAN12	ZNF552
ADH6	C11orf52	DBP	FGD3	HIST1H2B	KLHL24	NFE2	PITX2	SARDH	SULT1A1	TSSK6	ZNF572
ADIRF	C11orf54	DDX58	FGFR2	D	KRBOX4	NHSL1	PITX2	SEPSECS	SYBU	TTC30A	ZNF599
AGTRAP	C12orf76	DEGS2	FMO4	HIST1H3G	LAMA1	NMNAT3	PITX2	SERPINA6	SYF2	TTC30B	ZNF618
AGXT	C14orf80	DEPTOR	FOXJ1	HIST3H2A	LDHD	NMNAT3	PLA2G12B	SERPINF2	TARBP2	TTLL1	ZNF688
AIMP1	C14orf93	DGCR6	FOXO3	HOGA1	LETMD1	NR2F2	PLCH1	SESN1	TBC1D2	TXNIP	ZNF763
AKAP9	C19orf54	DHFR2	FRAT1	HORMAD2	LGSN	NR2F2	PLEKHM3	SESN3	TBX6	UBALD2	ZNF836
AMACR	C1orf116	DOCK9	FZD2	HOXA4	LOX	NTF3	PMM1	SETDB2	TCF4	UPK1A	ZSCAN2
AMOT	C1orf210	DRC7	G0S2	HOXA5	LYPD3	NUDT13	PNRC1	SH2B1	TCP11L2	USP51	
ANK3	C21orf58	EFNA1	GABRA4	HOXA6	MAF	NUDT18	POLR3GL	SH3RF2	TCTN2	VMAC	NM_00124
ANO1	C3orf58	EID2B	GATM	HOXB13	MAP2K6	NUDT2	PPEF1	SI	TESK2	VSTM5	2776
ANXA2R	C4orf33	ENHO	GDPD2	HOXC5	MAT1A	NUDT6	PPM1M	SIRT4	TFEC	WBSCR27	
AQP7	C5orf38	EPHX2	GDPGP1	HOXC6	MATN2	NUPR1	PROCA1	SIX5	THAP8	WNT1	
ATP10B	CAB39L	EPOR	GLI4	HOXC6	MB	NYNRIN	PRR15L	SLC23A1	THOC5	YPEL2	
BBS12	CALCOCO1	ERBB3	GPR162	HPDL	MDM1	OIT3	PRRT2	SLC40A1	TMEM135	YPEL3	
BCL2L11	CCDC170	ERICH4	GRAMD1C	HTR1D	METTL7A	ORAI3	PRUNE1	SLC44A2	TMEM187	ZBTB4	
BCL6	CCDC28A	ESPN	GRAMD3	IFIT3	MIA2	OSR2	PTH1R	SLC46A3	TMEM86B	ZC4H2	
BCL6	CCNG2	EVL	GRB7	IKBKB	MMP11	P2RY1	PYROXD2	SLC4A8	TMEM8B	ZFAND4	
BCO1	CDKN2C	EXOC3L4	GRIK4	IP6K2	MUSTN1	P2RY6	RAB37	SLC5A9	TNNI3	ZFP14	
BDH1	CEP126	FAM134B	GRIN2C	IRF2	MXD4	PCED1B	RAB3IL1	SMLR1	TNRC6B	ZFYVE1	
BFSP1	CHST9	FAM179A	GTF2I	IRF2BPL	MXI1	PCSK4	RASGEF1B	SORBS2	TPGS1	ZMYM5	
BIN1	CLDN19	FAM214A	HBP1	JMY	MYBPH	PDCD4	RB1CC1	SORBS2	TRAF3IP2	ZNF160	

Table B.1 NW-Control vs W-Control – Pathway analysis on 128 upregulated genes

KEGG 2016

Term	Overlap	Combined Score	Genes
HTLV-I infection_Homo sapiens_hsa05166	14/258	20.80	EGR1, JUN, CDKN1A, FZD9, SLC2A1, HLA-C, WNT9A, FOS, RELB, FOSL1, ZFP36, MYC, MAP3K14, ATF3
TNF signaling pathway_Homo sapiens_hsa04668	10/110	20.76	EDN1, JUN, CCL20, LIF, FOS, CXCL3, PTGS2, MAP3K14, JUNB, BIRC3
Pathways in cancer_Homo sapiens_hsa05200	14/397	13.16	JUN, CDKN1A, CXCL8, MMP1, ITGA2, FZD9, SLC2A1, CXCR4, LAMC2, WNT9A, FOS, PTGS2, MYC, BIRC3
Osteoclast differentiation_Homo sapiens_hsa04380	8/132	11.15	FOSL1, JUN, FOSB, TNFRSF11B, FOS, MAP3K14, JUNB, RELB
Cytokine-cytokine receptor interaction_Homo sapiens_hsa04060	11/265	11.12	IL11, CXCL8, TNFRSF12A, CCL20, CLCF1, LIF, CXCR4, TNFRSF11B, INHBA, CXCL3, TNFRSF21

WikiPathways 2016

Term	Overlap	Combined Score	Genes
TGF-beta Signaling Pathway_Homo sapiens_WP366	11/132	16.67	JUN, KLF6, CDKN1A, MMP1, MYC, ITGA2, FOSB, FOS, JUNB, SKIL, ATF3
Integrated Pancreatic Cancer Pathway_Homo sapiens_WP2377	10/192	10.86	EGR1, IL11, JUN, CDKN1A, ANXA1, GPRC5A, MYC, INHBA, PTGS2, JUNB
Wnt Signaling Pathway_Mus musculus_WP403	6/58	9.77	FOSL1, JUN, PLAU, MYC, FZD9, LDLR
TWEAK Signaling Pathway_Homo sapiens_WP2036	5/42	9.48	JUN, TNFRSF12A, MAP3K14, BIRC3, RELB
Quercetin and Nf-kB/ AP-1 Induced Cell Apoptosis_Homo sapiens_WP2435	4/16	9.47	JUN, MMP1, FOS, PTGS2

Reactome 2016

Term	Overlap	Combined Score	Genes
Cytokine Signaling in Immune system_Homo sapiens_R-HSA-1280215	15/620	10.20	DUSP4, DUSP5, EGR1, IL11, TNFRSF12A, LIF, HLA-C, TNFRSF11B, DUSP6, EREG, RELB, IRAK2, CLCF1, MAP3K14, BIRC3
MAPK targets/ Nuclear events mediated by MAP kinases_Homo sapiens_R-HSA-450282	4/30	9.74	DUSP4, JUN, FOS, DUSP6
Toll Like Receptor 3 (TLR3) Cascade_Homo sapiens_R-HSA-168164	6/97	9.05	DUSP4, JUN, IRAK2, FOS, DUSP6, BIRC3
MyD88-independent TLR3/TLR4 cascade_Homo sapiens_R-HSA-166166	6/97	9.02	DUSP4, JUN, IRAK2, FOS, DUSP6, BIRC3
TRIF-mediated TLR3/TLR4 signaling_Homo sapiens_R-HSA-937061	6/97	8.98	DUSP4, JUN, IRAK2, FOS, DUSP6, BIRC3

Table B.2 NW-Control vs NW-PAR2 activated – Pathway analysis on 410 upregulated genes

KEGG 2016

Term	Overlap	Combined Score	Genes
TNF signaling pathway_Homo sapiens_hsa04668	15/110	19.13	EDN1, JUN, JAG1, CSF1, CCL20, LIF, FOS, TNFRSF1B, PTGS2, TRAF3, CREB3L1, BCL3, MAP3K14, JUNB, BIRC3
Pathways in cancer_Homo sapiens_hsa05200	24/397	11.36	JUN, EGLN3, CDKN1A, CXCL8, MMP1, ZBTB16, ITGA2, SLC2A1, CXCR4, LAMC2, FOS, PTGS2, TGFBR2, SHH, BMP2, CCNE2, CCND1, TRAF3, CCNE1, MYC, ITGA6, TCEB1, BIRC3, FGFR1
MAPK signaling pathway_Homo sapiens_hsa04010	18/255	10.61	DUSP4, DUSP5, JUN, DUSP2, DUSP1, BDNF, NFATC3, FOS, DUSP6, DUSP7, RELB, TGFBR2, NR4A1, MYC, RASA2, FLNC, MAP3K14, FGFR1
Small cell lung cancer_Homo sapiens_hsa05222	10/86	9.76	CCND1, CCNE2, TRAF3, CCNE1, ITGA2, MYC, ITGA6, LAMC2, PTGS2, BIRC3
Cytokine-cytokine receptor interaction_Homo sapiens_hsa04060	18/265	9.58	IL11, CXCL8, TNFRSF12A, CSF1, CCL20, LIF, CXCR4, TNFRSF11B, TNFRSF10A, IL2RG, TNFRSF1B, TNFRSF10D, TGFBR2, BMP2, CLCF1, PLEKHO2, RELT, TNFRSF21

WikiPathways 2016

Term	Overlap	Combined Score	Genes
TGF-beta Signaling Pathway_Homo sapiens_WP366	19/132	19.99	TGIF1, KLF10, JUN, CDKN1A, MMP1, SHC1, ITGA2, TNC, FOS, THBS1, TGFBR2, KLF6, CCND1, MYC, FOSB, SIK1, JUNB, SKIL, ATF3
Spinal Cord Injury_Homo sapiens_WP2431	15/119	11.95	EGR1, ANXA1, CXCL8, BDNF, FOS, PTGS2, RHOB, NR4A1, ZFP36, GJA1, VCAN, CCND1, MYC, PLXNA2, SOX9
Spinal Cord Injury_Mus musculus_WP2432	13/96	10.71	EGR1, ANXA1, BDNF, FOS, RHOB, NR4A1, VCAN, ZFP36, GJA1, CCND1, MYC, PLXNA2, SOX9
Apoptosis Modulation and Signaling_Homo sapiens_WP1772	12/93	10.06	JUN, TRAF3, PEA15, PMAIP1, TNFRSF11B, TNFRSF10A, FOS, TNFRSF1B, MAP3K14, MCL1, TNFRSF10D, BIRC3
Integrated Pancreatic Cancer Pathway_Homo sapiens_WP2377	17/192	9.57	EGR1, IL11, JUN, CDKN1A, ANXA1, BDNF, PTGS2, THBS1, SHH, GPRC5A, CCND1, WT1, CCNE1, MYC, TFF1, JUNB, FGFR1

Reactome 2016

Term	Overlap	Combined Score	Genes
Signaling by FGFR1_Homo sapiens_R-HSA-5654736	22/336	14.63	DUSP4, DUSP5, DUSP2, CDKN1A, DUSP1, SHC1, IL2RG, DUSP6, FGFRL1, EREG, DUSP7, NR4A1, SPRED2, SPRED1, FLRT3, PEA15, RASA2, PIP5K1A, SPRY2, VCL, HBEGF, FGFR1
MAPK family signaling cascades_Homo sapiens_R-HSA-5683057	20/284	14.33	DUSP4, DUSP5, JUN, DUSP2, DUSP1, SHC1, IL2RG, ETV4, DUSP6, MMP10, EREG, DUSP7, SPRED2, SPRED1, MYC, PEA15, RASA2, VCL, HBEGF, FGFR1
Signaling by FGFR_Homo sapiens_R-HSA-190236	22/366	13.87	DUSP4, DUSP5, DUSP2, CDKN1A, DUSP1, SHC1, IL2RG, DUSP6, FGFRL1, EREG, DUSP7, NR4A1, SPRED2, SPRED1, FLRT3, PEA15, RASA2, PIP5K1A, SPRY2, VCL, HBEGF, FGFR1
Signaling by EGFR_Homo sapiens_R-HSA-177929	21/355	13.60	DUSP4, DUSP5, DUSP2, CDKN1A, DUSP1, SHC1, IL2RG, DUSP6, EREG, DUSP7, NR4A1, SPRED2, SPRED1, PEA15, RASA2, PIP5K1A, SPRY2, SPRY1, VCL, HBEGF, FGFR1
Signaling by FGFR4_Homo sapiens_R-HSA-5654743	20/332	13.51	DUSP4, DUSP5, DUSP2, CDKN1A, DUSP1, SHC1, IL2RG, DUSP6, EREG, DUSP7, NR4A1, SPRED2, SPRED1, PEA15, RASA2, PIP5K1A, SPRY2, VCL, HBEGF, FGFR1

Table B.3 NW-Control vs W-control – Gene ontology terms for 128 upregulated genes

GO terms Biological Processes 2015

Term	Overlap	Combined Score	Genes
Cytokine Signaling in Immune system_Homo sapiens_R-HSA-1280215	15/620	10.20	DUSP4, DUSP5, EGR1, IL11, TNFRSF12A, LIF, HLA-C, TNFRSF11B, DUSP6, EREG, RELB, IRAK2, CLCF1, MAP3K14, BIRC3
MAPK targets/ Nuclear events mediated by MAP kinases_Homo sapiens_R-HSA-450282	4/30	9.74	DUSP4, JUN, FOS, DUSP6
Toll Like Receptor 3 (TLR3) Cascade_Homo sapiens_R-HSA-168164	6/97	9.05	DUSP4, JUN, IRAK2, FOS, DUSP6, BIRC3
MyD88-independent TLR3/TLR4 cascade_Homo sapiens_R-HSA-166166	6/97	9.02	DUSP4, JUN, IRAK2, FOS, DUSP6, BIRC3
TRIF-mediated TLR3/TLR4 signaling_Homo sapiens_R-HSA-937061	6/97	8.98	DUSP4, JUN, IRAK2, FOS, DUSP6, BIRC3

GO terms Cellular Components 2015

Term	Overlap	Combined Score	Genes
focal adhesion (GO:0005925)	12/352	17.25	ANXA1, CSRP1, PLAU, ITGA2, SPRY4, PLAUR, PIP5K1A, LIG4, FLNC, L1CAM, PLEC, EPHA2
cell-substrate adherens junction (GO:0005924)	12/358	17.23	ANXA1, CSRP1, PLAU, ITGA2, SPRY4, PLAUR, PIP5K1A, LIG4, FLNC, L1CAM, PLEC, EPHA2
cell-substrate junction (GO:0030055)	12/362	17.20	ANXA1, CSRP1, PLAU, ITGA2, SPRY4, PLAUR, LIG4, PIP5K1A, FLNC, L1CAM, PLEC, EPHA2
adherens junction (GO:0005912)	12/405	14.99	ANXA1, CSRP1, PLAU, ITGA2, SPRY4, PLAUR, LIG4, PIP5K1A, FLNC, L1CAM, EPHA2, PLEC
anchoring junction (GO:0070161)	12/419	14.68	ANXA1, CSRP1, PLAU, ITGA2, SPRY4, PLAUR, LIG4, PIP5K1A, FLNC, L1CAM, EPHA2, PLEC

GO terms Molecular Function 2015

Term	Overlap	Combined Score	Genes
cytokine activity (GO:0005125)	11/213	22.09	IL11, EDN1, CXCL8, CCL20, GDF15, CLCF1, LIF, TNFRSF11B, INHBA, CXCL3, AREG
growth factor activity (GO:0008083)	8/163	13.43	IL11, VGF, GDF15, CLCF1, LIF, INHBA, AREG, EREG
MAP kinase phosphatase activity (GO:0033549)	3/16	11.65	DUSP4, DUSP5, DUSP6
R-SMAD binding (GO:0070412)	3/22	11.34	JUN, ANKRD1, FOS
MAP kinase tyrosine/serine/threonine phosphatase activity (GO:0017017)	3/15	11.33	DUSP4, DUSP5, DUSP6

Table B.4 NW-Control vs NW-PAR2 activated – Gene ontology terms for 410 upregulated genes

GO terms Biological Process 2015

Term	Overlap	Combined Score	Genes
cellular response to external stimulus (GO:0071496)	22/185	30.03	KLF10, EGR1, JUN, CDKN1A, SPHK1, SLC2A1, TNC, TNFRSF10A, FOS, PTGS2, HIGD1A, FOSL1, GJA1, NUAK2, AXL, ADORA2B, ANKRD1, PMAIP1, ITGA6, SOX9, UPP1, MAP3K14
regulation of protein serine/threonine kinase activity (GO:0071900)	31/416	25.66	CDKN1A, SHC1, CXCR4, THBS1, SPRED2, RGS2, SPRED1, CCND2, CCND1, SFN, DUSP4, DUSP5, EDN1, DUSP2, DUSP1, SPRY4, TNFRSF10A, CDC25A, DUSP6, DUSP7, BMP2, RGCC, CCNE2, ADORA2B, CCNE1, CCNYL1, SPRY2, SPRY1, TRIB1, FGFR1, CDK5R1
response to extracellular stimulus (GO:0009991)	26/313	25.40	CDKN1A, SLC2A1, TNC, TNFRSF11B, PTGS2, HIGD1A, ZFP36, NUAK2, CCND1, PMAIP1, UPP1, SLC25A25, KLF10, EGR1, JUN, BDNF, ITGA2, SPHK1, FOS, SSTR2, TGFBR2, FOSL1, VGF, AXL, ADORA2B, ITGA6
negative regulation of phosphorylation (GO:0042326)	26/325	24.60	ERRFI1, CDKN1A, SPRED2, RGS2, SPRED1, UBASH3B, MYC, SFN, DUSP4, DUSP5, JUN, DUSP2, DUSP1, TESC, SPRY4, LIF, KLF4, DKK1, DUSP6, DUSP7, MYADM, SPRY2, F2RL1, SPRY1, TRIB1, BIRC3
tissue morphogenesis (GO:0048729)	27/358	22.83	CSF1, TNC, CXCR4, AREG, SHH, GJA1, GBX2, MYC, ANKRD1, GCNT3, SOX8, SOX9, EDN1, JAG1, NFATC3, MICAL2, KLF4, ETV4, TGFBR2, ALDH1A3, BMP2, KRT17, WT1, SNAI1, VCL, FGFR1, EPHA2

GO terms Cellular Component 2015

Term	Overlap	Combined Score	Genes
anchoring junction (GO:0070161)	26/419	18.64	FHL2, TNC, GJA1, CSRP1, PLAU, PIP5K1A, FLNC, ANXA1, ITGA2, SPRY4, RDX, PLAUR, KAZN, LIG4, L1CAM, YWHAZ, RHOB, PPFIBP1, ZYX, ITGA6, KIFC3, SSX2IP, FERMT2, VCL, EPHA2, PLEC
adherens junction (GO:0005912)	25/405	18.44	FHL2, TNC, GJA1, CSRP1, PLAU, PIP5K1A, FLNC, ANXA1, ITGA2, SPRY4, RDX, PLAUR, LIG4, L1CAM, YWHAZ, RHOB, PPFIBP1, ZYX, ITGA6, KIFC3, SSX2IP, FERMT2, VCL, EPHA2, PLEC
focal adhesion (GO:0005925)	23/352	18.29	ANXA1, ITGA2, SPRY4, RDX, FHL2, PLAUR, TNC, LIG4, L1CAM, YWHAZ, RHOB, GJA1, PPFIBP1, CSRP1, PLAU, ZYX, PIP5K1A, ITGA6, FLNC, VCL, FERMT2, PLEC, EPHA2
cell-substrate adherens junction (GO:0005924)	23/358	18.27	ANXA1, ITGA2, SPRY4, RDX, FHL2, PLAUR, TNC, LIG4, L1CAM, YWHAZ, RHOB, GJA1, PPFIBP1, CSRP1, PLAU, ZYX, PIP5K1A, ITGA6, FLNC, VCL, FERMT2, PLEC, EPHA2
cell-substrate junction (GO:0030055)	23/362	18.24	ANXA1, ITGA2, SPRY4, RDX, FHL2, PLAUR, TNC, LIG4, L1CAM, YWHAZ, RHOB, PPFIBP1, GJA1, CSRP1, PLAU, ZYX, PIP5K1A, ITGA6, FLNC, FERMT2, VCL, PLEC, EPHA2

GO terms Molecular Function 2015

Term	Overlap	Combined Score	Genes
MAP kinase phosphatase activity (GO:0033549)	6/16	21.08	DUSP4, DUSP5, DUSP2, DUSP1, DUSP6, DUSP7
MAP kinase tyrosine/serine/threonine phosphatase activity (GO:0017017)	6/15	20.61	DUSP4, DUSP5, DUSP2, DUSP1, DUSP6, DUSP7
RNA polymerase II core promoter proximal region sequence-specific DNA binding transcription factor activity (GO:0000982)	17/204	17.68	TGIF1, EGR1, JUN, BATF3, NFATC3, NR1D1, KLF4, ETV4, ETS2, NR4A1, WT1, MYC, CREB3L1, BHLHE40, SNAI1, SOX9, ATF3
transcription regulatory region sequence-specific DNA binding (GO:0000976)	21/340	16.59	KLF10, TGIF1, EGR1, JUN, BATF3, FOXF2, NFATC3, NR1D1, BHLHA15, FOS, KLF4, ETV4, ETV5, ETS2, FOSL1, MYC, SNAI1, SOX8, SOX9, JUNB, ATF3
sequence-specific DNA binding RNA polymerase II transcription factor activity (GO:0000981)	23/397	16.47	TGIF1, EGR1, CSRNP1, JUN, BATF3, FOXF2, NFATC3, AHR, BHLHA15, NR1D1, KLF4, ETV4, ETV5, ETS2, NR4A1, WT1, MYC, CREB3L1, BHLHE40, SNAI1, SOX8, SOX9, ATF3

APPENDIX C

Leader cell identification

C.1 Dll4 staining

In order to test the hypothesis that PAR2-induced actin cabling prevented leader cell formation, resulting in reduced Caco2 sheet migration, Caco2 cells were plated and wounded according to the staining protocol. At 24 h, cells were fixed and stained for Dll4 (sc18640 Santa Cruz, 1:200). Unfortunately, the goat IgG control antibody staining was similar to the primary Dll4 antibody (Figure C.1) suggesting that the apparent Dll4 immunoreactivity was in fact not specific to Dll4 protein.

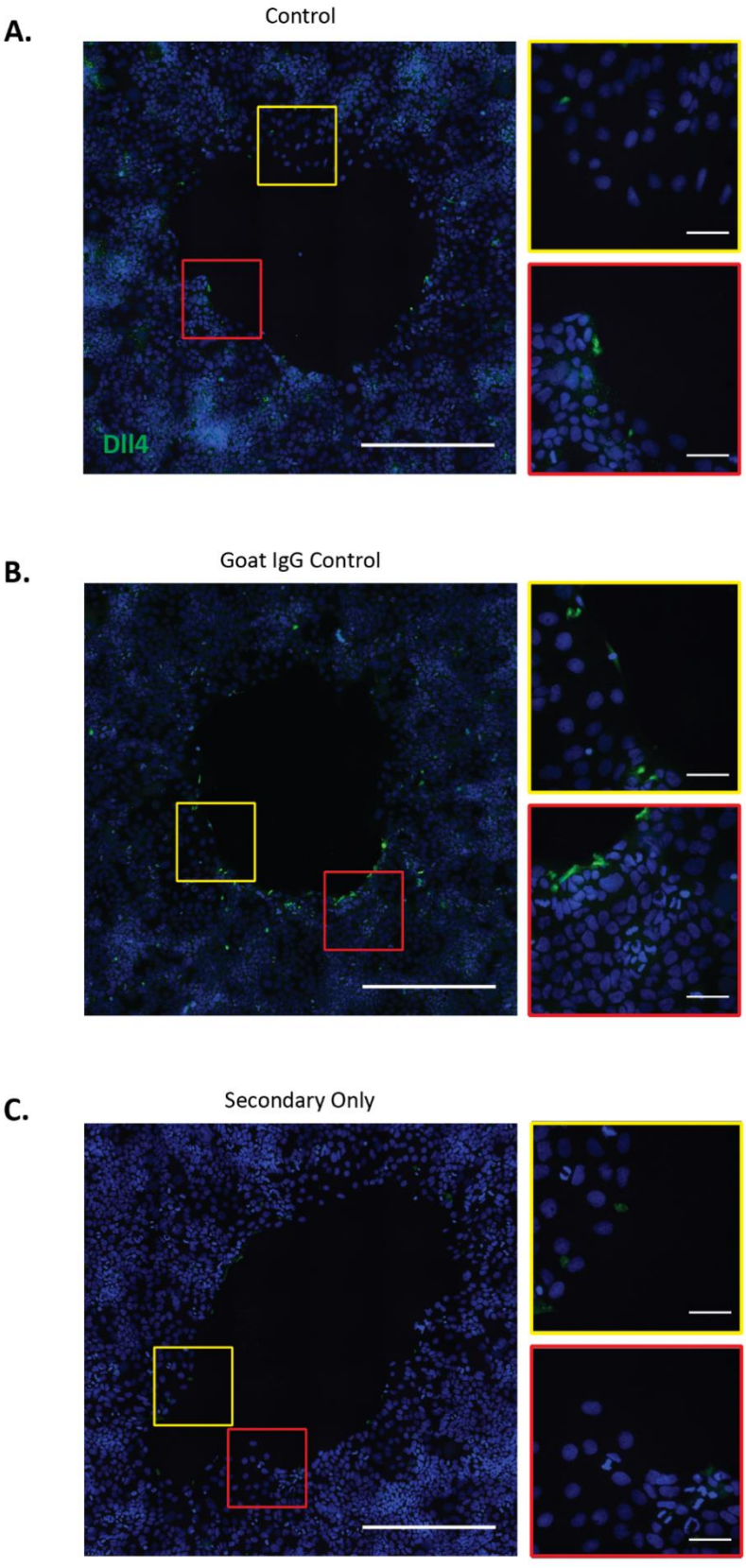
A.
Control
Dll4
B.
Goat IgG Control
C.
Secondary Only

Figure C.1 Dll4 staining in Caco2 cells could not identify leader cells.

A: In control wounds, although there was some positive staining in cells that were part of protrusions into the wounded area (red insert), there was no positive staining in other areas where leader cells would be expected (yellow insert). B: Using the IgG control, a similar wound-edge staining was observed compared to the primary Dll4 antibody. C: Secondary only control. *Scale bars – stitched image: 400 µm; 20X image: 50 µm.*

APPENDIX D

Primary Intestinal Epithelial Cells

D.1 Methods[3]

D.1.1 Generating L-WRN cell conditioned media

L-WRN cells were kindly provided by Dr. Kristi Baker (University of Alberta, originally purchased from ATCC CRL-3276). The conditioned media from L-WRN cells, containing Wnt-3A, R-spondin 3, and noggin was used to make the culture media for all primary cells. The detailed method of generating conditioned media when starting with a cryovial of L-WRN cells is as follows:

The cryovial of L-WRN cells was quickly thawed in a 37°C water bath, and immediately transferred to 25 mL pre-warmed L-WRN cell media made from DMEM (high glucose), supplemented with sodium pyruvate (1 mM), L-glutamine (4 mM), penicillin (100 U/mL), streptomycin (0.1 mg/mL) and FBS (10% v/v). It is important to note that these cells were very fragile after thawing, and centrifugation as well as excess pipetting were avoided. The media containing the cells was transferred to a 150 cm^2 flask and incubated at 37°C with 5% CO_2. The following day, media was changed to include G418 (500 µg/mL) and hygromycin (500 µg/mL) in the complete media listed above. Cells were grown until confluency (2 d). Once confluent, the cells were washed with 20 mL PBS-EDTA (without

[3] These methods were developed and optimized within the lab by Michael Dicay (MacNaughton lab manager) and Dr. Marilyn Gordon (MacNaughton lab post-doctorate).

Ca^{2+} or Mg^{2+}, 0.5 mM), and then 1 mL of trypsin-EDTA (0.25% wt/v in PBS-EDTA) was used to carefully coat the surface before returning the flask to the incubator for 3-5 min to lift the cells. Once lifted, cells were suspended in 12 mL of complete L-WRN cell media, and gently pipetted up and down 3 times. Another 120 mL of complete L-cell media was added to the flask with the cell suspension, for a total of 132 mL. The cell suspension was divided into 5 new 150 cm^2 flasks with 25 mL per flask. The leftover suspension (8 mL) was either discarded, or used in the following section to freeze stock vials of L-WRN cells. The 5 new flasks were incubated for 3 days, with a media change on the second day. The culture media did not contain G418 or hygromycin to avoid any carryover of the drugs into the conditioned media. By the third day, the cells were over-confluent with a number of cell aggregates coming off. Cells were then washed with 10 mL/flask of **washing media**, which was made with DMEM/F12 with HEPES, containing L-glutamine (2.5 mM), penicillin (100 U/mL), streptomycin (0.1 mg/mL) and FBS (10% v/v). The washing media was aspirated, and 25 mL of **primary culture media (PCM)** was added. PCM was made with Advanced DMEM/F-12 containing L-glutamine (2 mM), penicillin (100 U/mL), streptomycin (0.1 mg/mL) and FBS (20% v/v). The flasks were incubated for 24 h, at which time the conditioned media was recovered into a 50 mL centrifuge tube, and new PCM was added to the flask. The tubes containing the conditioned media were spun at 2,000 x *g* for 5 min at r.t. and the supernatant was carefully decanted into a 1 L bottle (total 125 mL) and stored at 4°C. Every 24 h for 72 h, the conditioned media was collected the same way and stored in the same bottle. After the fourth collection, an equal volume of PCM (500 mL)

was added. The **final L-WRN conditioned media** was mixed well, divided into 15 mL or 50 mL centrifuge tubes, and stored at -20°C. Depending on how much conditioned media is required, the 5^{th}-8^{th} and 9^{th}-12^{th} collections can be prepared the same way as the described 1^{st}-4^{th} collection. Importantly, conditioned media can be stored at -20°C for at least 3 mo without a decrease in activity. After thawing, conditioned media should be stored at 4°C and used within 1 wk.

D.1.1.1 Freezing Stock Vials of L-WRN Cells

The leftover suspension (8 mL) from the previous section was placed into a 150 cm^2 flask with 17 mL of L-WRN cell media. The following day, media was changed to include G418 (500 µg/mL) and hygromycin (500 µg/mL) in the L-WRN media. Cells were grown until confluency (2 d). Once confluent, the cells were washed with 20 mL PBS-EDTA, and then 1 mL of trypsin-EDTA was used to carefully coat the surface before returning the flask to the incubator for 3-5 min to lift the cells. Once lifted, cells were suspended in 9 mL of complete L-WRN cell media, and gently pipetted up and down 3 times. Ten 75 cm^2 flasks were seeded with 1 mL of cell suspension and 14 mL of L-WRN media, and grown until confluent (2 d). Again, the cells were washed with 10 mL PBS-EDTA, and 1 mL of trypsin-EDTA was used to lift the cells. Cells were suspended by adding 9 mL of washing media, and gently pipetted up and down 3 times. The cell suspension (10 mL) was transferred to a 15 mL centrifuge tube and spun at 1200 rpm (need to convert to g) for 3 min at r.t. Supernatant was aspirated, and the cells were resuspended in 3 mL of freezing media by gently pipetting up and down 5 times. **Freezing media** was made fresh with washing media

containing FBS (10% v/v) and DMSO (10% v/v). The cell suspension was transferred into cryovials (1 mL/vial) to yield a total of 30 tubes from 10 flasks. Vials were stored at -80°C or in liquid nitrogen until needed.

D.1.2 Preparation of a 3D colonoid culture from mouse large intestine

Before harvesting the mouse colon, Matrigel was set to thaw on ice and a 24 well plate was warmed in an incubator. Additionally, basal crypt media (BCM) was prepared using Advanced DMEM/F12 (ADF) supplemented with Glutamax (2 mM), HEPES (10 mM), penicillin (100 units/mL), streptomycin (0.1 mg/mL), N2 Supplement (1x), B27 supplement (1x) and N-acetyl cysteine (NAC, 1 mM). Complete crypt culture media (CCCM) was then prepared by mixing basal crypt media (BCM) and L-WRN conditioned media at a 1:1 ratio and supplemented with human epidermal growth factor (hEGF, 50 ng/mL).

The colon was harvested and placed in a petri dish with cold PBS. After removing the serosal fat, the colon was cut longitudinally and washed twice with ice cold sterile PBS. Next, the entire colon was transferred to a 1.5 mL Eppendorf with PBS (1 mL) to be minced with scissors. The minced colon was transferred to a new 50 mL tube containing cold PBS (20 mL) for washing. To wash, the tubes were manually shaken (30 sec), then spun at 243 x *g* (30 sec, r.t.). PBS was removed and the minced colon was washed twice more. After the third wash, 30 mL of ice cold crypt isolation buffer (2 mM EDTA, 43.4 mM sucrose, 0.5 mM DTT in PBS) was added to the tube and incubated at 4°C with gentle rocking (30 min).

It is important to note that all pipettes and pipette tips used in subsequent steps were pre-coated with a solution of PBS containing 2% FBS (PBS2) to avoid tissue becoming stuck to the sides of the pipettes. Glass pipettes should not be used.

Following incubation with the crypt isolation buffer, tubes were spun at 300 x *g* (30 sec), and the supernatant was aspirated. Cold PBS (10 mL) was added, and tissue was pipetted up and down (x 6). The tissue pieces were allowed to settle at the bottom of the tube, and the supernatant (fraction 1) was removed and placed in a separate 50 mL Falcon tube labeled "A". This PBS step was repeated and the supernatant (fraction 2) was also added to tube "A" and set aside on ice. Tube "A" is used only as a back-up in the event there is little or no pellet in fractions 3 – 7. Additional cold PBS (10 mL) was added to the settled pieces of tissue, which was again pipetted up and down (x 6), allowed to settle, and the supernatant (fraction 3) was transferred to a separate 50 mL Falcon tube labeled "B". This was repeated 4 more times, and fractions 4-7 were added to tube B. Next, a cell strainer (mesh size 100 µm) was coated with PBS2, and used to filter the contents of tube B into a new 50 mL Falcon tube. Tube B was centrifuged at 300 x *g* (4°C, 5 min). The supernatant was aspirated leaving approximately 100 µL on the pellet. The pellet was then resuspended in cold ADF (1 mL) and transferred to a 1.5 mL Eppendorf tube which was spun at 20817 x *g* (30 sec, r.t.). All of the supernatant was carefully aspirated and the pellet was plated.

To plate the cells, a pre-chilled pipette tip was used to transfer Matrigel (360 µL) to the pellet and resuspended taking care not to introduce bubbles. Next, the Matrigel-cell

mixture (30 µL) was applied to the center of 16 wells of a pre-warmed 24 well plate, with careful attention to avoid introducing air bubbles in the Matrigel. The plate was then quickly inverted and placed in the incubator to set (30 min), which encouraged the droplet to have good 3D structure.

After 30 min, CCCM (500 µL/well) containing Y27632 (ROCK inhibitor, 10 µM) and Primocin (0.1 mg/mL) was carefully added down the side of each well and the plate was then placed in a 37°C incubator (with 5% CO_2). The following day, and every 2 days thereafter, media was changed with regular CCCM.

D.1.3 Plating a 2D monolayer from a 3D enteroid culture

Cells were plated in 12 wells of a 24 well plate with or without Transwell inserts, that were either coated or uncoated. To coat the wells or inserts, 250 µL of a 1:30 Matrigel:ADF mix was added for 1-2 h at 37°C. Excess solution was removed, and warm CCCM (400 µL) lacking NAC (lack of NAC promotes monolayer growth) but containing Y27632 (10 µM) and Primocin (0.1 mg/mL) was placed in each pre-coated well until the cell suspension was added.

Media was aspirated from each organoid-containing Matrigel dome, and cold ADF (1 mL) was added. Domes were vigorously pipetted and transferred to a cold solution of trypsin-EDTA. Six domes were pooled into 6 mL of trypsin-EDTA for a final volume of 12 mL, and the solution was incubated on ice for 30 min.

A second incubation step was then performed in a water bath at 37°C for 10 min. Trypsin was inactivated by adding 15 mL cold washing media, and the tube was manually shaken to mix (30 sec). Tubes were then centrifuged at 300 x *g* (5 min, 4°C). The supernatant was aspirated leaving approximately 200 µL on the pellet, PBS (1 mL) added and the pellet resuspended using a pipette tip pre-coated with PBS2 and transferred to a 1.5 mL Eppendorf tube. Tubes were spun at 20817 x *g* (30 sec) and supernatant was aspirated. Next, using a pipette tip pre-coated with PBS2, the pellet was resuspended with warm CCCM (1.3 mL) lacking NAC but containing Y27632 (ROCK inhibitor, 10 µM) and Primocin (0.1 mg/mL). The suspension was then added to the pre-coated wells (100 µL/well), with constant pipetting of the cell suspension to ensure even plating. The plate was rocked gently to distribute cells in the wells and then placed in 37°C incubator (with 5% CO_2).

D.2 Results[4]

D.2.1 PAR2 signaling in primary mouse intestinal epithelial cells

Mouse primary intestinal epithelial cells isolated from WT and PAR2-deficient mice were plated in a 24 well plate that was either Matrigel-coated or uncoated. Cells were grown as a 2D culture from 3D enteroids for 13 days, then treated with 2fO or 2fLI (2 μM) for 5 min (ERK) or 2-6 h (COX-2). Whole cell lysates were analyzed by western blot. Phosphorylation of ERK in only WT primary cells confirmed PAR2-signaling was induced (Figure D.1 A), and this signaling was independent of the presence or absence of Matrigel coating. When WT cells were treated with 2fLI for 2 or 6 h, COX-2 expression was increased (Figure D.1 B) with both coated and uncoated conditions, but this effect was not seen in PAR2-deficient cells. These data were produced with cells isolated from a single mouse.

D.2.2 Optimizing visualization of primary intestinal epithelial cells for wound healing experiments

In order to test the effect of PAR2-activation on wound healing in primary cells, similar to the previous experiments performed in cell lines, it is necessary to visualize the cells clearly. When cells were plated on Transwell supports, the contrast provided from the Transwell made it difficult to visualize the monolayer of cells, and impossible to determine

[4] The cells used in the following experiments were prepared and plated by Michael Dicay or Marilyn Gordon, and experiments were performed by Elizabeth Fernando.

the wound edge (Figure D.2 A), but when the cells were plated directly in a Matrigel-coated plastic well, it was possible to visualize cell boundaries (Figure D.2 B).

Next, primary cells were plated within a coated 24 well plate that had a glass coverslip placed in the bottom of the well, and grown for 13 days. Although a wound healing experiment was planned, when an initial image was captured using the IncuCyte microscope it was evident that the cells had not grown to form a complete monolayer. Cells were left on the IncuCyte microscope for 24 h to visualize growth (Figure D.3). Cells appeared to move slightly within 24 h, but it was unlikely that they would become confluent if left to grow.

On day 14, the plate was removed from the IncuCyte microscope, the cells were fixed in 4% PFA, and the glass coverslips were used for immunofluorescence staining. ZO-1 (white) was detected at the intercellular junctions (Figure D.4 A), and lamellipodia formation was seen in cells at the edges of confluence (F-actin, green, Figure D.4 B).

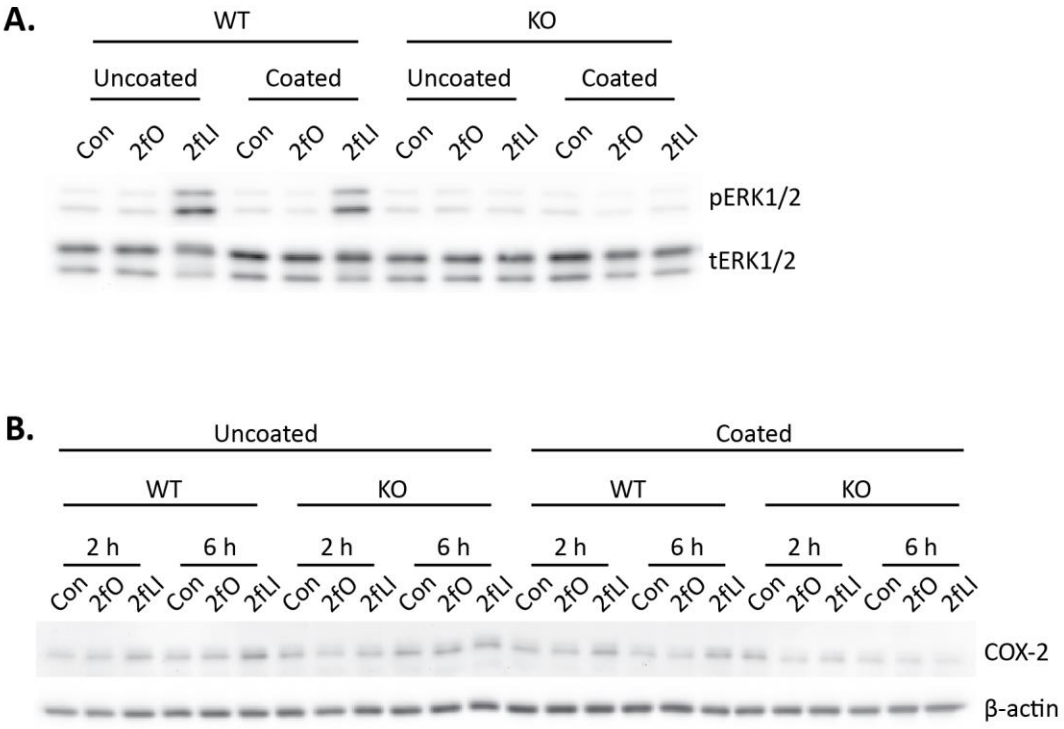

Figure D.1 Signaling in primary intestinal epithelial cells, with and without Matrigel coating.

Primary cells isolated from WT or Par2-deficient mice were plated with or without Matrigel coating (1:30) in a 24-well plate, without a Transwell support. A: PAR2 signaling was confirmed by treating cells for 5 min with 2fO or 2fLI (2 μM), and control cells were left untreated. Whole-cell lysates were analyzed by western blotting for pERK1/2 and tERK1/2. B: Cells were treated with 2fO or 2fLI (2 μM) for 2 h or 6 h, and whole-cell lysates were analyzed by western blotting for COX-2 and β-actin.

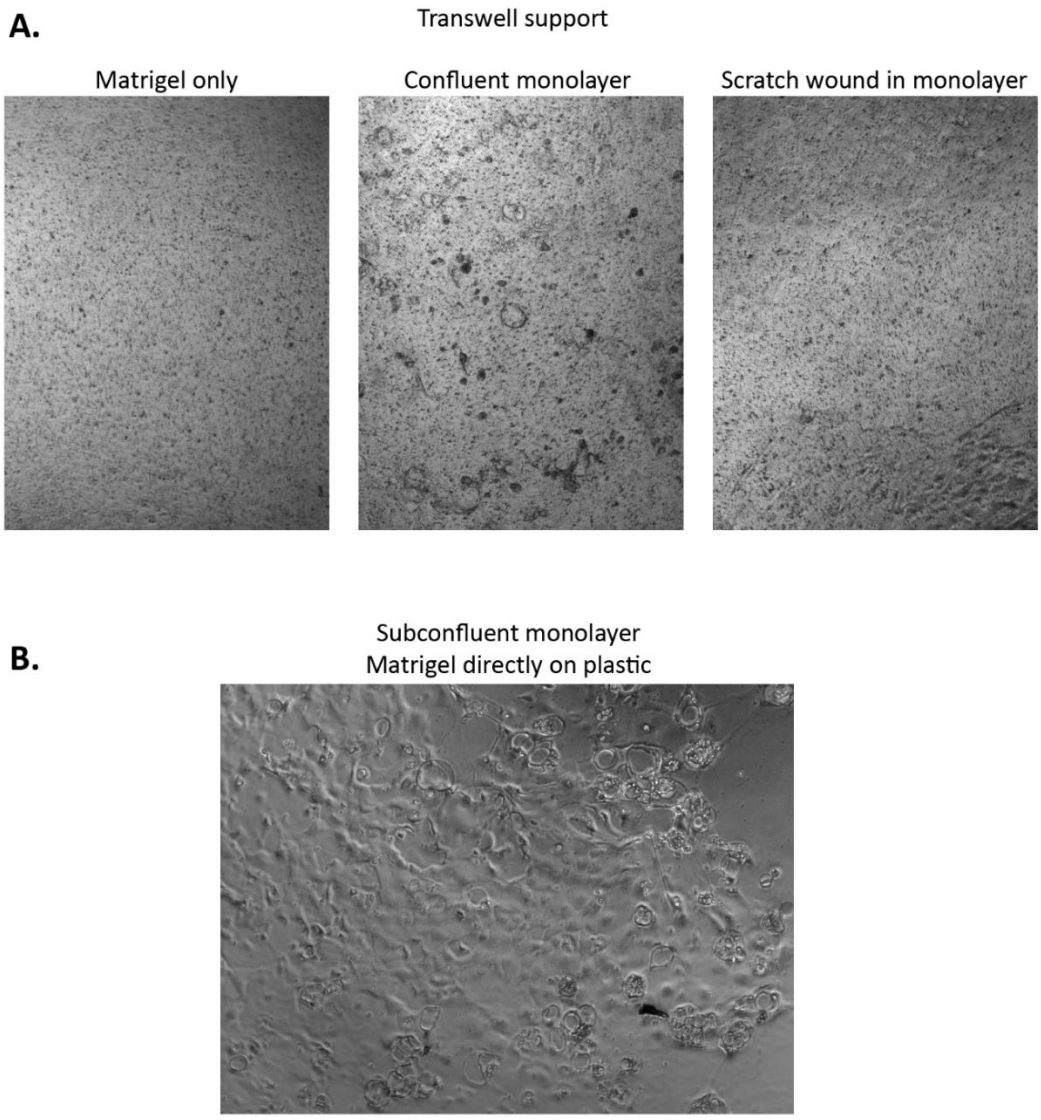

Figure D.2 Visualizing primary intestinal epithelial cells grown in a 2D monolayer.

A: Due to the high contrast provided by the Transwell insert, visualizing the primary cells was very difficult on a phase-contrast microscope, and wounds that were created in a confluent monolayer could not be quantified. B: Cells were easier to visualize when plated without a Transwell support.

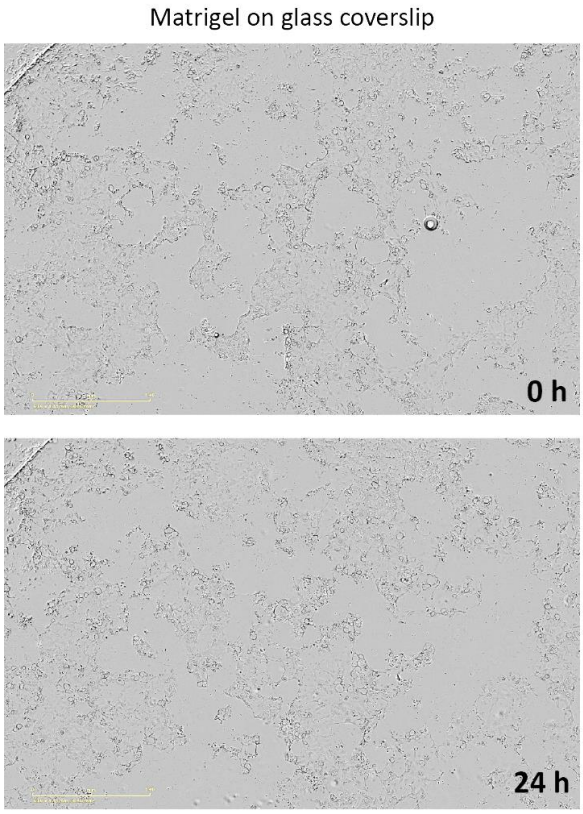

Figure D.3 Primary intestinal epithelial cells do not reach confluence when grown in 2D without a Transwell support.

Primary cells were plated in a 24-well plate that had a glass cover slip placed on the bottom, which was coated with 1:30 Matrigel. After 10 days, cells were wounded and imaged using whole-well scanning on the Incucyte microscope for 24 h. Representative images are shown at 0 h and 24 h.

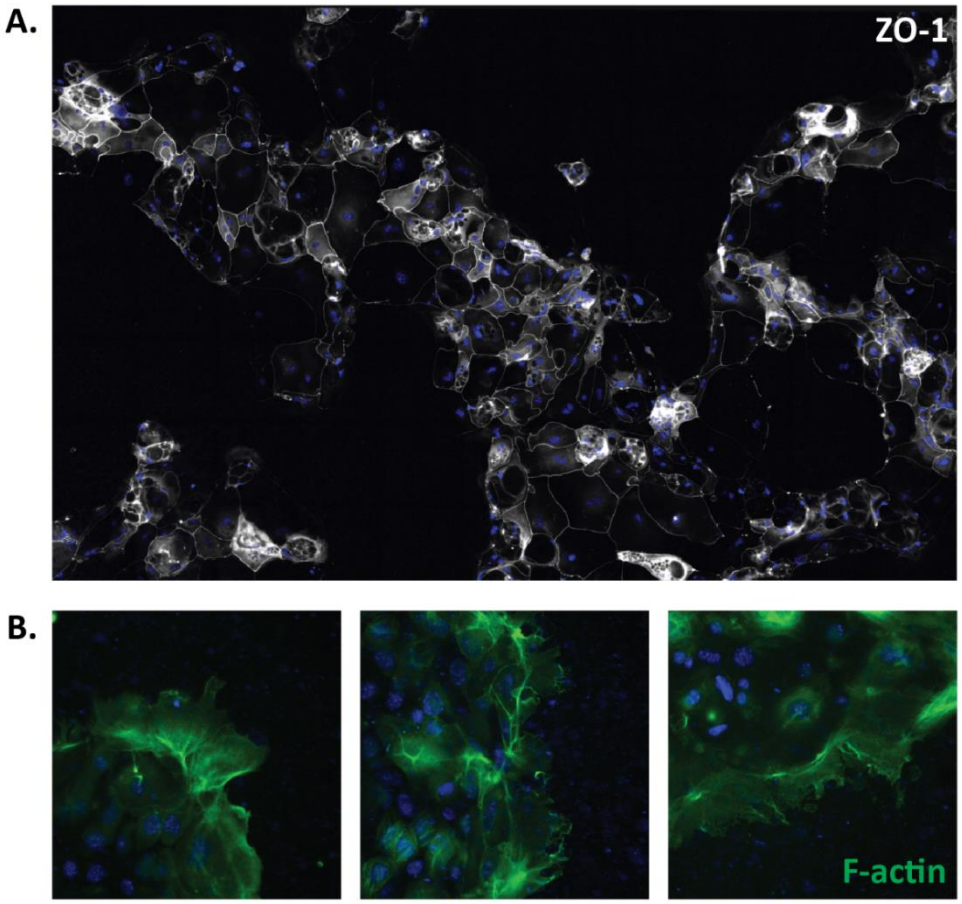

Figure D.4 ZO-1 and F-actin immunofluorescent staining of primary intestinal epithelial cells.

Cells were grown on a Matrigel-coated glass coverslip but did not reach confluence. A: ZO-1 staining (white) localized to the intercellular junctions. B: F-actin staining with phalloidin (green) in cells at the edge of cell patches. (DAPI blue)

D.3 Discussion

The novel method developed of culturing primary mouse intestinal epithelial cells in 2D will be a valuable tool in order to assess the translational potential of the previous work on PAR2 signaling and PAR2-dependent wound healing in intestinal epithelial cell lines. The preliminary data using primary cells indicated that PAR2 signaling was functional in 2D cultures, and COX-2 expression was increased with PAR2 activation. However, these results will need to be repeated using cells isolated from multiple mice in order to confirm the effect.

Additional trouble shooting is required in order to optimize a wound healing protocol in the 2D primary cell cultures due to the difficulty in imaging the cells. Since the primary cells only form monolayers when they are grown on semi-permeable supports such as Transwells (data from M. Dicay, not shown), live-cell videos will be difficult to acquire due to the contrast of the Transwell. However, if the size of the starting wound can be accurately reproduced, cells can be fixed and stained at many time points in order to visualize the cells and wounded area, by staining either components of the cell-cell junctions or the F-actin.